Development of a novel growth method for AlN bulk single crystals using elemental aluminum and nitrogen gas

PeiTsen Wu

2015

Abstract

Aluminum nitride (AlN) is a promising material for ultraviolet (UV) emitters due to its large direct bandgap of ~6 eV at room temperature. However, the device fabrication technologies of nitride-based UV light-emitting diodes (LEDs) are still immature. The absence of suitable bulk substrates is the most fatal problem. It has led to the fabrication of AlN on foreign substrates such as sapphire and SiC. The large mismatches in both the thermal expansion coefficients and lattice parameters between AlN and foreign substrates cause cracks and high-density defects in the AlN films. Therefore, AlN bulk crystals for homoepitaxy are highly expected. Although extensive efforts have been devoted to fabricating AlN bulk crystals, the current common growth methods such as hydride vapor phase epitaxy (HVPE) and sublimation involve some restrictions: dangerous source precursors, extremely high growth temperatures up to 2000°C, etc. In order to break such restrictions, we propose a new approach in this thesis, where only Al metal and N_2 gas are used. Those are much safer and less polluting materials, compared with the source precursors of the common growth methods.

In Chap. 2, novel, environmentally-friendly growth methods are discussed. A simple thermodynamic analysis suggested that a reaction of $Al_{(s,l,g)}+1/2N_{2(g)} = AlN_{(s)}$ is possible at a reasonable temperature. However, if N_2 gas is directly supplied on Al powders, AlN crust forms on the powder surface. Consequently, the AlN crust covers the Al metal source and prevents the growth processes from proceeding. Therefore, Al vapor and N_2 gas should separately be transferred onto the substrate surface. To do this, we designed and constructed a suitable furnace equipped with two temperature zones; one is for source and the other is for growth. These zones can be operated at different temperatures. Furthermore, the source zone

is divided into the upper and lower channels. N_2, which is a main reaction gas, is supplied into the upper channel, whereas Al metal is placed in the lower channel, to which Ar is supplied as a carrier gas of heat generated Al vapor. Those gases join together in the growth zone.

In Chap. 3, the reactivity between Al and N_2 was initially confirmed. For this, N_2 gas was introduced into the lower channel to directly react with Al powders in the source zone. Successful synthesis of AlN powders was demonstrated. Subsequently, to synthesize AlN whisker and film crystals on c-plane sapphire substrates, Al vapor was carried to the growth zone by Ar gas and reacted with separately-supplied N_2 gas. Through adjusting growth conditions, we found that low V/III ratios (that is, $[N_2]/[Al]$ ratio) during the growth result in AlN whiskers, whereas high V/III ratios result in films.

In Chap. 4, the details of self-separation of AlN from sapphire and AlN thick film growth are discussed. The self-separation was attributed to the decomposition of sapphire substrates. The self-separation phenomenon cushions the effect of tensile strain within the growth plane effectively. Thus, we consider that it can be used to avoid cracks even in thick AlN. By optimizing the growth condition (particularly, V/III ratio in vapor), we achieved a growth rate of 16 μm/hr. The structural properties of the 16-μm-thick AlN film were assessed by X-ray diffraction measurements. The ϕ-scan of the AlN $\{1\bar{1}02\}$ asymmetric planes showed that the crystal was in the single phase exclusive of other rotation domains. The ω-scan profiles of the AlN (0002) symmetric and $(1\bar{1}02)$ asymmetric planes have full widths at half maximum of 290 and 291 arcsec, respectively. From these values, the edge and screw dislocation densities were estimated to be 4.8×10^8 and 1.8×10^8 /cm^2, respectively. These results strongly suggest that this new method is promising for AlN bulk growth.

Acknowledgements

I would like to first express my sincere thanks and gratitude to my advisors, Professor Yoichi Kawakami for guidance, kind support, helpful advice and giving me a chance to study in Kawakami laboratory. Without his encouragement, I would have not been able to complete this work.

I would like to thank Professor Shizuo Fujita and Professor Gikan Takaoka for their kind encouragement, valuable discussion and suggestion during discussions and my thesis defense. I would also like to deeply appreciate Professor Mitsuru Funato, for his assistance, guidance and valuable discussion throughout my graduate study. He is one of the best teachers I have ever had.

And, sincere thanks to all the members in Kawakami Laboratory for their kindness and supports. Thank you. Thank our secretaries, Miki Watanabe and Keiko Furuyama, for their support and concern daily. To Dr. Akio Kaneta, Dr. Ryota Ishii and Dr. Takao Oto, thanks your helpful advice and assistance in the optical measurements. To Dr. Ryan G. Banal, Dr. Junichi Nishinaka, Mr. Ken Kataoka, Mr. Shuhei Ichikawa, thank your helpful discussion and suggestion during my researching. To Dr. Pedro Favuzzi, Miss QuinFeng Meng and all my friends, thank to your friendship and encouragement.

Lastly, I would like to appreciate my parents, sister and brother for their continuous love and support. I LOVE YOU!

September, 2015

PeiTsen Wu

Contents

Chapter 1 – Introduction

1.1 Research Background

1.1.1 Evolution of Illumination

Making use of illumination started a new chapter in history of humanity. The control of fire was a turning point in the development of civilization. Through a series of the evolution of illumination, Joseph Wilson Swan achieved a pivotal invention, the first electric light in the middle of the 19th century. Although that incandescent bulb was not bright enough nor did it have a long life time to be practical, it was an innovation of illumination. After that, many inventors challenged the improvement of incandescent bulb. In 1879, Thomas Edison devised a carbon filament that burned for forty hours. A cheaper, more convenient, and brighter lighting source was invented at last. Thereafter, electric lighting became ubiquitous illumination in the world.

In the middle of the 19th century, a more efficient lighting source compared with incandescent bulbs was invented. That was a fluorescence lamp. The fluorescent lamp was first invented by Heinrich Geissler in 1856 and commercialized in 1895 by Daniel McFarlan Moore. Fluorescent lamps consist of a tube containing mercury vapor and phosphor coated on the tube inside. An electric current that flows through the tube excites mercury atoms, and when they relax to the ground state, ultraviolet (UV) light is emitted. Subsequently, a phosphor on the inside wall absorbs the UV light and radiates visible light. Since the luminous efficacy of fluorescent lamps is several times better than incandescent bulbs with comparable light output, fluorescent lamps have been the main stream of illumination. However, because mercury vapor is a well-known hazardous gas, fluorescent lamps are

classified as a hazardous waste.

The most recent revolutionary illumination is light-emitting diodes (LEDs) based on semiconductor materials. Due to the high energy conversion efficiency, long lifetime, durability, safety, and environmentally-friendliness, LEDs are expected to replace traditional incandescent bulbs and fluorescent lamps. The first LED was reported by Henry Joseph Round in 1907 [1]. He discovered a phenomenon named electroluminescence when using silicon carbide and a cat's whisker detector (*i.e.* point contact). However, he did not understand the mechanism clearly. The detailed investigations of the luminescence phenomenon observed with metal–SiC rectifiers were reported by Oleg V Lossev in 1928 [2]. By the late 1960's, the growth technologies of SiC films were more matured, and p-n junction devices were fabricated, leading to blue LEDs [3]. However, the electro-optic conversion efficiency of SiC LEDs was only ~0.005%. Although SiC LEDs were sold commercially in 1990s, the best SiC LEDs emitting blue light at 470 nm had an efficiency of only 0.03 % [4]. In the past decades, one can hardly see improvement in blue SiC LEDs, because SiC has an indirect bandgap. (Recently, progress of SiC-based power electronic devices is remarkable.)

The era of III–V compound semiconductors started in the early 1950s. III–V compound semiconductors were expected to supersede SiC due to their direct bandgaps. Rubin Braunstein of the Radio Corporation of America (RCA) discovered infrared emission from gallium arsenide (GaAs) and other semiconductor alloys in 1955. In 1961, James R. Biard and Gary Pittman developed GaAs infrared LEDs at Texas instruments. This was the first demonstration of the modern LEDs although the LEDs did not emit visible light [5]. Then, infrared (870–980 nm) LEDs and laser diodes (LDs) based on GaAs were reported by groups working at RCA, GE, IBM, and MIT in 1962. In the same year, the first visible (red) LEDs were developed by Nick Holonyak. With further work through the 1970s, more colors became available. In 1972, M. George Craford, a Holonyak's former graduate student, developed the

first yellow LEDs and improved about 10 times the brightness of red and red-orange LEDs. Furthermore, the first efficient blue LEDs were demonstrated in the mid-1990s by Isamu Akasaki, Hiroshi Amano, and Shuji Nakamura [6-8].

With the rapid development of technologies in the past two decades, nowadays, LEDs bring a great evolution of illumination. LEDs are widely used in various applications such as traffic signals, automotive headlamps, outdoor (stadium) lightings, full-color displays, back lightings of liquid crystal display, and artwork lightings.

1.1.2 Ultraviolet Emitters

After the development of high-efficiency visible light-emitters, nowadays, the researchers are taking a great interest in the shorter emission wavelength region such as UV region (Fig. 1.1).

The UV spectral region spans from 400 to 10 nm in wavelength, which is shorter than that of visible light but longer than that of X-rays. In general, UV light can be classified into four parts: UV-A (320 – 400 nm), UV-B (290 – 320 nm), UV-C (200 – 290 nm) and vacuum-UV (10 – 200 nm). UV light was first observed by J. W. Ritter in 1801. Afterward, Wheatstone invented a mercury vapor lamp in 1835, and Stokes made a "closed" arc lamp that emitted UV rays of 185 nm, using Al electrodes in a quartz tube in 1850. 66 years later, the first commercially viable Hg vapor lamp was manufactured by P. C. Hewitt. In 1936, the first UV light source for the sterilization was demonstrated by General Electric Company. In 1970, the first excimer laser using Xe was developed by N. Basov et al. To date, there are several kinds of UV applications such as UV light therapy, air-/water-purification, UV lithography, germicidal and biological instrumentation systems, UV photocatalytic effect, and curing. However, a choke point for UV emitters at shorter wavelengths is that almost all of the existent UV light sources use discharge of gas mixtures, such as ArF excimer gas lasers,

(a)

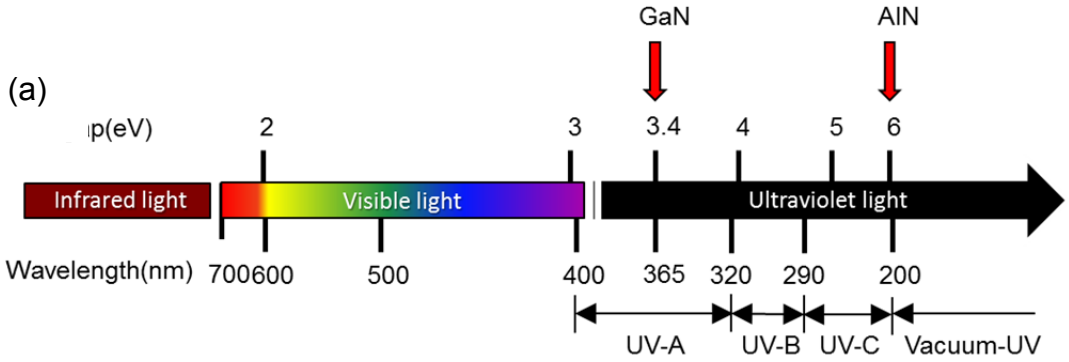

(b)

Applications	Wavelength
White LEDs	260-340nm
High-density optical recording	250-270nm
Water purification	250-340nm
Medical treatment	300-350nm

Figure 1.1: (a) Optical spectrum from IR to UV light. (b) Some applications of UV light.

mercury-vapor lamps, Xe, XeCl, KrCl, and D_2 lamps. In addition to short lifetime, those sources are hazardous to the health and environment. Therefore, solid-state LEDs and LDs are considered as good substitutes since they are compact, safe, and environmentally friendly, and have long life time. Recently, $Al_xGa_{1-x}N$ has attracted great attention because its energy band gap can be tuned by changing the alloy composition, and covers 200 – 400 nm of the UV spectrum [9-12]. However, the external quantum efficiency (EQE) of fully packaged AlGaN-based UV LEDs emitting below 285 nm is below 15% (Fig. 1.2) [13-23]. Reasons of this low EQE are discussed in the next section.

1.1.3 Properties and Challenges of AlN

AlN has not been found in nature. It was first synthesized from molten Al and N_2 gas in 1862 by F. Briegleb and A. Geuther [24]. At ambient conditions, the wurtzite structure is

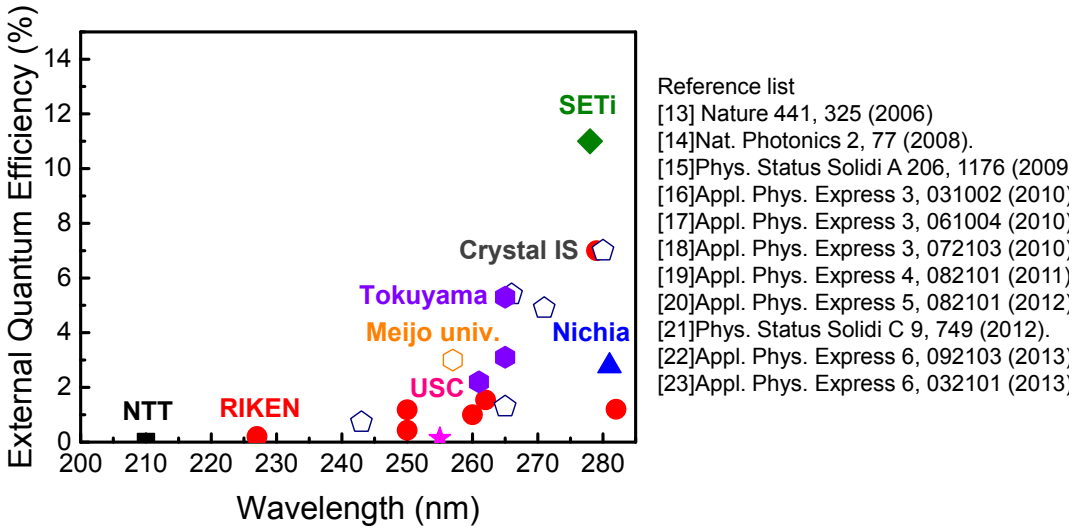

Figure 1.2: Reported external quantum efficiencies in AlGaN based UV-LEDs.

thermodynamically stable for AlN (Fig. 1.3).

The experimentally determined *a* and *c* lattice parameters of high purity AlN are 0.31111 and 0.49808 nm, respectively [25]. AlN possesses excellent thermal conductivity, high hardness, and good dielectric properties. Therefore, AlN has already been utilized as microelectronic packages and substrates.

AlN has the largest direct bandgap among the representative III–nitride compound semiconductors (about 6.0 eV at room temperature) and is considered as a promising material for the UV LEDs and LDs. In 2006, an AlN p-i-n junction UV LED with an emission wavelength of 210 nm was realized [13]. However, the growth technologies of nitride-based UV LEDs are still immature. The absence of suitable bulk substrates is the most fatal problem. It has led to the fabrication of AlN on foreign substrates such as sapphire and SiC.

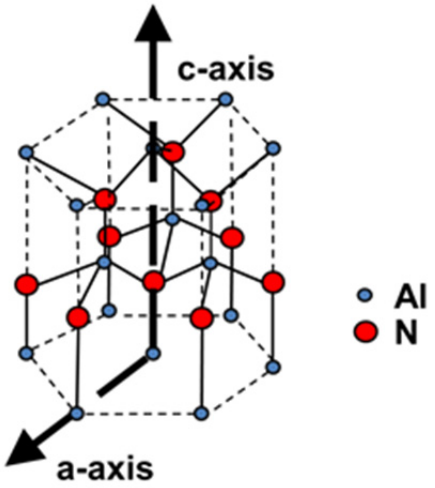

Figure 1.3: Schematic of the AlN crystal structure.

Table 1.1: Physical properties of AlN, GaN, sapphire, 6H-SiC, and Si.

(at 300K)

Materials	AlN [26]	GaN [27]	Sapphire [28]	6H-SiC [29]	Si [30]
Bandgap (eV)	~6.0 (D*)	~3.4 (D)	~8.7 (ID)	~3.0 (ID)	~1.1 (ID)
Crystal structure	Wurtzite	Wurtzite	Corundum	6H	Diamond
Lattice constant (Å)	a=3.111 c=4.981	a=3.189 c=5.196	a=4.785 c=12.991	a=3.081 c=15.117	5.43
Melting point (°C)	3000 (decompose)	>2500	2050	2800	1412
Thermal conductivity ($W\ cm^{-1}\ K^{-1}$)	2.85	1.30	0.35	4.20	1.63
Thermal expansion coefficient (K^{-1})	5.3×10^{-6} (//c) 4.2×10^{-6} (//a)	3.9×10^{-6} (//c) 3.5×10^{-6} (//a)	6.7×10^{-6} (//c) 5.0×10^{-6} (//a)	3.4×10^{-6} (//c) 3.3×10^{-6} (//a)	2.6×10^{-6}

*D: direct bandgap, ID: indirect bandgap

Table 1.1 lists the physical properties of AlN, GaN, sapphire, SiC, and Si. Due to the large lattice mismatch between III-nitride materials and substrates such as sapphire or Si, the presence of high-density dislocations in the device is inevitable (Fig. 1.4). Furthermore, the thermal expansion mismatch causes stress, occasionally resulting in cracks in the epilayer.

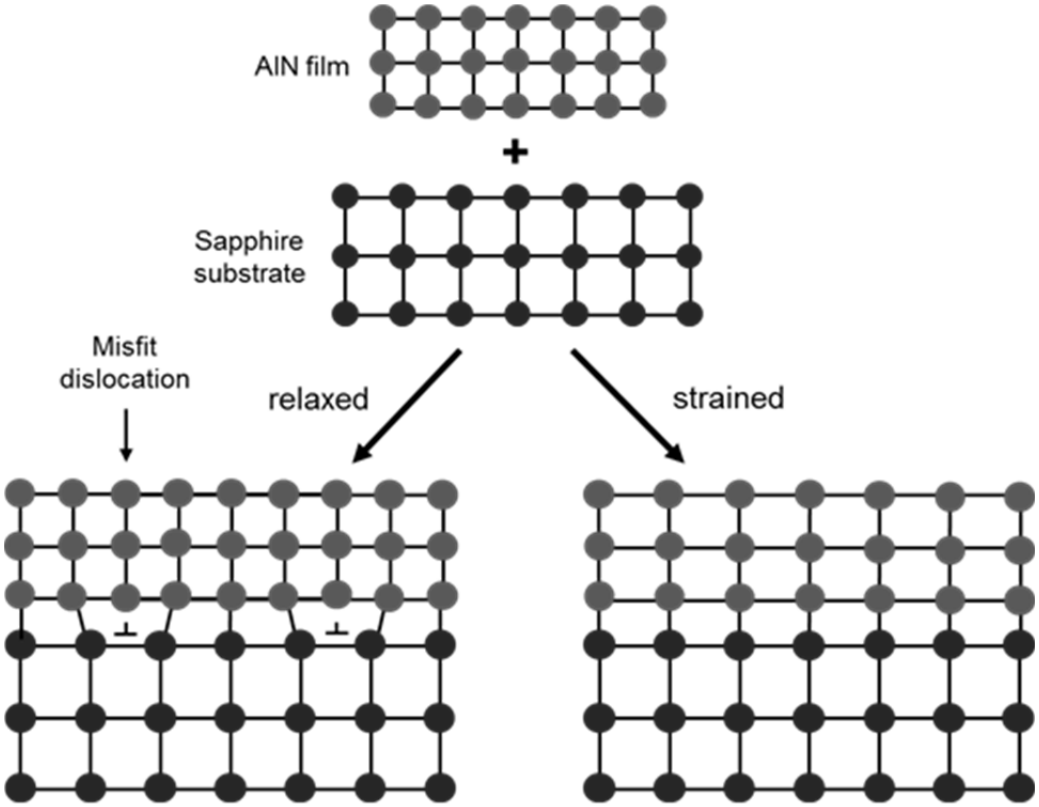

Figure 1.4: Formation of dislocations and strain during heteroepitaxial growth.

Consequently, the performance of nitride-based UV LEDs is limited, as mentioned above. To circumvent those problems, AlN bulk crystals for homoepitaxy are expected.

1.2 Growth Methods of AlN Bulk Crystals

Figure 1.5 shows the development of AlN-related crystal growth methods. AlN was initially synthesized in 1862 by heating Al fillings under a N_2 atmosphere [24]. In 1960, the first AlN single crystals were fabricated with this direct nitridation method by K. M. Taylor and C. Lenie [31]. The synthesis reaction of Al and N_2 was performed at high temperatures ranging from 1800 to 2000°C. AlN crystals prepared in their work were in the forms of thin plate with a diameter of 2 – 3 mm or six-sided prismatic needles with a diameter of up to 0.5 mm and a length of 30 mm. However, this method had no significant progress in the subsequent decades

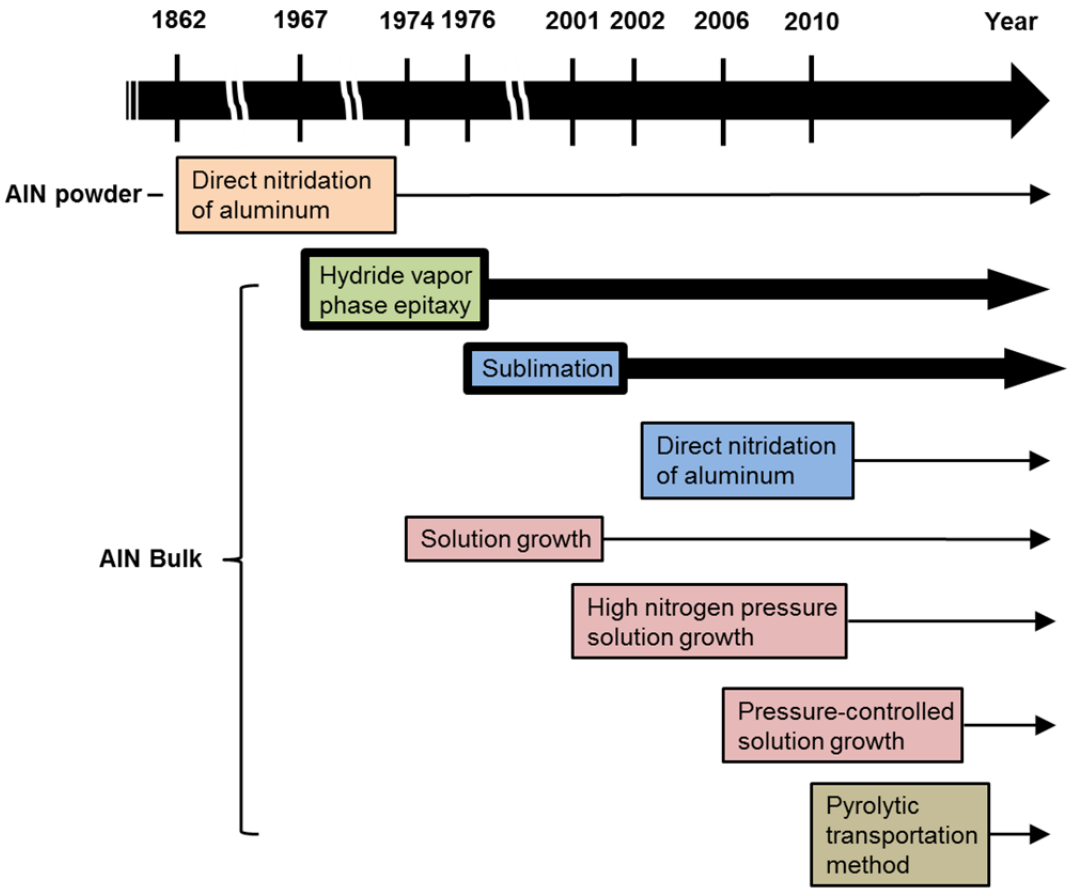

Figure 1.5: Significant achievements in AlN bulk crystal growth.

until 2002, when R. Schlesser and Z. Sitar achieved AlN c-plates with a size up to 10×5 mm^2 surface area by spontaneous nucleation at 2100ºC for 2 hours [32]. The growth rates were up to 5 mm/h in the (0001) plane and 0.2 mm/h along the [0001] c-axis. However, this attempt was not suitable for long-term growth because an AlN crust covers the Al metal source and gradually decreases the Al vapor. Thus, although AlN crystal was first synthesized by this method, to date, it was mainly developed for the sintering of AlN polycrystalline ceramics and whiskers.

The AlN crystal bullets were first obtained by G. A. Slack and T. F. McNelly in 1976 with sublimation (or Physical vapor transport, PVT) method [33,34]. After that, many crystal growth methods have been developed for bulk AlN single crystals in the past several decades (Fig. 1.5). The major approaches are:

- Sublimation (or PVT) method,
- Hydride vapor phase epitaxy (HVPE),
- Solution growth.

The details of those methods are explained in the following.

1.2.1 Sublimation Method

Sublimation method is the most common technology of bulk AlN crystal growth. For sublimation growth, AlN powder source is sublimed at a high temperature in a N_2 atmosphere [35-53]. A schematic of a reactor is shown in Fig. 1.6.

AlN powder source is contained at the bottom of a crucible, and decomposes to gaseous Al and N_2 at an elevated temperature. Owing to the thermal gradient, the vapors transport to the top of the crucible where a lower temperature promotes the re-crystallization of AlN. The whole process follows the reaction:

$$AlN_{(s)} = Al_{(g)}+N_{2(g)}.$$

Since AIN powders usually begin to sublimate at temperatures over 1800ºC, the

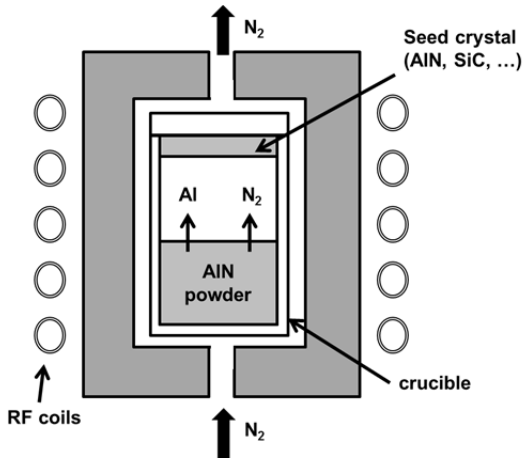

Figure 1.6: Schematic of a sublimation growth furnace for AlN crystals.

sublimation growth requires high process temperatures in a range of 1800 – 2300ºC. Consequently, seed crystals for the AlN sublimation growth are AlN or SiC, which possess melting points higher than 2600ºC. (When seeds or substrates are not used, whisker-type AlN can spontaneously form on the crucible wall.) However, at such extreme temperatures, along with the chemically aggressive nature of Al vapor, the crucible and related heat insulation materials may be unstable and react with the source materials. Accordingly, impurities from the materials of growth furnace limit the purity and optical properties of bulk AlN crystals grown by the sublimation method [55]. Furthermore, the commercially available AlN powder (purity: at most 5N) contains high concentrations of impurities, such as oxygen, silicon, carbon, and hydroxides. To overcome these problems is a big challenge.

1.2.2 Hydride Vapor Phase Epitaxy

In the HVPE process, AlN is formed via a chemical reaction between aluminum chloride gas and NH_3. The first fabrication of AlN crystal by HVPE was reported in 1967 by I. Akasaki et al. [55]. Recently, a colorless and transparent AlN thick layer with a growth rate of 25 μm/hr was achieved [25]. Similar to the sublimation method, HVPE is considered as a prospective technology for the bulk AlN crystal growth and has been developed rapidly in recent years [56-72].

A schematic of the HVPE reactor is shown in Fig. 1.7. Commonly, HVPE reactors for III-nitrides (GaN, AlN or InN) consist of (at least) two zones: a source zone for generating chloride gas of group III metal and a growth zone where the III-chloride gas reacts with NH_3 to yield nitride crystals. In the source zone, the group III source metal is volatilized at a certain temperature and reacts with the HCl vapor to generate III-Cl_3, III-Cl_2, and III-Cl. It should be noted that the source zone temperature determines the dominant III-chloride [59,73].

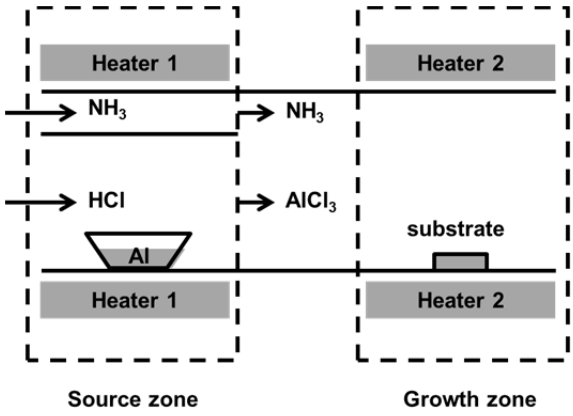

Figure 1.7: Schematic of the AlN HVPE system.

HVPE is currently more matured for the GaN growth, where GaCl is the main reactant. Since the GaN HVPE process possesses a high growth rate up to 1000 μm/hr, AlN crystal growth using this method is expected. Generally, HVPE is carried out in a hot-wall quartz (SiO_2) reactor. In the case of GaN HVPE, the reactivity of Ga-chloride, including the main reactant gas of GaCl, is moderate against quartz. However, Al-chloride gas species are very corrosive. Hot AlCl reacts violently with quartz, and eventually destroys the reactor. Therefore, AlN bulk growth with HVPE was very difficult. In order to overcome this problem, the use of $AlCl_3$ was initially demonstrated experimentally [59], and then the thermodynamic behavior of Al-chloride gases involved in HVPE was computed by Y. Kumagai [65, 73].

Figure 1.8(a) shows the calculation results. From the results, the main gaseous species in the source zone at low temperatures is $AlCl_3$ and that at high temperatures above 790ºC is AlCl. Because the reactivity order of Al-Cl compounds is $AlCl > AlCl_2 > (AlCl_3)_2 > AlCl_3$, the temperature of the source zone should be around 500ºC to generate $AlCl_3$ and to reduce the damages for the reactor.

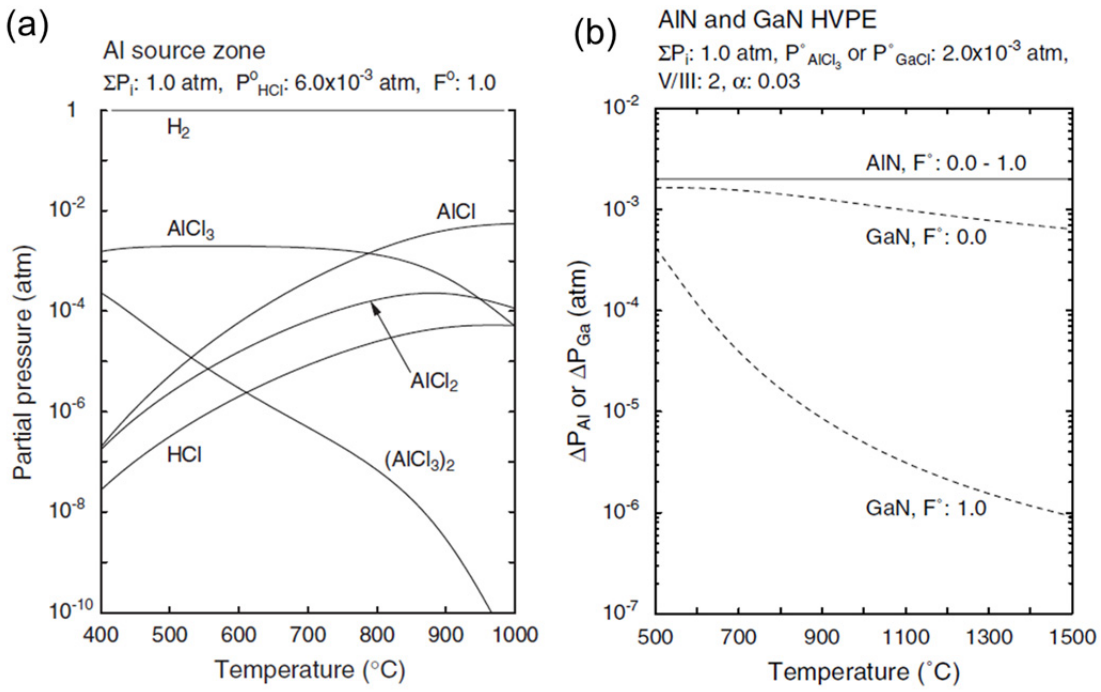

Figure 1.8: (a) Equilibrium partial pressures of gaseous species in the source zone as functions of source zone temperature [73]. (b) Dependence of the driving force for the HVPE of AlN using $AlCl_3$ and that of GaN using GaCl [65].

On the other hand, in the growth zone, the major chemical reaction is:

$$AlCl_{3(g)}+NH_{3(g)} = AlN_{(s)}+3HCl_{(g)}+H_{2(g)}$$

The driving force is defined as the difference between input and output equilibrium partial pressures of molecules of interest. For AlN growth, the driving force $\Delta P^0_{AlCl_3}$ is described as $\Delta P^0_{AlCl_3} = P^0_{AlCl_3} - \left[P_{AlCl_3} + P_{AlCl_2} + P_{AlCl} + 2P_{(AlCl_3)_2}\right]$, where P is a partial pressure of a subscript gas and P^0 is the input partial pressure. The driving force is almost equal to $P^0_{AlCl_3}$ in the temperature range of $500 - 1500$ºC as shown in Fig. 1.8(b). It means that a high growth rate of AlN is expected even at high growth temperatures regardless of the carrier gas. Note that variable F is the ratio of the number of hydrogen atoms to the number of hydrogen plus inert gas (IG) atoms in the reactor [65].

However, the growth process with HVPE involves HCl, a well-known strong mineral acid. Furthermore, the by-products and excess reactants in this method are highly corrosive. Therefore, the removal of these waste gases is a thorny problem.

1.2.3 Solution Growth

Figure 1.9 shows a schematic of the apparatus for the solution growth method. A seed is mounted on a shaft. Then, the shaft with the seed is dipped into a solution containing Al- and N-sources at a high N_2 pressure, and AlN is expected to crystallize from the solution onto the seed. Because the solution growth takes place under nearly the thermal equilibrium condition, the defect density can be reduced drastically. In 1974, the growth of AlN crystals from solution was performed using Ca_3N_2 flux by Dugger [74]. In 2000, Na flux was applied for AlN bulk crystal growth by Yano et al. [75]. In the case of using molten Ca_3N_2 flux, Ca_3N_2 is the N-source, and Al powders are chosen as the Al-source. The chemical reaction is considered as:

$$Ca_3N_{2(l)}+2Al = 2AlN_{(s)}+3Ca_{(s)}.$$

The melting point of Ca_3N_2 is 1195°C. Therefore, the growth temperature of AlN crystals in

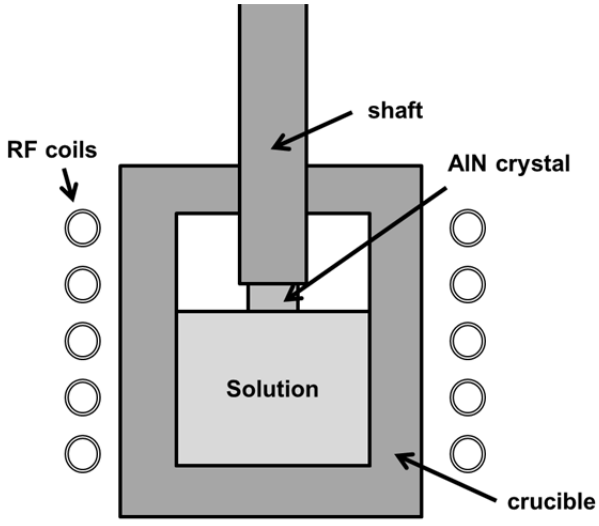

Figure 1.9: Schematic of a growth apparatus of the solution growth method.

this case is around 1200ºC. Note that the lowest growth temperature is determined by the melting point of solvents. Other prospective solvents include Li_3N [76, 77], NaN_3 [78], Mg_3N_2 [79], Be_3N_2 [80], and so on. Especially, since Li_3N has the melting point (813ºC) lower than the typical AlN growth temperature and high probability of N transfer, it is considered as a promising solvent. Besides, certain metal solvents, such as Sn-Ca-Al flux [81], Cu-Al [82] and Ga-Al flux [83] were also reported.

In comparison with sublimation and HVPE, the solution growth is the least developed. So far, although the colorless A1N single crystals with a growth rate of 10 μm/hr have been achieved via the solution method, the growth rate is still insufficient for bulk crystal growth. Further improvements are needed.

1.2.4 Another Emerging Method

Recently, another growth method for bulk AlN crystals has been proposed. That is pyrolytic transportation method (or carbon-thermal reduction method). Pyrolytic transportation method is based on the phase stability diagram of the Al_2O_3–AlN–C–N_2–CO system [84, 85].

This method was first developed by O. Serpek in 1905. Initially, it was proposed for synthesizing AlN powders [86]. However, the reaction mechanism was taken little notices until 1973. At that time, T. Sakai and M. Iwata produced AlN powders from mixtures of Al_2O_3 and C under a N_2 atmosphere at 1800ºC [87]. They found the direct solid state reaction of Al_2O_3–AlN–C to occur (where CO was added to promote the reduction reaction). After that, the phase diagram of the Al_2O_3–AlN–C system was calculated by several research groups, and finally a single crystal AlN thin film was achieved via this method by H. Fukuyama et al. in 2006 [88]. Subsequently, 48 mm long stick-like AlN crystals were obtained with a growth rate of 1.6 mm/hr in this method [89].

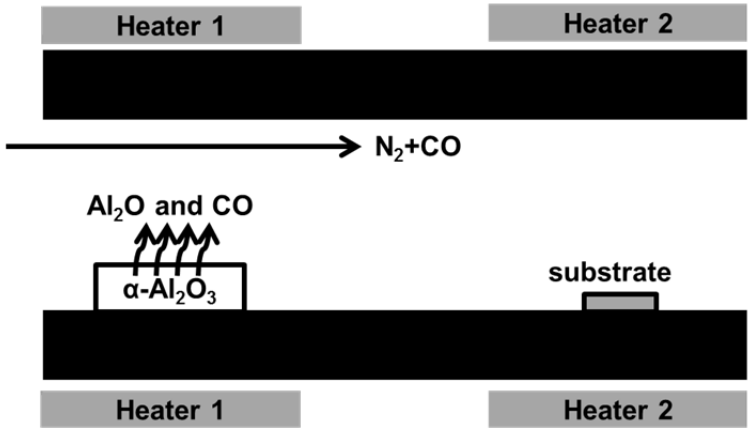

Figure 1.10: Schematic of experimental apparatus for pyrolytic transportation method.

A horizontal graphite furnace and a two-zone reactor are used in Ref. [89], as shown in Fig. 1.10. α-Al_2O_3 powders as the Al-source are placed in the source zone and are heated at 1950°C to generate Al_2O gas via a reducing reaction with graphite. Then, Al_2O gas is transported to the growth zone and reacts with N_2 gas under a N_2 atmosphere at 1750°C. The chemical reaction equations are as following:

$$Al_2O_{3(s)}+2C_{(s)} = Al_2O_{(g)}+CO_{(g)},$$

$$Al_2O_{(g)}+N_{2(g)}+CO_{(g)} = 2AlN_{(s)}+CO_{2(g)}.$$

The obtained high growth rate suggests that this growth method is promising. However, since C and CO are two of the main reactant materials, large quantities of C impurities exist in the AlN crystals grown with this method. Besides, CO_2, which is a byproduct of the growth process, is a significant greenhouse gas and a major source of ocean acidification. That is, C and CO are the keys to fabricating AlN bulk crystals with a high growth rate, but also cause some critical problems.

Table 1.2: Comparison of the common AlN bulk crystal growth methods.

	Sublimation	HVPE	Pyrolytic transportation
Raw materials	AlN, N_2(g)	Al, HCl(g), H_2(g), NH_3(g)	α-Al_2O_3 powder, N_2(g)
Growth Temp. (°C)	~2000	<1500	~1750
Growth rate (μm/hr)	>500	25[25]	>1000
Impurities	More than HVPE (From AlN powder and crucible materials)	O, H, Si, Cl…	O, C…
Dislocation Density (cm^{-2})	10^2~10^3 [25] (AlN seed growth)	>10^7 [66,71] (sapphire/SiC)	>sublimation
Transmittance at 220–300nm (%) (with ~100 μm thickness)	~18%[25]	~63%[25]	

1.3 Research Purpose and Motivation

As introduced in the previous sections, in order to improve the performance of nitride-based UV LEDs, AlN bulk crystals for homoepitaxy are expected. However, the current common technologies for AlN bulk crystals are still in development and have some critical restrictions as summarized in Tab. 1.2., where the solution growth is excluded because of its low growth rate. Therefore, in order to break through the restrictions, the main purpose of this thesis is to propose and develop a new approach for AlN bulk crystal growth. One of the most remarkable features is to use only element Al and N_2 gas as source materials. Although the growth principle of our method is the same as that of the direct nitridation method mentioned in Sec. 1.2, we demonstrate that a specially designed and developed growth machine can avoid the Al crust problem. Another important issue is a choice of the seed crystal (*i.e.* substrate). In this study, we select sapphire because it is cost effective and

abundant. Therefore, our proposed method may offer a more cost-effective and environmentally-friendly route to grow AlN crystals, compared with the previous methods. In the last of this thesis, single-phase, thick AlN films are successfully obtained with a reasonable growth rate after the optimization of the growth conditions. The achievements clearly indicate that the proposed growth process is quite promising for AlN bulk crystal growth.

1.4 Thesis Outline

This thesis consists of five chapters. In Chap. 1, the introductions including the history of LEDs, the challenges of AlN-based UV-LEDs, the existent growth technologies for AlN bulk crystals, and the research motivation have been presented.

In Chap. 2, the growth method and the growth furnace proposed in this thesis are described. Compared with the previous reports of AlN crystal growth by direct nitridation method, the improvements in this work are also mentioned.

In Chap. 3, successful synthesis of AlN powders, whickers, and films by the proposed method is experimentally demonstrated. Then the key factors that determine AlN crystal morphologies are discussed through adjusting the growth conditions. In addition, the optical properties of these AlN crystals are described.

In Chap. 4, first, the self-separation phenomenon of AlN from sapphire is discussed. It is demonstrated that this phenomenon effectively prevents cracks from being induced in AlN on sapphire. Then, toward the bulk AlN growth, the effects of the growth conditions such as V/III ratio, substrate pretreatment, and substrate species on the growth behavior are discussed.

According to the obtained experiments results, the conclusions and future works are presented in Chap. 5.

References

[1] H. J. Round, Electrical World, 49, 309 (1907).

[2] O. V. Lossev, Philosophical Magazine, Series 7, 6, 1024 (1928).

[3] E. E. Violin, A. A. Kalnin, V. V. Pasynkov, Y. M. Tairov, D. A. Yaskov, Silicon Carbide 1968, Pergamon Press, 231 (1969).

[4] J. A. Edmond, H. S. King, C. H. Carter, Physica B, 185, 453 (1993).

[5] J. R. Biard, G. Pittman, US Patent 3293513 (1962).

[6] I. Akasaki, H. Amano, Y. Koide, K. Hiramatsu, N. Sawaki, J. Cryst. Growth 98, 209 (1989).

[7] H. Amano, M. Kito, K. Hiramatsu, I. Akasaki, Jpn. J. Appl. Phys. 28, L2112 (1989).

[8] S. Nakamura, T. Mukai, M. Senoh, Appl. Phys. Lett. 64, 1687 (1994).

[9] H. Morkoc, Handbook of Nitride Semiconductors and Devices, Vol. 3: GaN-based Optical and Electronic Devices (2009).

[10] J. I. Pankove, T. D. Moustakas, Gallium nitride II: Semiconductors and Semimetals, Vol. 57 (1999).

[11] J. Han, M. H. Crawford, R. J. Shul, J. J. Figiel, M. Banas, L. Zhang, Y. K. Song, H. Zhou, A. V. Nurmikko, Appl. Phys. Lett. 73, 1688 (1998).

[12] T. Nishida, N. Kobayashi, Phys. Status Solidi A 176, 45 (1999).

[13] Y. Taniyasu, M. Kasu, T. Makimoto, Nature 441, 325 (2006).

[14] A. Khan, K. Balakrishnan, T. Katona, Nat. Photonics 2, 77 (2008).

[15] H. Hirayama, S. Fujikawa, N. Noguchi, J. Norimatsu, T. Takano, K. Tsubaki, N. Kamata, Phys. Status Solidi A 206, 1176 (2009).

[16] H. Hirayama, Y. Tsukada, T. Maeda, N. Kamata, Appl. Phys. Express 3, 031002 (2010).

[17] C. Pernot, M. Kim, S. Fukahori, T. Inazu, T. Fujita, Y. Nagasawa, A. Hirano, M. Ippommatsu, M. Iwaya, S. Kamiyama, I. Akasaki, H. Amano , Appl. Phys. Express 3, 061004 (2010).

[18] J. R. Grandusky, S. R. Gibb, M. C. Mendrick, L. J. Schowalter, Appl.Phys. Express 3, 072103 (2010).

[19] J. R. Grandusky, S. R. Gibb, M. C. Mendrick, C. Moe M. Wraback and L. J. Schowalter, Appl. Phys. Express 4, 082101 (2011).

[20] M. Shatalov, W. Sun, A. Lunev, X. Hu, A. Dobrinsky, Y. Bilenko, J. Yang, Appl. Phys. Express 5, 082101 (2012).

[21] T. Mino, H. Hirayama, T. Takano, N. Noguchi, K. Tsubaki, Phys. Status Solidi C 9, 749 (2012).

[22] T. Kinoshita, T. Obata, T. Nagashima, H. Yanagi, B. Moody, S. Mita, S. Inoue, Y. Kumagai, A. Koukitu, Z. Sitar, Appl. Phys. Express 6, 092103 (2013).

[23] J. R. Grandusky, J. Chen, S. R. Gibb, M. C. Mendrick, C. G. Moe, L. Rodak, G. A. Garrett, M. Wraback, L. J. Schowalter, Appl. Phys. Express 6, 032101 (2013).

[24] F. Briegleb, A. Geuther, Ann. Chem, 123, 228 (1862).

[25] Y. Kumagai, Y. Kubota, T. Nagashima, T. Kinoshita, R. Dalmau, R. Schlesser, B. Moody, J. Xie, H. Murakami, A. Koukitu, Z. Sitar, Appl. Phys. Express 5, 055504 (2012).

[26] W. M. Yim, R. J. Paff, J. Appl. Phys. 45 1456 (1974).

[27] C. Roder, S. Einfeldt, S. Figge, D. Hommel, Phys. Rev. B 72, 085218 (2005).

[28] E. R. Dobrovinskaya, L. A. Lytvynov, V. Pishchik, Sapphire: Material, Manufacturing, Applications, 109 (2009).

[29] Z. Li, R.C. Bradt, J. Am. Ceram. Soc. 69, 863 (1986).

[30] Y. Okada, Y. Tokumaru, J. Appl. Phys. 56, 314 (1984).

[31] K. M. Taylor, C. Lenie , J. Electrochem. Soc. 107, 308 (1960).

[32] R. Schlesser, Z. Sitar, J. Crystal Growth 234, 349 (2002).

[33] G.A. Slack, T.F. McNelly, J. Crystal Growth 34, 263 (1976).

[34] G.A. Slack, T.F. McNelly, J. Crystal Growth 42, 560 (1977).

[35] C.M. Balkas, Z. Sitar, T. Zheleva, L. Bergman, R. Nemanich, R.F. Davis, J. Crystal Growth 179, 363 (1997).

[36] R. Schlesser, R. Dalman, Z. Sitar, J. Crystal Growth 241, 416 (2002).

[37] J.H. Edgar, L. Liu, B. Liu, D Zhuang, J Chaudhuri, M Kuball, S Rajasingam, J. Crystal Growth 246, 187 (2002).

[38] B. Raghothamachar, M. Dudley, J.C. Rojo, K. Morgan, L.J. Schowalter , J. Crystal Growth 250, 244 (2003).

[39] S.Yu. Karpov, A.V. Kulik, I.N. Przhevalskii, M. Ramm, Y. Makarov, Phys. Status Solidi C 0, 1989 (2003).

[40] E.N. Mokhov, O.V. Avdeev, I.S. Barash, T.Yu. Chemekova, A.D. Roenkov, A.S. Segal, A.A. Wolfson, Yu.N. Makarov, M.G. Ramm, H. Helava, J. Crystal Growth 281, 93 (2005).

[41] B.M. Epelbaum, M. Bickermann, A. Winnacker, J. Crystal Growth 275, e479 (2005).

[42] D. Zhuang, Z.G. Herro, R. Schlesser, Z. Sitar, J. Crystal Growth 287, 349 (2006).

[43] Yu.N. Makarov, O.V. Avdeev, I.S. Barash, D.S. Bazarevskiy, T.Yu. Chemekova, E.N. Mokhov, S.S. Nagalyuk, A.D. Roenkov, A.S. Segal, Yu.A. Vodakov, M.G. Ramm, S. Davis, G. Huminic, H. Helava, J. Crystal Growth, 310, 881 (2008).

[44] C. Hartmann, J. Wollweber, C. Seitz, M. Albrecht, R. Fornari, J. Crystal Growth, 310, 930 (2008).

[45] B.M. Epelbaum, M. Bickermann, S. Nagata, P. Heimann, O. Filip, A. Winnacker, J. Crystal Growth 305, 317 (2007).

[46] M. Miyanaga, N. Mizuhara, S. Fujiwara, M. Shimazu, H. Nakahata, T. Kawase, J. Crystal Growth 300, 45 (2007).

[47] M. Bickermann, B.M. Epelbaum, O. Filip, P. Heimann, S. Nagata, A. Winnacker, Phys. Status Solidi C 5, 1502 (2008).

[48] H. Kamata, K. Naoe, K. Sanada, N. Ichinose, J. Crystal Growth 311, 1291 (2009).

[49] I. Nagai, T. Kato, T. Miura, H. Kamata, K. Naoe, K. Sanada, H. Okumura, J. Crystal Growth 312, 2699 (2010).

[50] L. Liu, J.H. Edgar, J. Crystal Growth 220, 243 (2000).

[51] A.S Segal, S.Yu Karpov, Yu.N. Makarov, E.N. Mokhov, A.D. Roenkov, M.G. Ramm, Yu.A. Vodakov, J. Crystal Growth 211, 68 (2000).

[52] B. Wu, R. Ma, H. Zhang, M. Dudley, R. Schlesser, Z. Sitar, J. Crystal Growth 253, 326 (2003).

[53] V. Noveski, R. Schlesser, S. Mahajan, S. Beaudoin, Z. Sitar, J. Crystal Growth 264, 369 (2004).

[54] G. A. Slack, J. Whitlock, K. Morgan, L.J. Schowalter, MRS Proc. 798, 293 (2003).

[55] I. Akasaki, M. Hashimoto, Solid State Commun. 5, 851 (1967).

[56] Yu. Melnik, D. Tsvetkov, A. Pechnikov, I. Nikitina, N. Kuznetsov, V. Dmitriev, Phys. Status Solidi A 188, 463 (2001).

[57] D. Tsvetkov, Yu. Melnik, A. Davidov, A. Shapiro, O. Kovalenkov, J.B. Lam, J.J. Song, V. Dmitriev, Phys. Status Solidi A 188, 429 (2001).

[58] O.Y. Ledyaev, A.E. Cherenkov, A.E. Nikolaev, I.P. Nikitina, N.I. Kuznetsov, M.S. Dunaevski, A.N. Titkov, V.A. Dmitriev, Phys. Status Solidi C 0, 474 (2002).

[59] Yu. Melnik, V. Soukhoveev, V. Ivantsov, V. Sizov, A. Pechnikov, K. Tsvetkov, O. Kovalenkov, V. Dmitriev, A. Nikolaev, N. Kuznetsov, E. Silveira, J. Freitas Jr., Phys. Status Solidi A 200, 22 (2003).

[60] D.F. Bliss, V.L. Tassev, D. Weyburne, J.S. Bailey, J. Crystal Growth 250, 1 (2003).

[61] Y. Kumagai, T. Yamane, A. Koukitu, J. Crystal Growth 281, 62 (2005).

[62] T. Yamane, H. Murakami, Y. Kangawa, Y. Kumagai, A. Koukitu, Phys. Status Solidi C 2, 2062 (2005).

[63] O. Kovalenkov, V. Soukhoveev, V. Ivantsov, A. Usikov, V. Dmitriev, J. Cryst. Growth 281, 87 (2005).

[64] D. S. Kamber, Y. Wu, B. A. Haskell, S. Newman, S.P. DenBaars, J.S. Speck, S. Nakamura, J. Cryst. Growth 297, 321 (2006).

[65] Y. Kumagai, K. Takemoto, J. Kikuchi, T. Hasegawa, H. Murakami, A. Koukitu, Phys. Stat. Solidi B 243, 1431 (2006).

[66] V. Soukhoveev, O. Kovalenkov, V. Ivantsov, A. Syrkin, A. Usikov, V. Maslennikov, V. Dmitriev, Phys. Status Solidi C 3, 1653 (2006).

[67] T. Nagashima, M. Harada, H. Yanagi, Y. Kumagai, A. Koukitu, K. Takada , J. Crystal Growth 300, 42 (2007).

[68] K. Tsujisawa, S. Kishino, Y.H. Liu, H. Miyake, K. Hiramatsu, T. Shibata, M. Tanaka, Phys. Status Solidi C 4, 2252 (2007).

[69] Y. Kumagai, T. Nagashima, A. Koukitu, Jpn. J. Appl. Phys. 46, L389 (2007).

[70] Y. Kumagai, J. Tajima, M. Ishizuki, T. Nagashima, H. Murakami, K. Takada, A. Koukitu, Appl. Phys. Express 1, 045003 (2008).

[71] Y. Kumagai, Y. Enatsu, M. Ishizuki, Y. Kubota, J. Tajima, T. Nagashima, H. Murakami, K. Takada, A. Koukitu, J. Crystal Growth 312, 2530 (2010).

[72] T. Nomura, K. Okumura, H. Miyake, K. Hiramatsu, O. Eryu, Y. Yamada, J. Crystal Growth 350, 69 (2012).

[73] Y. Kumagai, T. Yamane, T. Miyaji, H. Murakami, Y. Kangawa, A. Koukitu, Phys. Status Solidi C 0, 2498 (2003).

[74] C.O. Dugger, Mater. Res. Bull. 9, 331 (1974).

[75] M. Yano, M. Okamoto, Y.K. Yap, M. Yoshimura, Y. Mori, T. Sasaki, Diam. Relat. Mater. 9, 512 (2000).

[76] Y. Kangawa, T. Wakigawa, K. Kakimoto, Jpn. J. Appl. Phys. 46, 5785 (2007).

[77] Y. Kangawa, R. Toki, T. Yayama, B. M. Epelbaum, K. Kakimoto, Appl. Phys. Express 4, 095501, (2011).

[78] L. Li, X. Hao, N. Yu, D. Cui, X. Xu and M. Jiang, J. Crystal Growth 258, 268 (2003).

[79] H.Z. Ye, X.Y. Liu, B. Luan, Mater. Lett. 58, 2361 (2004).

[80] H. Jacobs, D. Schmidt, Curr. Top. Mater. Sci. 8, 387 (1982).

[81] H. Isobe, F. Kawamura, M. Kawahara, M. Yoshimura, Y. Mori, T. Sasaki, Jpn. J.Appl. Phys. 44, L488 (2005).

[82] K. Kamei, Y. Shirai, T. Tanaka, N. Okada, A.Yauchil, H. Amano, Phys. Status Solidi C 4, 2211 (2007).

[83] M. Adachi, K. Maeda, A. Tanaka, H. Kobatake, H. Fukuyama, Phys. Status Solidi A 208, 1494 (2011).

[84] P. Lefort, M. Billy, J. Am. Ceram. Soc. 76, 2295 (1993).

[85] W. Nakao, H. Fukuyama, K. Nagata, J. Am. Ceram. Soc. 85, 889 (2002).

[86] O. Serpek, Brit. Pat. No. 13579 (1906).

[87] T. Sakai, M. Iwata, Nippon Kagaku Kaishi 10, 1869 (1973).

[88] H. Fukuyama, S. Kusunoki, J. Appl. Phys. 100, 024905 (2006).

[89] K. Hironaka, T. Nagashima, S. Ikeda, M. Azuma, K. Takada, H. Fukuyama, J. Crystal Growth 312, 2527 (2010).

[90] B. Raghothamachar, R. Dalmau, B. Moody, S. Craft, R. Schlesser, J. Xie, R. Collazo, M. Dudley, Z. Sitar, Mater Sci Forum 717, 1287 (2012).

[91] V. Soukhoveev, O. Kovalenkov, V. Ivantosov, A. Syrkin, A. Usikov, V. Maslennikov, V. Dmitriev, Phys. Status Solidi C 3, 1653 (2006).

Chapter 2 – Design and Construction of Growth Apparatus

2.1 Introduction

As mentioned in Chap. 1, the current common growth methods of AlN bulk crystals have some restricts. Therefore, a new approach is proposed in this study. In Chap. 2, the basic concept of the growth approach in this thesis is described. Then, based on it, the growth apparatus is constructed.

2.2 Proposals of New Growth Methods

2.2.1 Direct Nitridation of Aluminum

The principal growth method in this study is based on direct nitridation of Al, which has so far been developed for the synthesis of AlN powder and whisker crystals [1-3]. The main advantage of this method over other common technologies of AlN crystal growth is that there is no side product in principle because the chemical reaction is extremely simple as:

$$Al_{(s,l,g)} + 1/2N_{2(g)} = AlN_{(s)}.$$

It is worth emphasizing that the source materials are just Al metal and N_2 gas, which are much safer and less polluting materials, compared with the source and ambient gases in the conventional methods. However, because N_2 gas is relatively non-reactive at typical growth temperatures and pressures due to its strong triple bond, it is generally believed that the growth of single crystal AlN from Al and N_2 requires excitation of the N_2 source in some way,

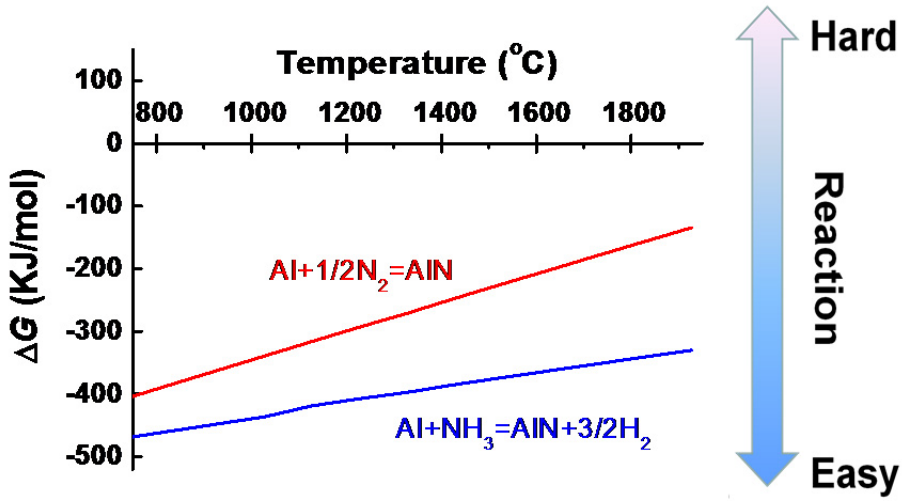

Figure 2.1: Estimations of the Gibbs free energy changes of the chemical reactions between Al and N_2, and between Al and NH_3. The pressure is 100 kPa.

as seen in sputtering deposition [4-6] and molecular beam epitaxy (MBE) [7-9]. A typical example is to use NH_3 instead of N_2. On the other hand, Al is a chemically reactive material.

To evaluate the possibility of the chemical reaction mentioned above to occur, the Gibbs free energy changes of $Al + 1/2N_2 = AlN$ and $Al + NH_3 = AlN + 3/2H_2$ are calculated. The standard Gibbs free energy change (ΔG) is a way to know the favor of the chemical reaction at a certain temperature and pressure. Briefly, $\Delta G < 0$ means that such a chemical reaction is favored. Figure 2.1 shows the calculated results at 100 kPa, where negative ΔG strongly suggests that the reaction between Al and N_2 may happen at a reasonable temperature, even though the value is higher than that of Al+ NH_3.

It is noteworthy that because the calculation assumes the atmospheric pressure, the growth does not require high vacuum, unlike MBE. However, simply applying the direct nitridation method to AlN bulk crystal growth causes some difficulties. The difficulties and our ideas to overcome them are described later in Secs. 2.3 and 2.4, respectively.

2.2.2 Thermite Method

Another method studied is based on a thermite reaction. The hint is from the pyrolytic transportation method which has been introduced in Chap. 1 (Sec. 1.2.4). The pyrolytic transportation method uses Al_2O_3 as a starting material, which is reduced to Al_2O gas with C. Then the Al_2O gas is transferred to the growth zone, and reacts with N_2 to produce AlN. The key point is to produce Al_2O gas in some way. (It is interesting to note that similarly, Ga_2O gas, which is generated through the reduction of Ga_2O_3 with H_2 [10] or oxidation of Ga with H_2O [11], is used for GaN growth.) Our idea to do that relies on the termite reaction.

Thermite is an antique refining method of Fe metal via a high exothermic reaction between Al and Fe_2O_3. This violent reaction is expressed as

$$Al + 1/6\ Fe_2O_3 = 1/2Al_2O + 1/3Fe.$$

This reaction reduces Fe_2O_3, and at the same time produces Al_2O and possibly related gases. These gases are expected to be Al precursors in AlN growth. Figure 2.2 shows the calculated Gibbs free energy changes for this reaction as well as the pyrolytic reaction of Al_2O_3 for comparison. Compared with the pyrolytic transportation method, thermite produces Al_2O related gases more easily.

The calculated results (Fig. 2.2) suggest that thermite method is applicable to AlN crystal growth, and to confirm this, we carried out preliminary experiments. Al [Fig. 2.3(a)] and Fe_2O_3 [Fig. 2.3(b)] powders were co-loaded, and N_2 gas was supplied at 1300°C. After the synthesis process, a mass of blackish powders were obtained as shown in Fig. 2.3(c).

Figure 2.4(a) shows X-ray diffraction (XRD) profiles. The upper is the simulated profile for polycrystalline AlN, while the lower is the experimental profile of the obtained powders. Nearly the same profiles indicate the successful fabrication of AlN by the proposed method. At the same time, however, additional peaks appear at around 42 – 45°, as shown in Fig.

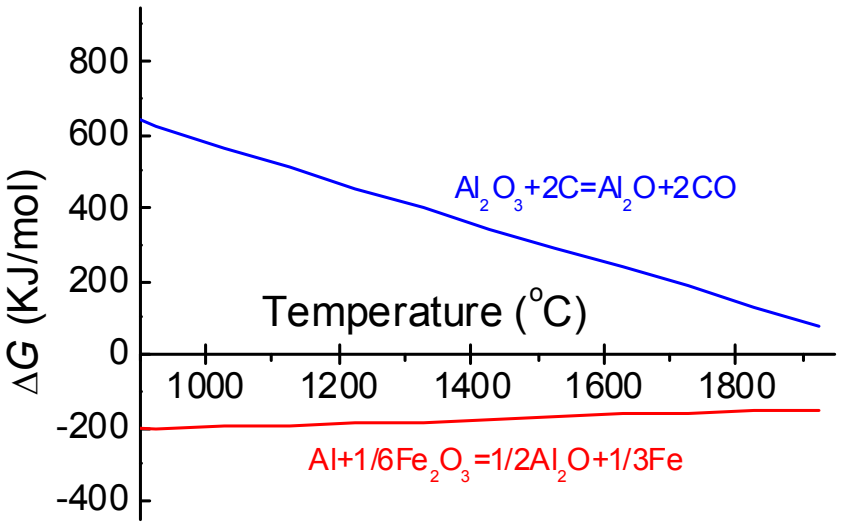

Figure 2.2: Gibbs free energy change calculations of the two reactions.

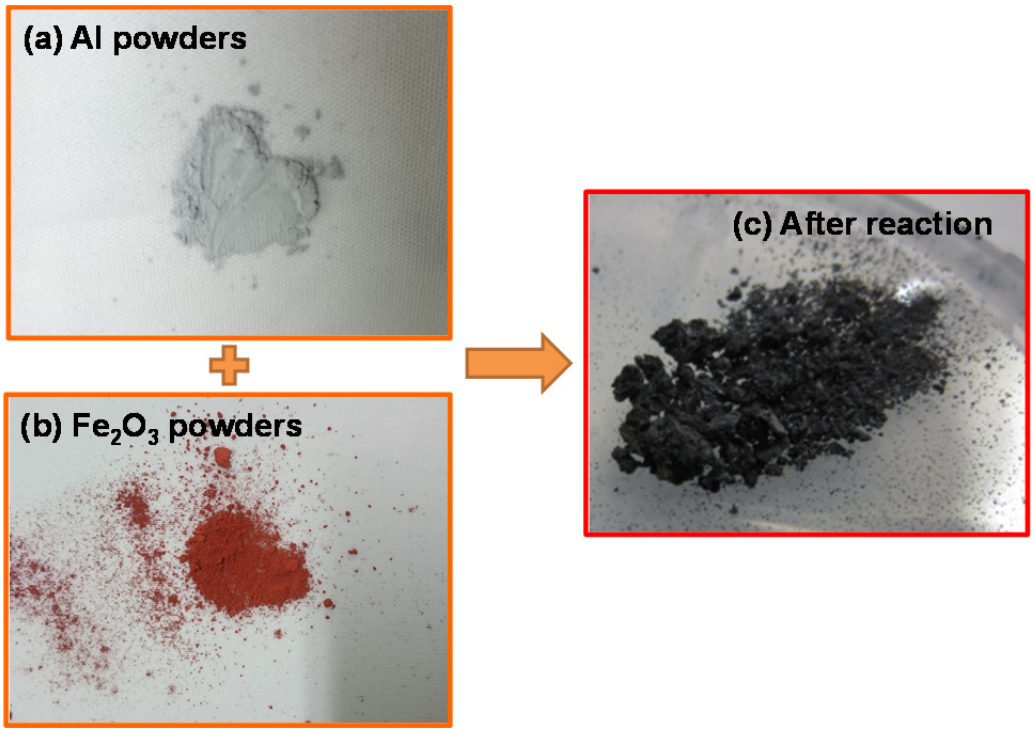

Figure 2.3: (a) Al powders, (b) Fe_2O_3 powders, and (c) powders after reaction.

2.4(b). Those peaks are attributed to Fe_3N, Fe, and Al_2O_3, which are by-products of the reaction. That is to say, Fe related impurities may be inevitable. Hence, we selected direct nitridation method to be the main growth method in this thesis.

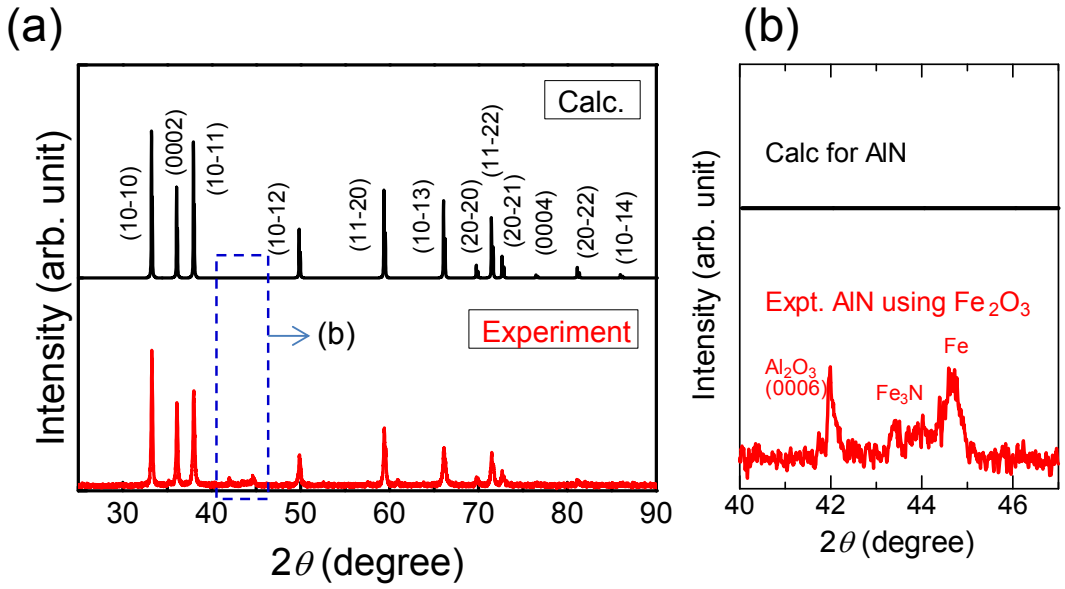

Figure 2.4: (a) XRD profile of AlN powders synthesized from Al and Fe_2O_3 (lower panel) and calculated AlN XRD profile (upper panel). (b) Magnified profiles in a 2θ range of 40 to 47°.

2.3 Difficulties in Single Crystal Growth with Direct Nitridation of Aluminum

As discussed with Fig. 2.1, the simple analysis based on the Gibbs free energy change indicated that the direct reaction between Al and N_2 is possible. However, it is difficult to apply the simple, direct reaction for AlN single crystal growth. To see the cause of it, let us review the previously reported AlN growth based on direct nitridation.

Figure 2.5 illustrates a schematic of a typical apparatus used to produce AlN sinters by direct nitridation [12]. Because the chemical reaction between Al and N2 gas proceeds spontaneously, N2 gas supplied onto the Al source generates AlN crust on the surface of the Al source. Consequently, the AlN crust covers the Al metal source and prevents the growth processes from proceeding. In addition, AlN powders grown by such growth methods are not always “pure” AlN powders, but occasionally AlN shell / Al core structures [13].

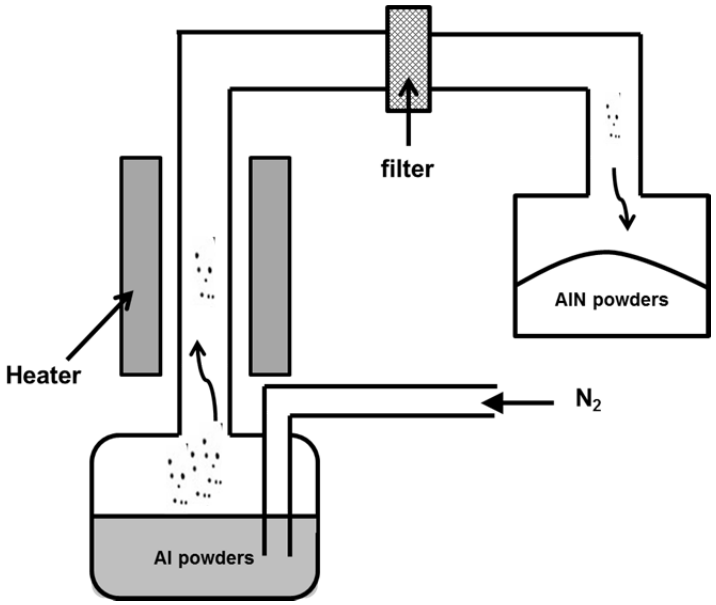

Figure 2.5: Schematic of the reactor for AlN powder sintering by direct nitridation method

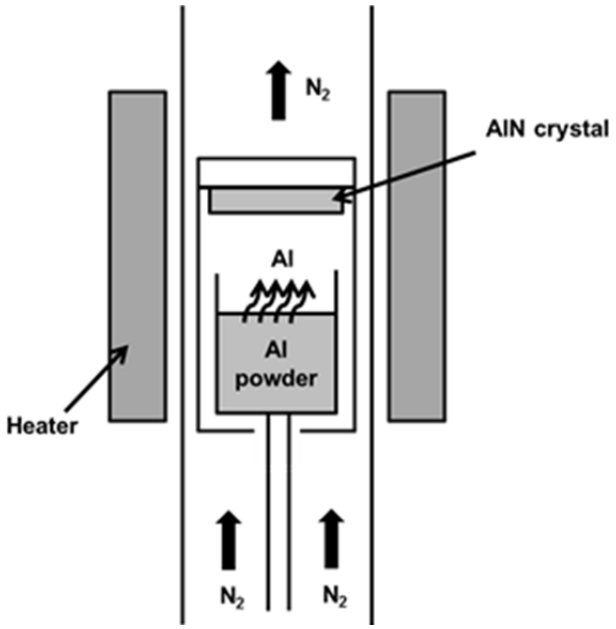

Figure 2.6: Schematic of the growth reactor of R. Schlesser and Z. Sitar [14].

In spite of the difficulty, in 2002, R.Schlesser and Z. Sitar demonstrated growth of bulky AlN crystals through direct nitridation [14]. However, they did not solve the AlN crust problem. The growth apparatus is schematically shown in Fig. 2.6. Al metal source was filled into the crucible mounted in a vertical tube. The vertical tube has an aperture (2 mm in diameters) to maintain equilibrium between the inside and outside N_2 pressure. That is, N_2 gas was supplied onto the Al metal source directly. Therefore, longer-term growth with this method was obstructed because of the formation of an AlN crust over the Al metal source [14, 15].

2.4 Development of a Novel Growth Method Based on Direct Nitridation

In order to overcome the aforementioned AlN crust problem and apply the direct nitridation method to bulk AlN growth, an original growth apparatus was designed and constructed in this study. Figure 2.7 shows a photograph and the schematic of the developed furnace. The horizontal reactor has two temperature zones. One is for Al source, and the other is for the growth. These zones can independently be operated at different temperatures. Furthermore, the source zone is divided into the upper and lower channels. An Ar carrier gas is introduced into the lower channel, where the Al vapor is produced by heating the zone. On the other hand, N_2 gas, which is a main reaction gas, is supplied into the upper channel in order to avoid premature reactions with the Al vapor before reaching the substrate. At last, those gases join together in the growth zone. In addition, depending on experiment purposes, either Ar or N_2 gas is supplied into the lower channel. With this growth apparatus, the Al vapor can be supplied continuously, and the processes of AlN crystal growth can proceed with a given growth rate.

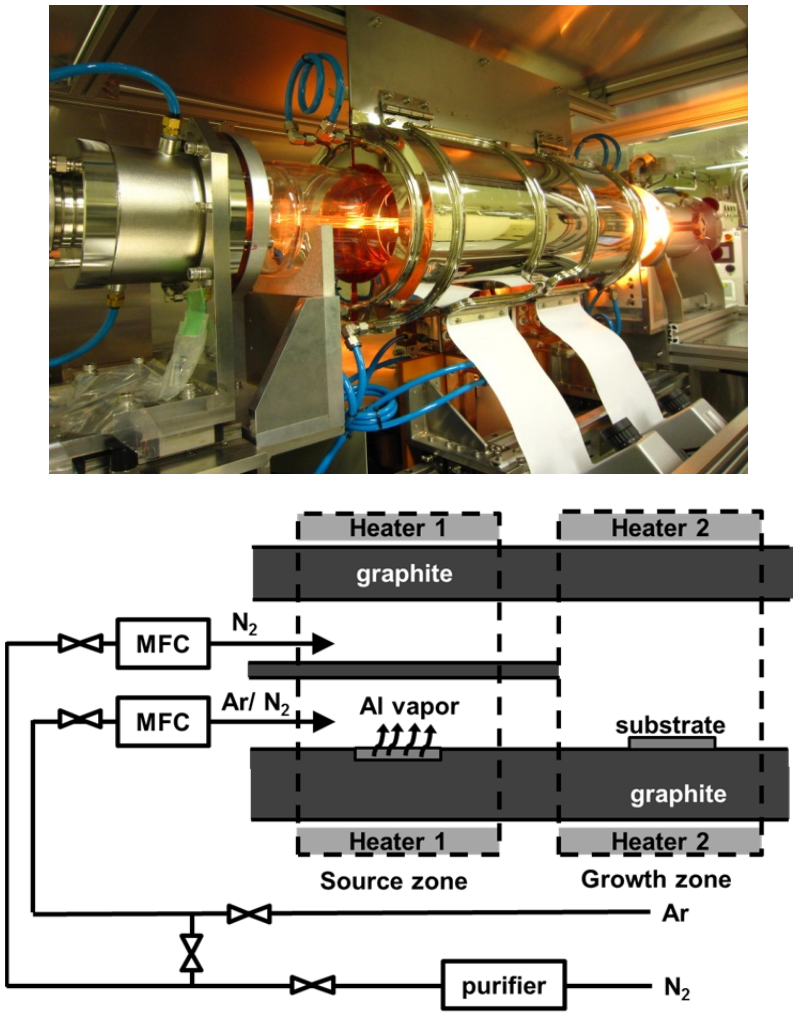

Figure 2.7: Photograph and schematic of the lab-made apparatus constructed in this thesis.

*MFC: mass flow controller

2.5 Control of Al Flow Rates

In comparison with the previous researches based on direct nitridation, a decisive difference of the proposed method is that N_2 gas is not supplied directly onto the Al source. Additionally, Al vapor is transported to the growth zone not through temperature gradient, but by Ar carrier gas. That is, the growth method in this study can be classified into vapor phase epitaxy. Hence, the control of the flow rate of Al vapor is an important point.

Firstly, the vapor pressure is strongly dependent on the nature of the substance and ambient

temperature. For Al, the vapor pressure P (mmHg) at a temperature T (K) can be estimated with [16]:

$$\log P = -16.45\times10^3/T + 12.36 - 1.023\log T.$$

Figure 2.8 shows the calculated Al vapor pressure as a function of temperature. The Al vapor pressure at 1300 and 1400°C are calculated to be 4.3×10^{-2} and 1.7×10^{-1} mmHg, respectively.

Secondary, the molar flow rate of Al at different temperature and pressure can be calculated from the ideal gas equation. For instance, with a source-zone temperature of 1400°C, an Ar flow rate of 1 SLM, and a reactor pressure of 10 kPa, an Al vapor pressure of 1.7×10^{-1} mmHg corresponds to an Al flow rate (n) of 100 μmol/min through the relationship of 1.7×10^{-1} mmHg × {(100 kPa/10 kPa) × (1673 K/273 K) × 1 SLM} = n/(mol/s) R × 1673 K, where R is the gas constant. Namely, with a reasonable flow rate of the Ar carrier gas, the Al flow rate can be comparable to those in metalorganic vapor phase epitaxy.

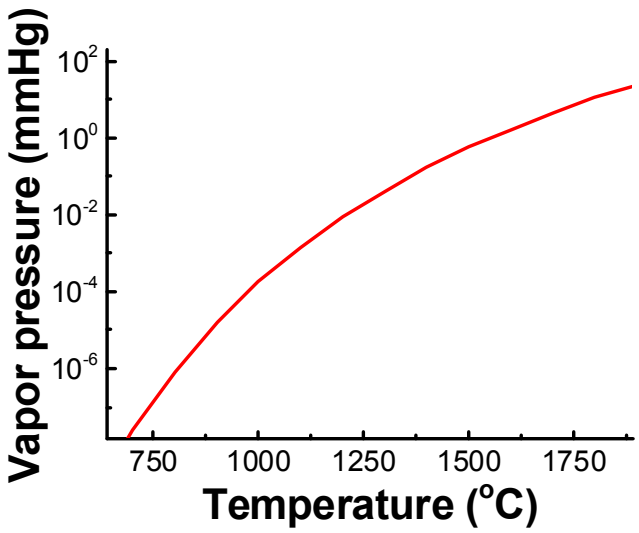

Figure 2.8: Estimation of Al vapor pressure as a function of temperature.

2.6 Summary

To avoid the restrictions in the common growth technologies of AlN bulk crystals, we proposed relatively simple two approaches. One is based on the thermite method. This method is to refine Fe from Fe_2O_3, during which Al_2O gas is produced. The Al_2O gas can be used as an Al precursor for AlN growth. In fact, preliminary experiments demonstrated successful syntheses of AlN powders, indicating potential use of this method for AlN growth. However, inclusion of Fe-related impurities was significant, so that we developed another approach. That approach is based on direct nitridation, where only Al metal and N_2 gas are used as source materials. A simple thermodynamic analysis suggested that the reaction of $Al+1/2N_2 = AlN$ is possible at a reasonable temperature. However, if N_2 gas is directly supplied onto Al powders, AlN is formed on the Al surface. Therefore, Al vapor and N_2 gas should separately be transferred onto the substrate surface. To do this, a suitable growth apparatus equipped with two flow cannels, each of which is for either Al vapor or N_2 gas, was designed and constructed.

References

[1] F. Briegleb, A. Geuther, Ann. Chem, 123, 228 (1862).

[2] K. M. Taylor, C. Lenie , J. Electrochem. Soc. 107, 308 (1960).

[3] R. Schlesser, Z. Sitar, J. Crystal Growth 234, 349 (2002).

[4] M.A. Auger, L. Vazquez, M. Jergel, O. Sanchez, J.M. Albella, Surf. and Coat. Tech. 180-181, 140 (2004).

[5] B. Mednikarov, G. Spasov, Tz. Babeva, J. Optoelectron Adv. Mater. 7, 1421 (2005).

[6] N. Matsunami, H. Kakiuchida, M. Sataka, S. Okayasu, Adv. Mater. Phys. Chem. 3, 101 (2013).

[7] S. Yoshida, S. Misawa, S. Gonda, J. Appl. Phys. 53, 6844 (1982).

[8] S. A. Nikishin, V. G. Antipov, S. Francoeur, N. N. Faleev, G. A. Seryogin, V. A. Elyukhin, H. Temkin, T. I. Prokofyeva, M. Holtz, A. Konkar, S. Zollner, Appl. Phys. Lett. 75, 484 (1999).

[9] V. G. Mansurov, A. Yu. Nikitin, Yu. G. Galitsyn, S. N. Svitashev, K. S. Zhuravlev, Z. Osvath, L. Dobos, Z. E. Horvath, B. Pecz, J. Cryst. Growth, 300, 145 (2007).

[10] M. Imade, H. Kishimoto, F. Kawamura, M. Yoshimura, Y. Kitaoka, T. Sasaki, Y. Mori, J. Crystal Growth 312, 676 (2010).

[11] T. Sumi, Y. Taniyama, H. Takatsu, M. Juta, A.Kitamoto, M. Imade, M. Yoshimura, M. Isemura, Y. Mori, Jpn. J. Appl. Phys. 54, 051001 (2015).

[12] G. Selvaduray, Mater. Sci. Technol. 9, 463 (1993).

[13] D. Zhang, F. Liu, L. Cai, X. Liu, Y. Li, J. Alloys Compd. 547, 91 (2013).

[14] R. Schlesser, Z. Sitar, J. Crystal Growth 234, 349 (2002).

[15] S.Y. Karpov, A.V. Kulik, M.S. Ramm, E.N. Mokhov, A.D. Roenkov, Y.A. Vodakov, Y. N. Makarov, Mater. Sci. Fourm 353, 779 (2001).

[16] J.C. Bailar, H.J. Emeléus, S.R. Nyholm, A.F. Trotman-Dickenson, Comprehensive Inorganic Chemistry, Pergamon, Oxford (1973).

Chapter 3 – Syntheses of AlN Powders, Whiskers, and Films

3.1 Introduction

In Chap. 2, we proposed to use the rection Al + N_2 = AlN for the growth of AlN single crystals. Fisrtly in this chapter, the reativity between Al metal and N_2 gas is confirmed by directly supplying N_2 gas on Al metal at a relatively low temperature (1300°C). Successful conversion from Al metal to AlN powder crystal is demonstrated by X-ray diffraction, cathodoluminescence, and energy dispersive X-ray spectroscopy. Subsequently, AlN is grown using the newly developed growth apparatus, where the Al vapor is tranferred by innert Ar gas to the growth zone, to avoid premature reaction between Al and N_2 gas. Varying the growth conditions, such as N_2/Al molar ratio (V/III ratio) and growth temperature, AlN whiskers and films are obtained on sapphire substrates. The decisive factors of the crystal morphologies of the obtained AlN crystals are discussed. All of the fabricated crystals (powder, whisker, and film) are emissive at deep levels at ~400 nm wavelength, suggesting another possible application as a near ultraviolet phosphor.

3.2 Confirmation of Reactivity between Al and N_2

First, the reaction between Al and N_2 gas is discussed. Al powders with a purity of ~4N (diameter: 45μm) were loaded in the crucible which was settled in the source zone. N_2 gas was introduced to directly react with Al powders. The process duration was 1 h, and the

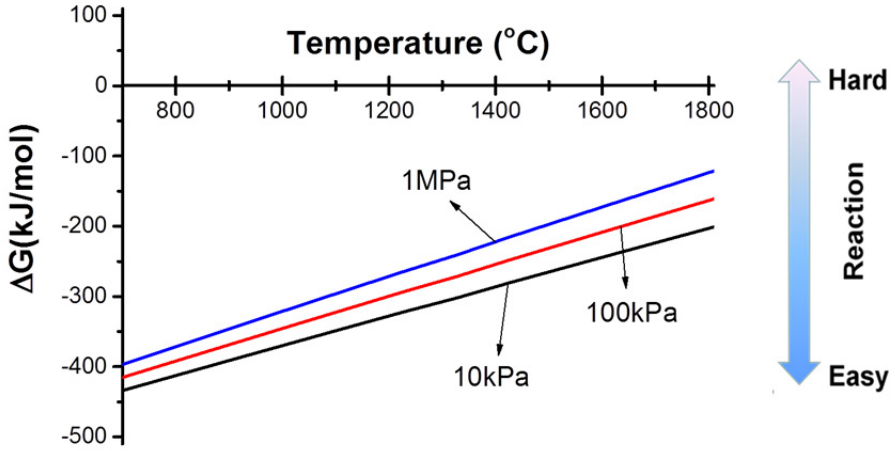

Figure 3.1: Gibbs free energy changes for Al + 1/2N_2 = AlN under different pressures.

source zone temperature was 1300°C. This relatively low temperature suppresses the evaporation of Al, and consequently, Al powder was directly nitrided within the source zone without sapphire substrates.

Let us consider the effect of the growth pressure on the reactivity. Figure 3.1 shows the calculated Gibbs free energy changes under different growth pressures. It is generally true that a lower pressure increases reactivity [1], and the trend is confirmed for Al+1/2N_2 = AlN. That is, to promote the reaction Al+1/2N_2 = AlN, the growth pressure should be lower, whereas to confirm the reactivity, it should be higher. Therefore, we chose 95 kPa in this section, and 10 kPa in the following growth section.

Figure 3.2 compares Al powders and the products after the reaction. Those are apparently different, suggesting a reaction between Al and N_2. To assess crystal structures of the sintered powders, X-ray diffraction (XRD) measurements were performed using the Cu Kα line. Calculated and experimental XRD profiles of the powders are shown in Fig. 3.3. In the experimental profile (lower panel), many peaks are observed. Their positions and relative intensities are quite well reproduced by a simulation (upper panel) assuming an AlN

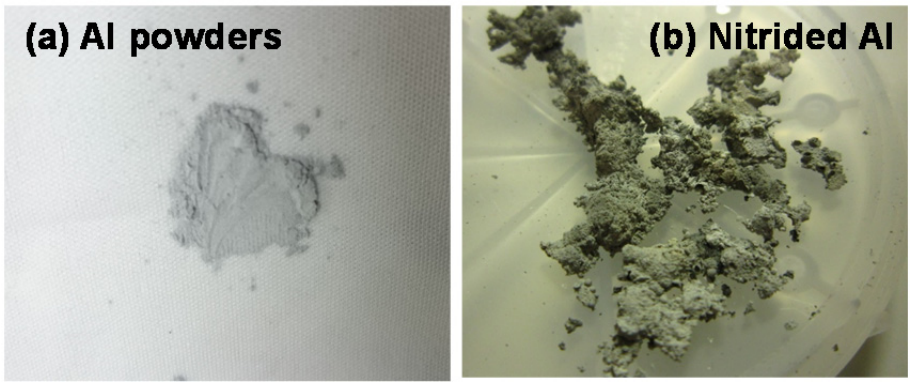

Figure 3.2: Photographs of (a) Al powders and (b) nitrided Al.

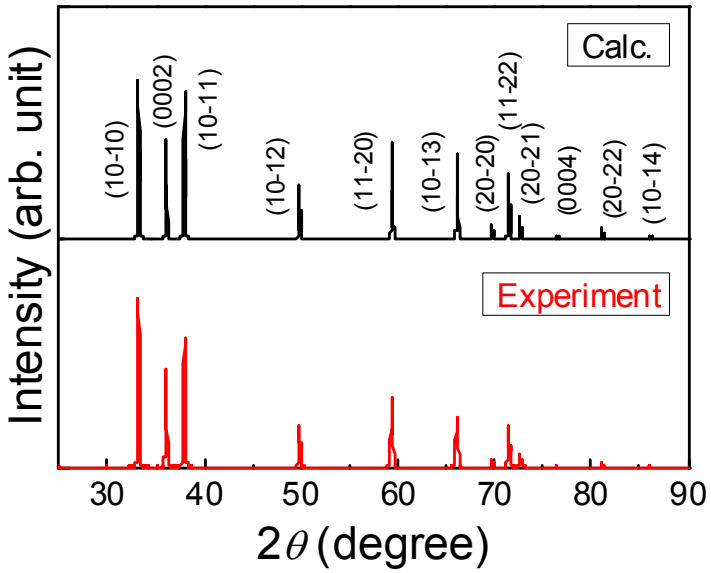

Figure 3.3: Calculated (upper panel) and experimental (lower panel) XRD profiles of AlN powders.

poly-crystal. Therefore, all of the observed peaks can unambiguously be assigned to different crystallographic planes, thereby confirming the synthesis of an AlN phase.

Figure 3.4 shows (a) cathodoluminescence (CL) spectrum, (b) scanning electron microscopy (SEM) image, (c) CL monochromatic mapping, and (d) energy-dispersive X-ray spectroscopy (EDS) profiles of the AlN powder crystals at room temperature (RT). The SEM and CL mappings were taken at the same position, and EDS spectra were taken at positions 1 to 4 designated in the SEM image.

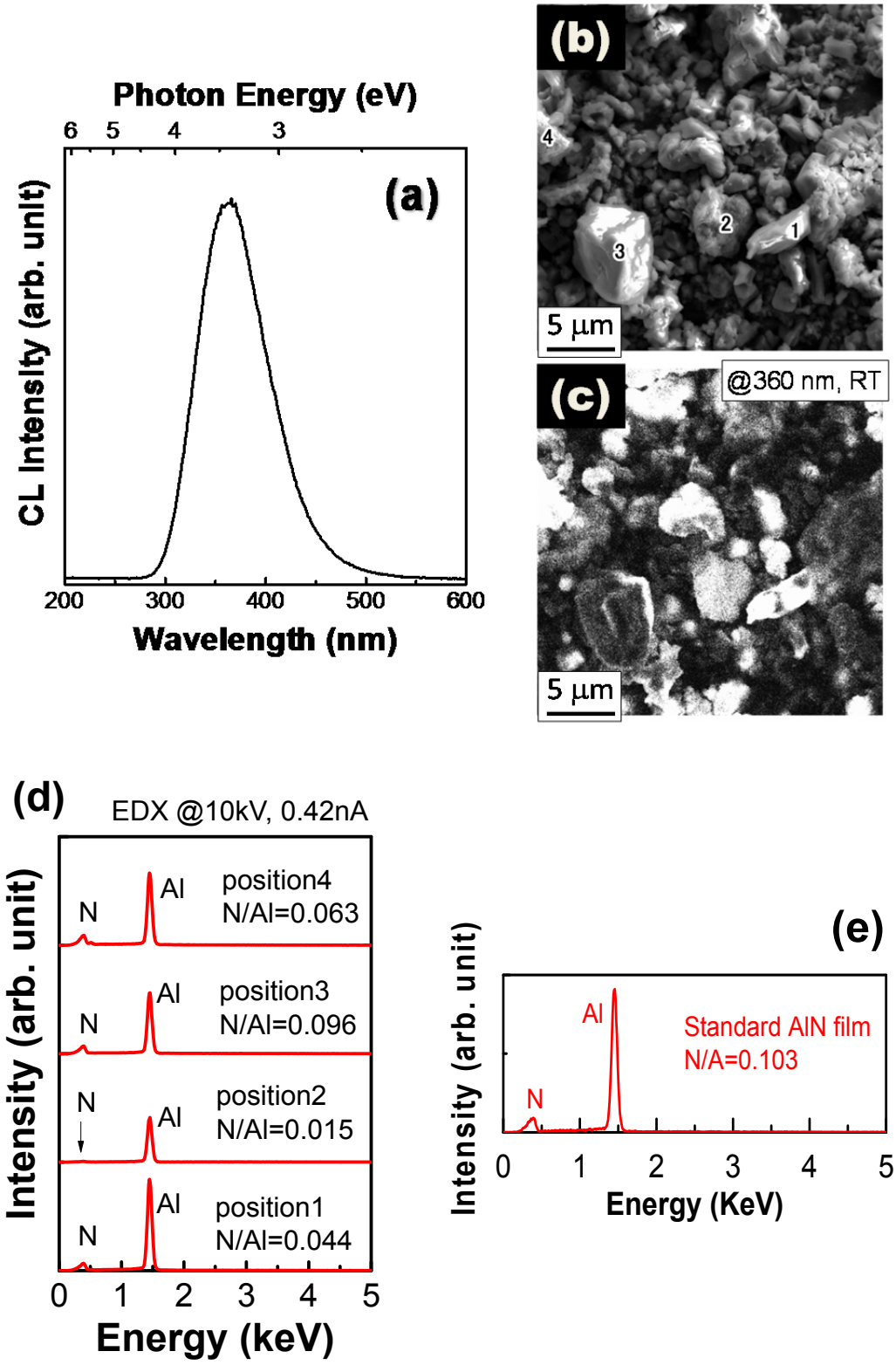

Figure 3.4: (a) CL spectrum, (b) SEM image, (c) CL monochromatic mapping at 360 nm, (d) EDX profiles of AlN powders, and (e) EDX profile of a standard AlN film. The measurements are at RT.

The CL peak wavelength is 357 nm [Fig. 3.4(a)]. Although this is much longer than the AlN band gap (6 eV ~ 207 nm), and no emission is observed from the band edge, the 357-nm emission is intense. We suppose that this emission is related to impurities and/or defect levels, as discussed below in Sec. 3.4. The SEM image in Fig. 3.4(b) shows that the diameter of the particles is a few μm after grinding. Figure 3.4(c) is a CL mapping monitored at 360 nm wavelength, which is around the emission peak. Comparing with the SEM image [Fig. 3.4(b)] reveals that many of the synthesized AlN particles are highly emissive. Those findings lead us to believe that our AlN powders can be used as a phosphor in the near UV spectral range.

In addition, the EDS profiles of AlN powder crystals were measured in the SEM chamber with an acceleration voltage of 10 keV and an electron beam current of 0.42 nA. As shown in Fig. 3.4(d), a N peak at ~0.39 keV and an Al peak at ~0.45 keV are found in each spectrum. By comparing the EDS spectra of the selected particles with that of an AlN standard film [Fig. 3.4(e)], which is a 2-μm-thick AlN layer grown on sapphire by metalorganic vapor phase epitaxy, we found that the N peak intensities of the powders are weak. As mentioned in Chap. 2 and confirmed in this section, the chemical reaction between Al and N_2 proceeds spontaneously. Therefore, Al powders heated under N_2 atmosphere tend to form AlN crust on Al (AlN shell/Al core structures), which may lead to the weaker N signal from the powders. In order to clarify the existence of the AlN shell/Al core structure in our powder samples, the experimental results are compared with a series of simulations.

The simulations were carried out through a program, Casino, which is a Monte Carlo simulation of electron trajectory for electron beam interacting with a bulk and thin foil. It is possible to evaluate the probabilities of electron scattering and X-ray generation by using probability functions. That means, the intensity of characteristic X-rays emitted from atoms irradiated with high-energy electrons can be predicted. To simulate an AlN crust on an Al bulk crystal, we assumed a two-dimensional layered structure of an AlN thin film on an Al

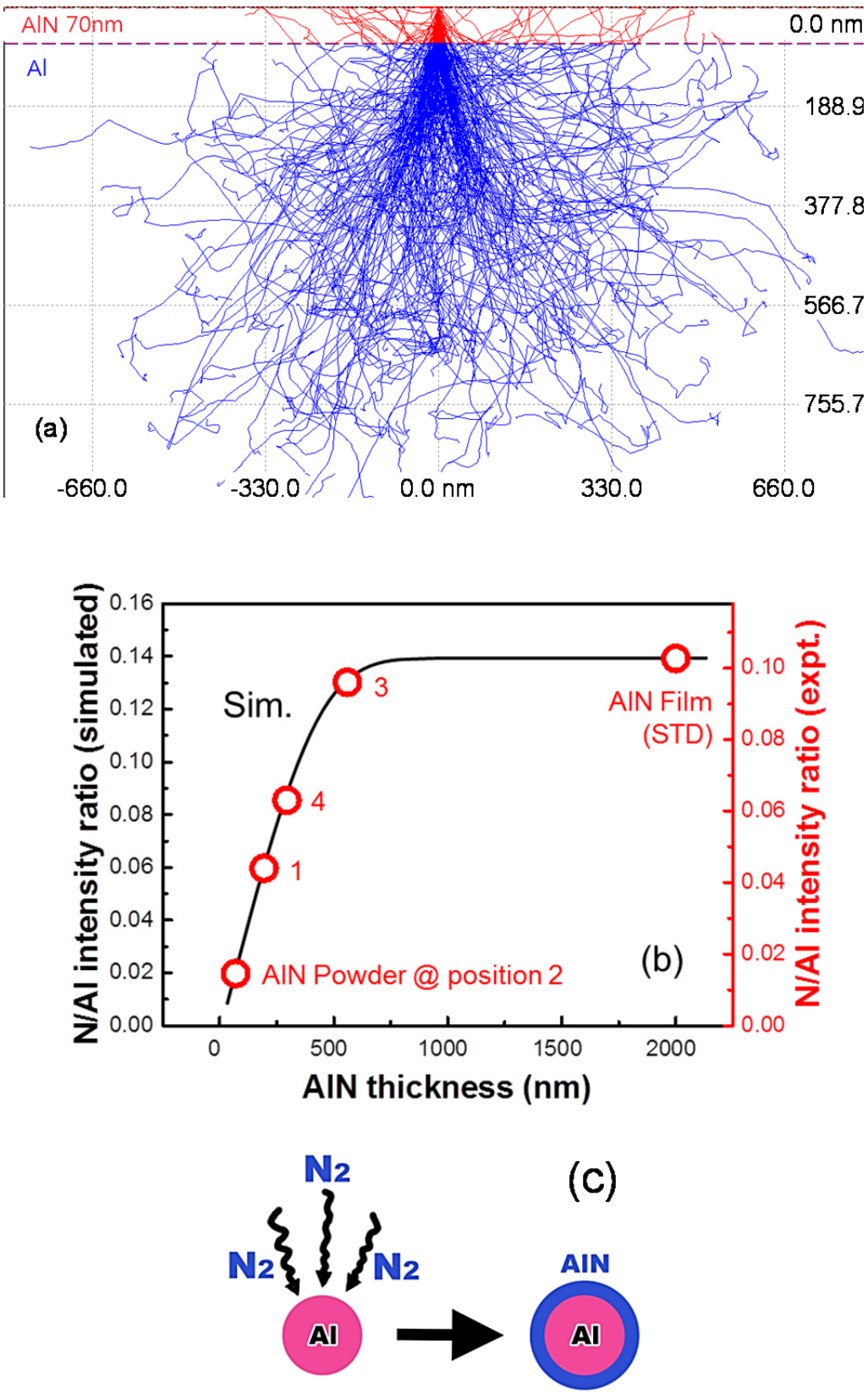

Figure 3.5: (a) Simulation of paths of 10 keV electrons by Casino, (b) Casino simulation results and experimental data with increasing AlN film thickness, and (c) a model of an Al core/AlN shell structure.

substrate. Figure 3.5(a) illustrates an example of the simulated electron paths. In this particular case, the AlN thickness is 70 nm, and irradiated electrons at 10 keV penetrate into the underlying Al layer. Therefore, both the AlN and Al layers can contribute to the Al signal. Consequently, the N/Al characteristic X-ray intensity ratio of the AlN/Al structure is smaller than that of pure AlN, and varies depending on the AlN crust layer thickness. Figure 3.5(b) shows the calculated results (solid curve). Also plotted in Fig. 3.5(b) are the experimental N/Al ratios derived from Figs. 3.4(d) and (e). To let the experimental N/Al of the standard AlN match with the simulated one, the scales of the left and right vertical axes of Fig. 3.5(b) were adjusted, which enables direct comparison between the simulations and experiments. For example, at position 2, the experimental N/Al ratio is 0.015, and consequently, the thickness of AlN crust can be read as ~75 nm. Similarly, the thicknesses of AlN crust at position 1, 3 and 4 are considered as 195, 295, and 560 nm, respectively. That is say, the AlN powders at the selected positions are all AlN/Al structures as shown in Fig.3.5 (c).

Besides, recall that the XRD profile of the fabricated powders (Fig. 3.3, lower panel) does not include signals of Al crystal. Hence we suppose that core Al is not in the crystalline phase.

The results shown in this section indicate that AlN crust forms over the Al metal source during the direct reaction between Al and N_2, and the growth of pure AlN is difficult by this method. Therefore, in the next step, we introduce Ar gas as a carrier gas.

3.3 Crystal Growth of AlN Whiskers and Films

3.3.1 Typical Growth Morphologies

In this section, we discuss the growth of AlN using Ar carrier gas and sapphire (0001) substrates placed in the growth zone. The source zone temperature was fixed at 1400°C, and the growth pressure was 10 kPa (as discussed in the previous section). By adjusting growth

conditions except the source zone temperature and pressure, AlN whisker and film crystals were fabricated. The XRD profiles and the SEM images of representative AlN whiskers and a film are shown in Figs. 3.6 (a) and (b), respectively.

For whiskers, apart from the (0006) sapphire peak located at 41.69°, the AlN (0002) and (10$\bar{1}$1) diffractions are observed at 36.02° and 37.90°, respectively, indicating preferable c-oriented growth. Although this finding is not necessarily consistent with the SEM image showing random orientation of the whiskers, the reason is unclear. The diameter of AlN whiskers was in the nanometer-order, and the length was of the order of several 100 μm. From these results, we expect that this growth method can be used for AlN nano-whiskers/wire formation.

In the case of AlN films, only the AlN (0002) diffraction is observed, confirming that the

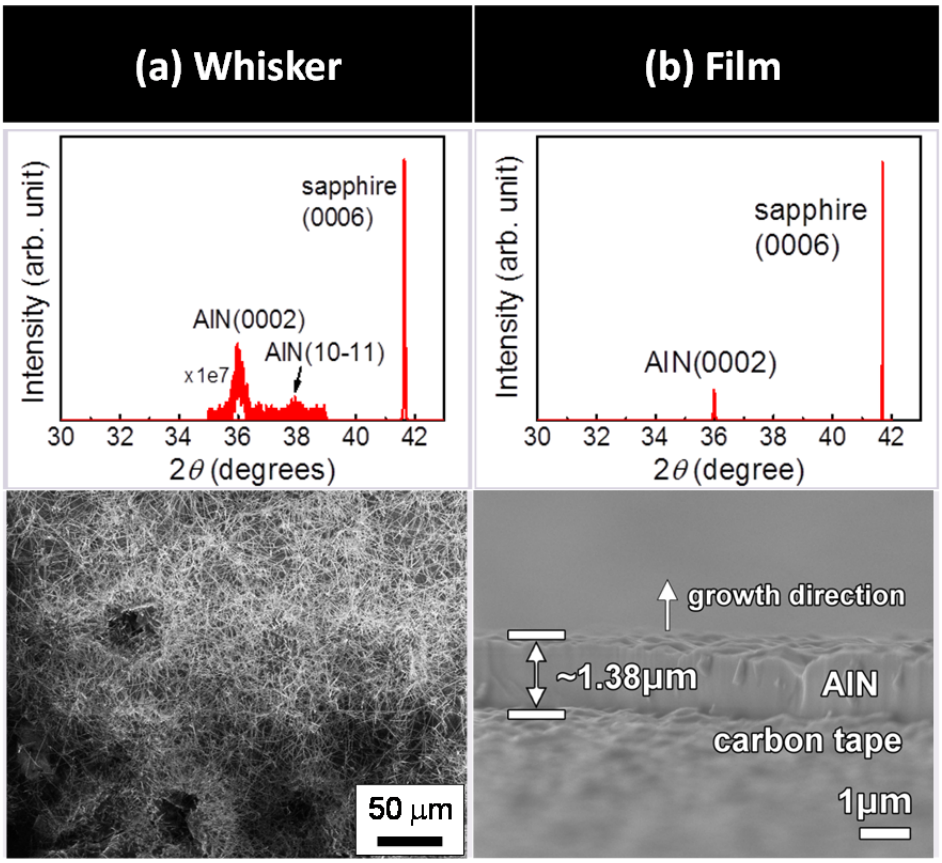

Figure 3.6: The XRD 2θ-ω profile (upper panel) and SEM images (lower panel) of (a) AlN whiskers and (b) film.

grown film is a c-oriented film. Interestingly, some of the AlN films prepared in this study were spontaneously separated from the sapphire substrates after the growth. This self-separation phenomenon will be discussed in Chap. 4. The bottom part of Fig. 3.6(b) shows the cross sectional SEM image for an AlN film. (Because the AlN film has already separated from the sapphire substrate before the SEM observation, it was stuck on a carbon tape.) The film thickness is 1.38 μm, which corresponds to a growth rate of 1.38 μm/hr. Although the surface is still rough, an AlN film can be fabricated with a reasonable growth rate. Further optimization of the growth condition is described in Chap. 4.

3.3.2 Factors Determining Crystal Morphologies

Now, let us discuss the cause of the morphology variations. In the case of AlN powder growth, N_2 gas was directly supplied on Al powder, which causes the direct reaction between them to produce powders. In the case of whiskers and films, N_2 gas is absent in the lower channel, whereas Ar was supplied to transport the Al vapor into the growth zone. Therefore, the growth condition of AlN powders is totally different from those of AlN whiskers and films. Comparatively, the growth conditions of AlN whiskers and films are similar. In the following, we discuss the difference of the growth conditions of AlN whiskers and films.

(a) Growth zone temperature: Figure 3.7 compares two samples prepared at different growth temperatures. At temperatures below 1550°C, AlN films were obtained successfully, whereas AlN whiskers were fabricated at 1600°C. The growth temperature is thus an important parameter to determine the crystal morphology. It should be noted that the thermal decomposition of sapphire substrate may occur at a temperature higher than 1600°C. Therefore, the upper limit of growth temperature of AlN film/whisker crystals on sapphire substrates is approximately 1600°C.

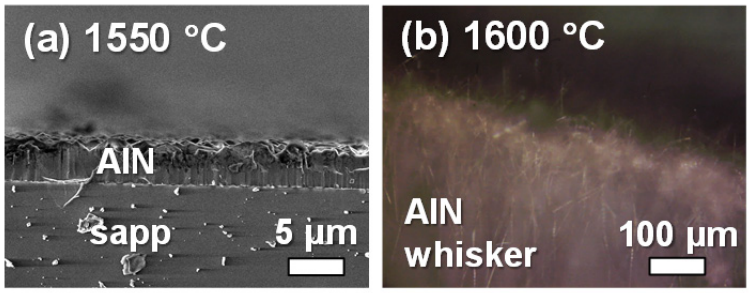

Figure 3.7: (a) SEM cross-section image of an AlN film grown on a sapphire substrate at 1550°C. (b) A plan view optical microscope image of AlN whiskers grown on a sapphire substrate at 1600°C.

(b) Al flow rate: Even at the same growth temperature of 1500°C and the same N_2 flow rate of 3 SLM, increasing Al vapor (*i.e.* decreasing V/III ratio) causes whisker formation, as shown in Fig 3.8. Here, the V/III ratio is defined as molar flow ratio of N_2 against Al, $[N_2]/[Al]$.

(c) N_2 flow rate: Figure 3.9 displays SEM images of AlN grown under different N_2 flow rates. The growth temperature was 1500°C, and the Al flow rate was 16 μmol/min. With high N_2 flow rates (*i.e.* high V/III ratios), AlN crystals would be films, whereas lower ratios bring whiskers.

From above (b) and (c), we consider that not the flow rates of Al and N_2, but their ratio (V/III ratio) can well describe the growth behavior. To demonstrate this idea, we compare the sample morphology as functions of growth temperatures and V/III ratios. Figure 3.10 shows the result, where a clear U-shape boundary between AlN film and whisker is seen, supporting our hypothesis. Basically, AlN films (whiskers) can be obtained under a higher (lower) V/III ratio. This trend is consistent with GaN metalorganic vapor phase epitaxy [2], in which a low V/III ratio reduces the driving force for film growth and promotes nanowire formation.

The U-shape boundary is explained as follows. As the growth temperature increases,

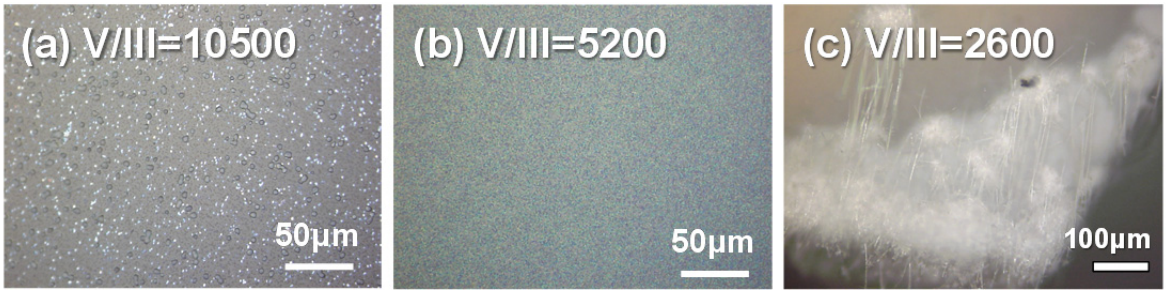

Figure 3.8: Optical microscope images of AlN crystals grown on sapphire substrates at 1500°C with Al flow rates of (a) 25, (b) 50, and (c) 100 μmol/min. The corresponding V/III ratios are (a) 10500, (b) 5200, and (c) 2600. The N_2 flow rate is constant at 3 SLM.

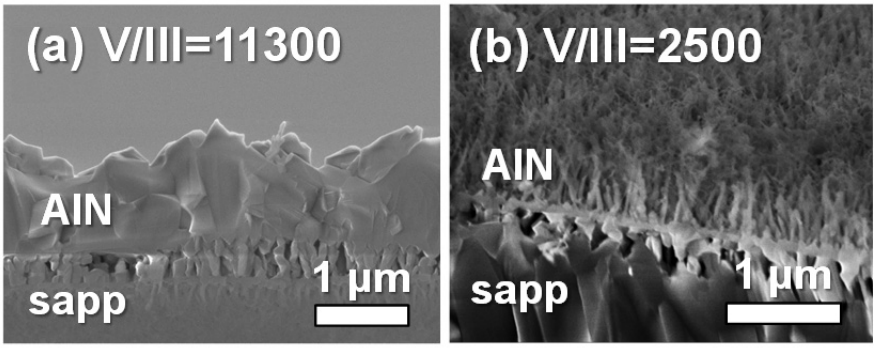

Figure 3.9: SEM images of AlN crystals grown on sapphire substrates at 1500°C under different N_2 flow rates of (a) 4 SLM (V/III = 11300) and (b) 2 SLM (V/III = 2500). The Al flow rate is constant at 16 μmol/min.

decomposition of N_2 is promoted, which increases the effective N concentration that contributes to the growth. This is why 1550°C needs a less input V/III ratio than 1500°C for the film growth. However, further increase in the temperature to 1600°C requires a higher V/III ratio, opposite to the expectation. This is understandable by considering that the reducing reaction of sapphire substrate caused by the Al vapor is enhanced at higher temperatures reducing the effective V/III ratio. That is, competition between decomposition of N_2 and sapphire dominates the growth morphology.

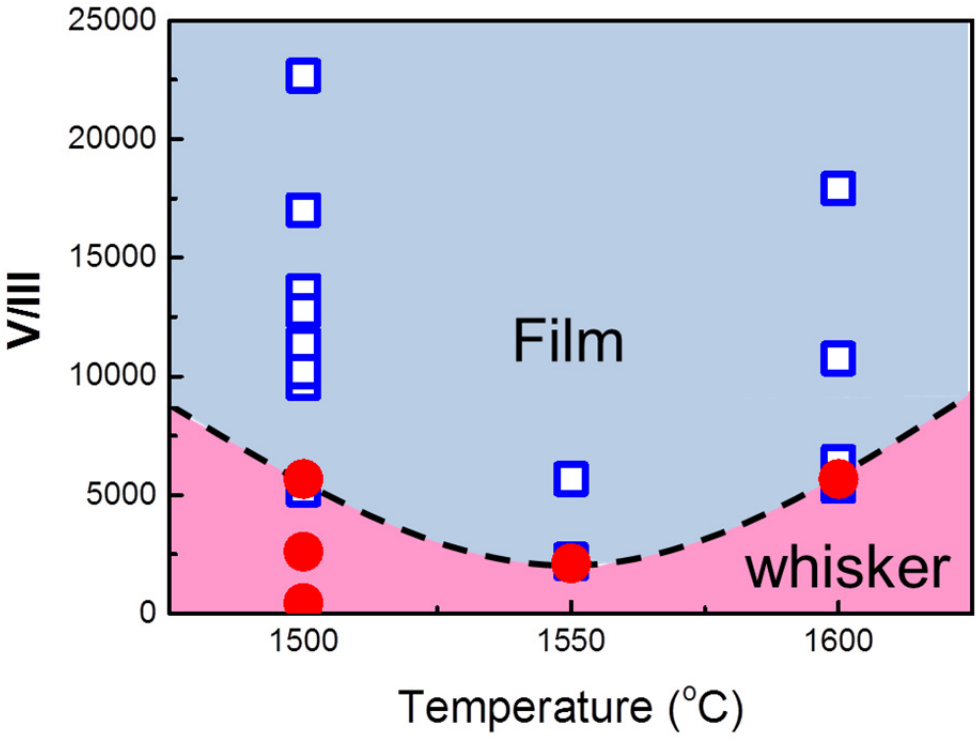

Figure 3.10: Plot of AlN crystal morphologies with various growth temperatures and V/III ratios.

If one wants to grow AlN films at lower temperatures via this growth method, the utilizations of radical nitrogen species may be a good choice. In addition, we also found that AlN whisker and film crystals can coexist under an appropriate growth condition. This result yields an interesting phenomenon, self-separation. The mechanism of self-separation will be discussed in Chap. 4.

3.4 Optical Properties of AlN Powders, Whiskers, and Films

The optical properties are investigated by photoluminescence (PL) and CL measurements. The excitation source in the PL measurements was an ArF excimer laser (193 nm) with a

pulse width of 4 ns. Figure 3.11 shows the PL spectra of AlN powders, whiskers, and a film acquired at RT and 13 K. Note that the PL spectrum of each sample was acquired with the same setting, so that the direct comparison of the intensities is reasonable.

The near bandgap emission was not observed, but deep level emissions were observed. Although the deep level emission energies are much smaller than the AlN band gap (6 eV ~207 nm), the emissions are intense. As shown in Fig. 3.11(a), the PL intensity of AlN powders is the strongest. If we assume that at low temperatures non-radiative processes are negligible and the consequent internal quantum efficiency is 100%, the PL intensity ratio provides an internal quantum efficiency at a measurement temperature. This procedure reveals that the internal quantum efficiency of our AlN powders, which possess the strongest emission intensity among three different morphologies, is as high as 59% [Fig. 3.11(b)]. This value is also higher than that of other typical nitride films [3, 4]. Alluring prospects of our AlN powders as UV phosphors are confirmed.

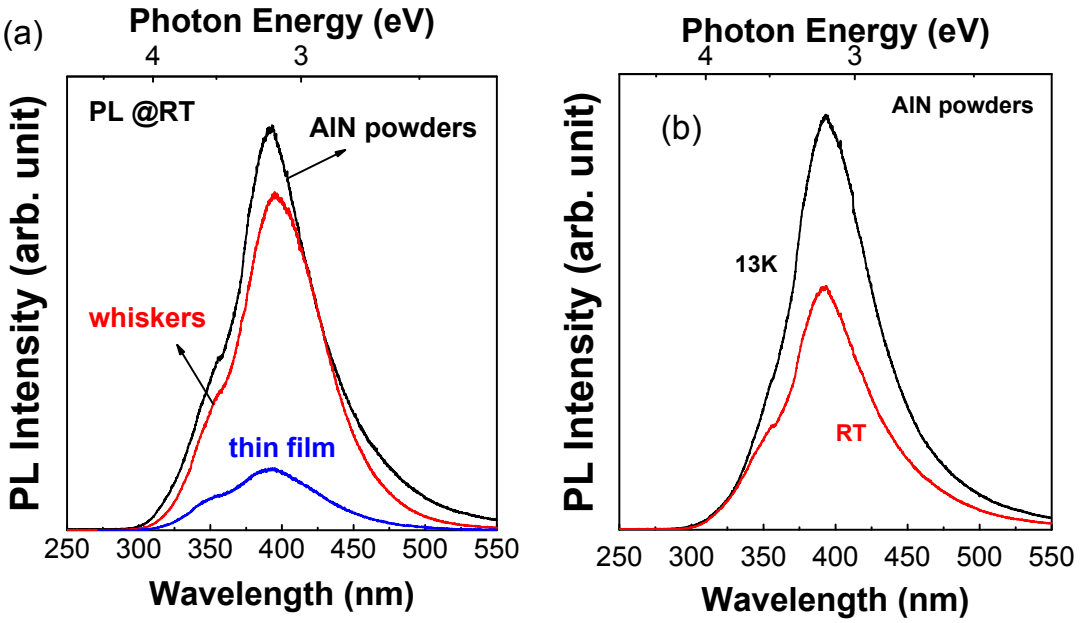

Figure 3.11: (a) PL spectra of AlN powders, whiskers, and film acquired at RT. (b) PL spectra of AlN powders acquired at 13 k and RT.

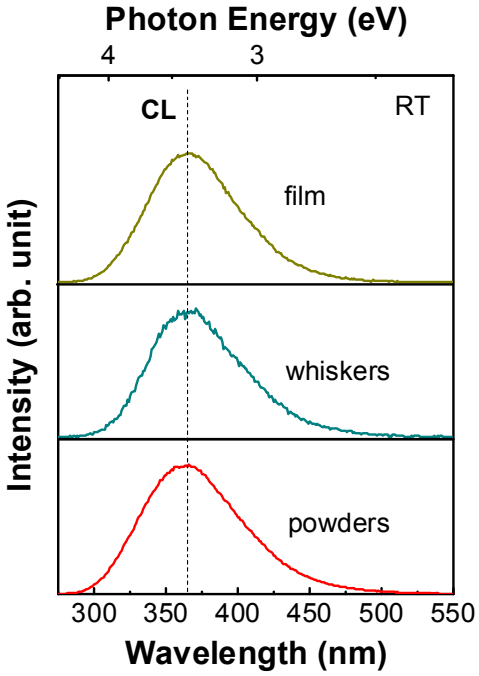

Figure 3.12: CL spectra of AlN (a) powders, (b) whiskers, and (c) a film acquired at RT.

Figure 3.12 compares the CL spectra of AlN powders, whiskers, and a film. As seen, the CL spectra span almost the same wavelength range. This suggests that those three types of AlN crystals prepared in this study possess the similar deep-level emissions.

To find a clue to the origins, the broad emission spectra were separated into three peaks through the Gaussian fitting. An example of a PL spectrum fit is shown for powders in Fig. 3.13; the emissions are peaking at 345, 394, and 411 nm. The possible origins of deep-level emissions are illustrated in Fig. 3.14 [5-15], where V_{Al} represents Al vacancy. According to references listed in Fig. 3.14, we tentatively assign the 345 nm emission (~3.59 eV) to C_N acceptor-related transition or $(V_{Al}\text{-}O_N)^{2-}$, the 394 nm emission (~3.15 eV) to V_{Al}^{3-} – deep donor transition, and the 411 nm emission (3.02 eV) to V_{Al}^{3-} – valence band transition.

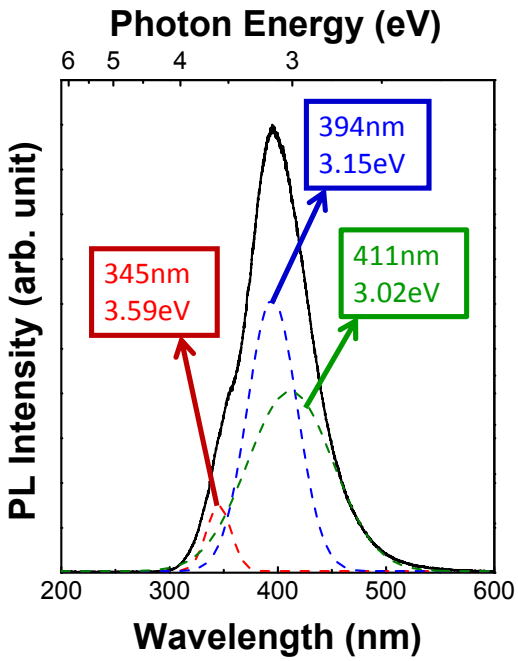

Figure 3.13: PL spectrum of AlN powders acquired at room temperature with the Gaussian line fitting.

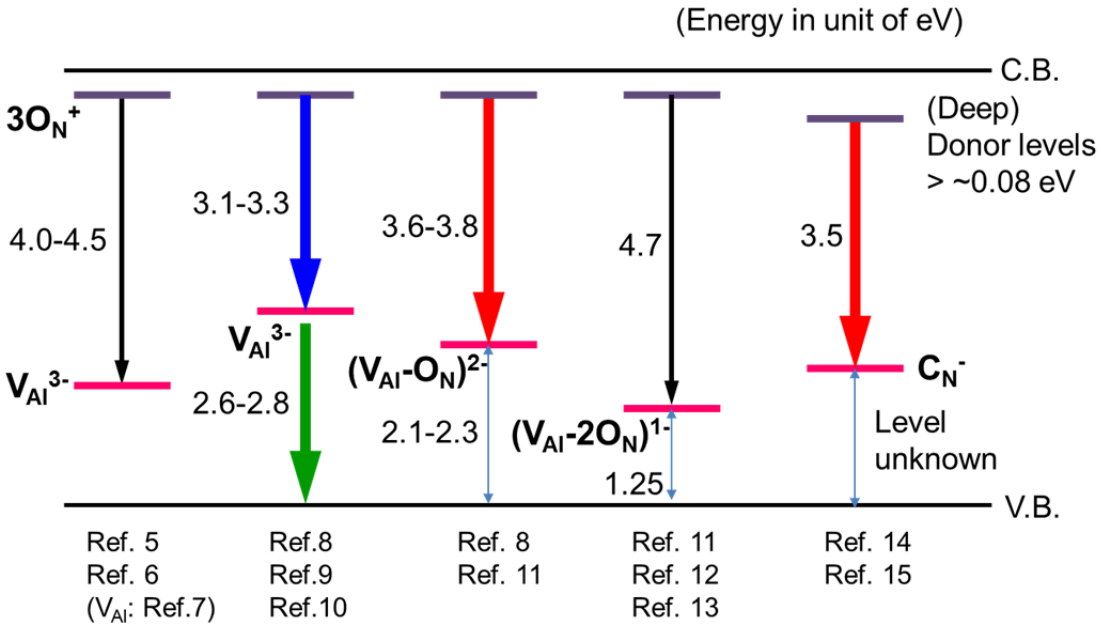

Figure 3.14: Summary of previously reported deep level emissions.

In order to confirm our assertion that two of deep level emissions are related to V_{Al}, we fabricated another AlN whisker sample under a significantly Al excess condition. To realize the Al excess condition, a sapphire substrate was directly soaked into the Al source, and N_2 was supplied on it. The CL mapping and spectra of that sample are shown in Figs. 3.15(a) and (b), respectively. The AlN whiskers exhibited a near band edge emission at around 6 eV (~210nm), which indicates that the excess Al condition successfully reduces the number of V_{Al}.

In addition, compared with the CL spectrum of another AlN whisker sample grown under the normal condition with much less Al (higher V/III ratio), it is found that the emission wavelength of the AlN whiskers grown under the Al-excess condition shifts to a shorter wavelength, as shown in Fig. 3.16. This is because an emission at ~325 nm (3.8 eV) becomes clearly observable. According to ref. [16], the origin of the 3.8 eV emission is related to O-impurities. They claim that since Al is a strong reducing agent and can reduce sapphire substrates (Al_2O_3), too excess Al will generate O-related impurities originating from sapphire substrates. Therefore, we consider that the origin of the 3.8 eV emission in our AlN whisker is O-impurity related emission. For future works, we may be able to do some special treatments such as annealing in Al atmosphere to further improve the optical properties.

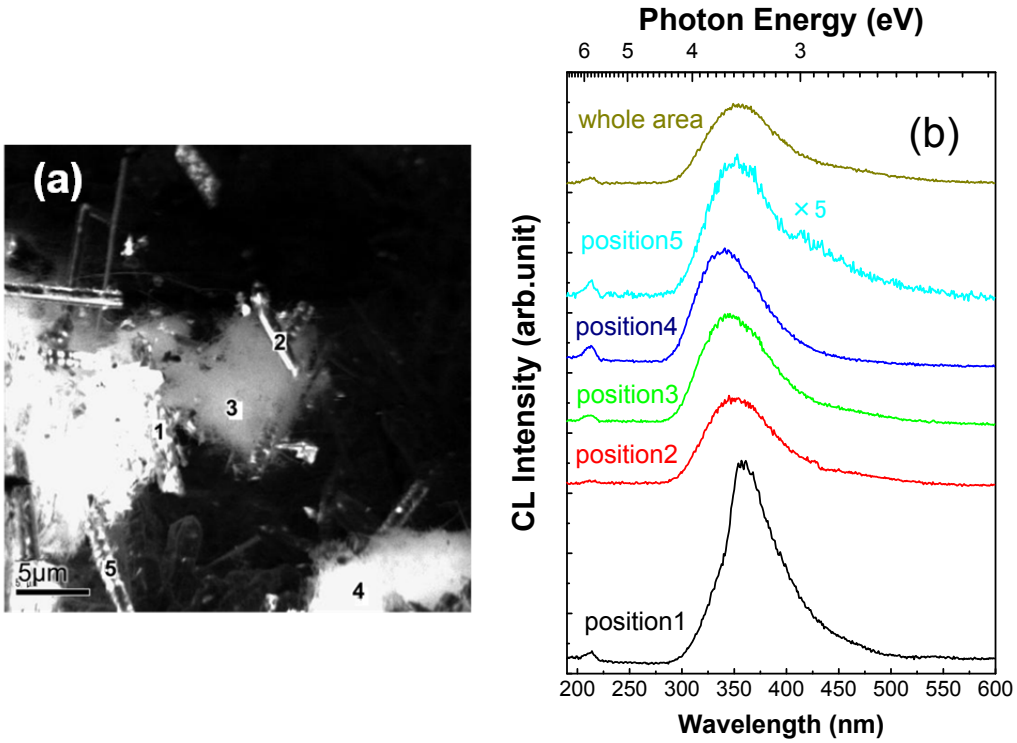

Figure 3.15: (a) CL mapping monitored at 360 nm and (b) spectra of AlN whiskers acquired at RT.

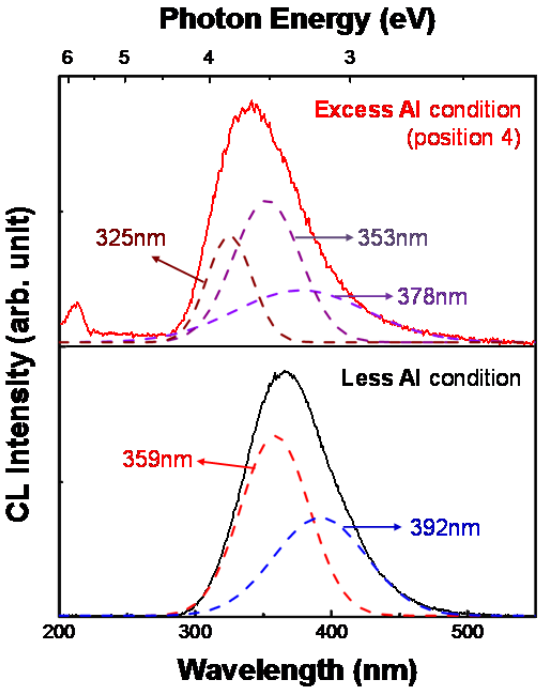

Figure 3.16: Effects of Al vacancy compensation treatment.

3.5 Summary

In this chapter, we confirmed the probability of the chemical reaction between Al metal and N_2 gas to produce AlN powders. Then we synthesized AlN whiskers and films by using just Al and N_2 gas as source materials and Ar carrier gas.

AlN powders were successfully sintered at 1300°C, 95 kPa for 1 hr. Al core/AlN shell structures were obtained, the properties of which were examined through EDX measurements and EDX simulations.

For AlN whisker and film growths, we found that the key factors which determine the morphologies of AlN crystal are the growth zone temperature and V/III ratio. Under higher V/III ratios, AlN crystals would be films, whereas lower ratios bring whiskers.

The optical properties were assessed by PL and CL. Although the main emissions of our samples are deep level emission, the emissions (especially those of AlN powders) are intense. The internal quantum efficiency of our AlN powders was as high as 59% at RT. According to previous reports, we supposed that the main deep level emissions are related to Al vacancies. This assignment was supported by an AlN whisker sample grown under an excess-Al condition that can compensate for the Al vacancies.

References

[1] See for example, O. Kubaschewski, C.B. Alcock, P.J. Spencer, Materials Thermochemistry, 6th ed. (Pergamon Press, 1993).

[2] K. Choia, M. Arita, Y. Arakawa, J. Crystal Growth 357, 58 (2012)

[3] K. Inoue, N. Hirosaki, R.J Xie, T. Takeda, J. Phys. Chem. C 113, 9392 (2009).

[4] R.G. Banal, Doctor thesis, Kyoto University (2009).

[5] E. Monroy, J. Zenneck, G. Cherkashinin, O. Ambacher, M. Hermann, M. Stutzmann, M. Eickhoff, Appl. Phys. Lett. 88, 071906 (2006).

[6] T. Mattila, R.M. Nieminen, Phys. Rev. B54, 16676 (1996).

[7] A. Dadgar, A. Krost, J. Christen, B. Bastek, F. Bertram, A. Krtschil, T. Hempel, J. Bläsing, U. Haboeck, A. Hoffmann J. Cryst. Growth 297, 306 (2006).

[8] K.B. Nam, M.L. Nakarmi, J.Y. Lin, H.X. Jiang, Appl. Phys. Lett. 86, 222108 (2005).

[9] A. Sedhain, L. Du, J.H. Edgar, J.Y. Lin, H.X. Jiang, Appl. Phys. Lett. 95, 262104 (2009).

[10] T. Koyama, M. Sugawara, T. Hoshi, A. Uedono, J. Kaeding, R. Sharma, S. Nakamura, S.F. Chichibu, Appl. Phys. Lett. 90, 241914 (2007).

[11] T. Mattila, R.M. Nieminen, Phys. Rev. B 55, 9571 (1997).

[12] I. Gorczyca, N.E. Christensen, A. Svane, Phys. Rev. B 66, 075210 (2002).

[13] N. Nepal, M. L. Nakarmi, J.Y. Lin, H.X. Jiang, Appl. Phys. Lett. 89, 092107 (2006).

[14] R. Collazo, J. Xie, B.E. Gaddy, Z. Bryan, R. Kirste, M. Hoffmann, R. Dalmau, B. Moody, Y. Kumagai, T. Nagashima, Y. Kubota, T. Kinoshita, A. Koukitu, D. L. Irving, Z. Sitar, Appl. Phys. Lett. 100, 191914 (2012).

[15] T. Nagashima, Y. Kubota, T. Kinoshita, Y. Kumagai, J. Xie, R. Collazo, H. Murakami, H. Okamoto, A. Koukitu, Z. Sitar, Appl. Phys. Express, 5, 125501 (2012).

[16] X. Tang, F. Hossain, K. Wongchotigul, M.G. Spencer, Appl. Phys. Lett. 72, 1501 (1998)

Chapter 4 – Growth of Thick AlN Films

4.1 Introduction

To improve the device performance of AlN-based solid state UV light sources, AlN bulk crystals for homoepitaxy are highly expected. In this chapter, we discuss the growth of thick AlN films by the new method developed in the previous chapters.

In Chap. 3, we found that a low (high) V/III ratio during the growth results in AlN whiskers (films). In this chapter, we demonstrate that this growth characteristic leads to self-separation of AlN from sapphire, which is a beneficial property for the growth of bulky crystals as it can suppress the formation of cracks and exclude *ex-situ* processes to remove the substrate. However, the excessive separation will lead to a poor crystal quality due to rolling of the separated AlN. Therefore, to control the degree of the self-separation, two techniques are examined in this chapter. After establishing the control of the self-separation phenomenon, the growth for thick crack-free AlN is optimized with a particular focus on the V/III ratio, which successfully achieves a growth rate of 16 μm/hr.

4.2 Self-separation of AlN from Sapphire

Sapphire is an extremely hard material and is difficult to remove from epilayers via chemical and/or mechanical milling techniques. Here, to solve this problem in AlN bulk crystals on sapphire, we propose a new procedure using the corrosion property of Al.

Figure 4.1 displays an example of self-separation, where a 6-μm-thick AlN film is

spontaneously separated from the sapphire substrate after growth. Sapphire is a heat-resistant material and is stable up to 1600°C, but Al vapor is a strongly reducing gas and is able to reduce oxide such as sapphire (α-Al_2O_3). Therefore, we consider that the reducing reaction of sapphire plays a key role in the observed self-separation phenomenon.

To confirm this hypothesis, a simple experiment was carried out. A sapphire substrate was placed near the Al source in the source zone and heated at 1400°C and 10 kPa. Only Ar gas was supplied. For comparison, another sapphire substrate was heated without the Al source. Figures 4.2(a) and (b) are the photographs of sapphire after heating without and with Al vapor,

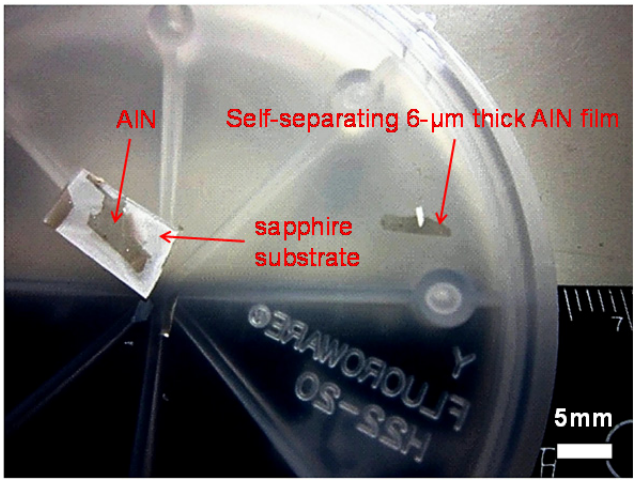

Figure 4.1: Photograph of a self-spared AlN film from a sapphire substrate.

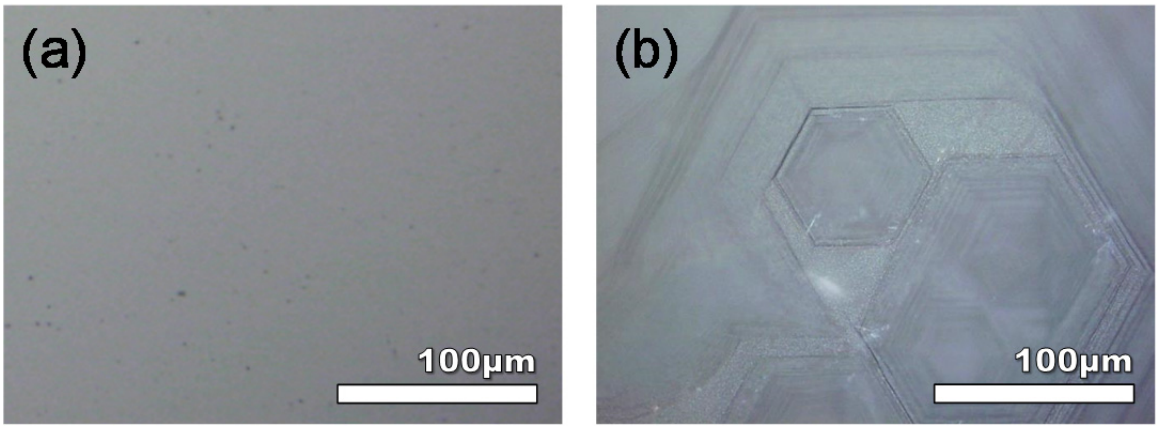

Figure 4.2: Optical microscope images of thermally treated sapphire substrates (a) without and (b) with Al vapor at 1400°C.

respectively. Comparison between those photographs indicates that Al vapor promotes decomposition of sapphire.

For the AlN growth, in addition to directly supplied Al vapor from the Al source, Al-related gases produced during the reduction process must be considered. Such additional Al-related gases decrease the local effective V/III ratio, which may lead to whisker formation, as discussed in Chap. 3. Figure 4.3 shows an AlN thin film (~200 nm) grown on sapphire substrate for 20 minutes. As expected, whiskers form only near the interface, where the effective V/III ratio is higher than the input V/III ratio due to sapphire decomposition. As the growth proceeds, the influence from the decomposition of the sapphire substrate is weakened gradually. Consequently, the V/III ratio recovers to the value determined by the gas flow rates and an AlN film is obtained. Because whiskers are physically weak, sapphire and an AlN film can be separated at that position. Figure 4.4 illustrates a schematic diagram of the proposed self-separation mechanism.

To further support our consideration, an AlN thin film was grown on a 6H-SiC (0001) substrate. Figure 4.5 compares the interfaces between (a) AlN/sapphire and (b) AlN/SiC. There are no whiskers near the AlN/SiC interface. In addition, the self-separating

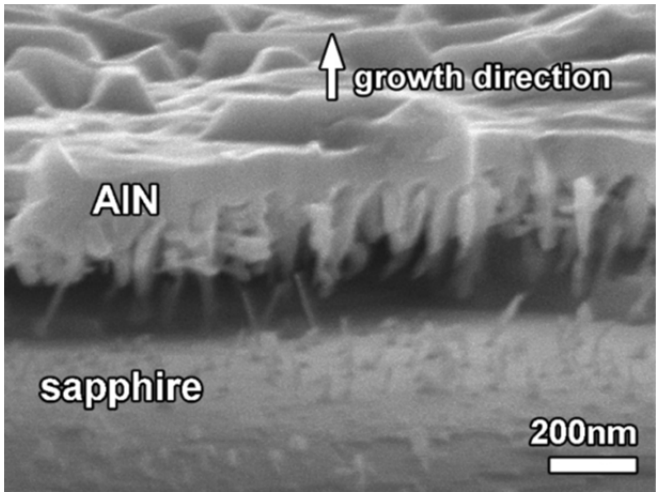

Figure 4.3: SEM image of the AlN/sapphire interface.

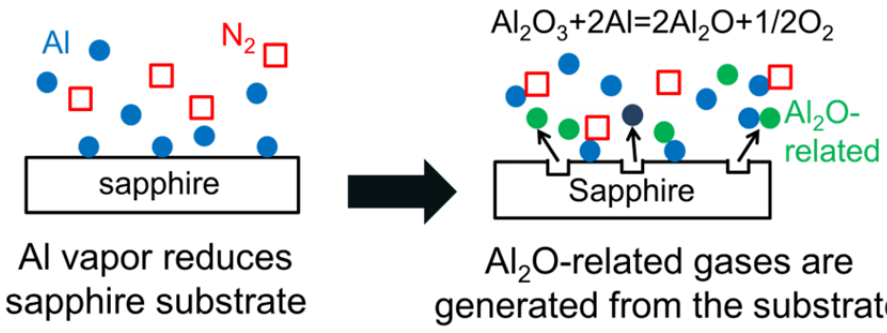

Figure 4.4: Schematic of the mechanism of AlN self-separated from a sapphire substrate.

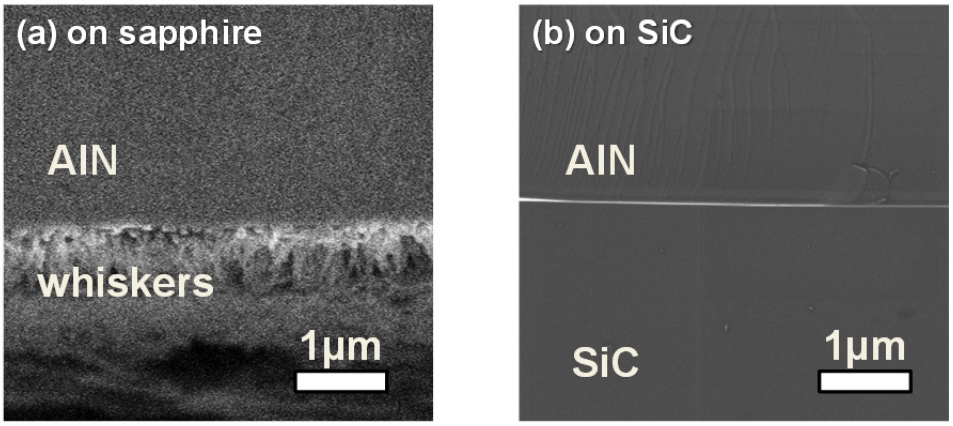

Figure 4.5: SEM cross-sectional images of AlN grown on (a) sapphire and (b) SiC.

phenomenon and the substrate decomposition were not observed in the AlN/SiC structure. All of these findings support our conclusion that the self-separation of AlN from sapphire is due to the reaction between Al and sapphire.

Moreover, we found another exploitable aspect of the self-separating phenomenon. That is the reduction of the stress in AlN films for crack-free AlN. It has often been reported that the large mismatch in the thermal expansion coefficients of sapphire and AlN causes tensile strain within the growth plane, and consequently leads to epilayer cracking [1,2]. Figure 4.6(a) displays a Nomarski microscopy image of the surface of a typical 1-μm-thick AlN film grown by metalorganic vapor phase epitaxy (MOVPE) on a sapphire (0001) substrate [3]. Many

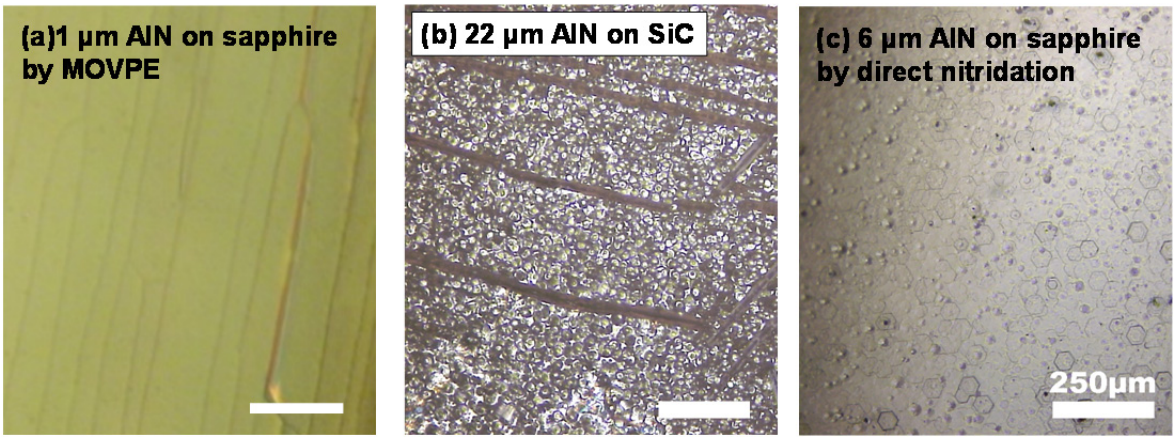

Figure 4.6: Optical microscope images of AlN grown on (a) sapphire by MOVPE (1 μm) (reproduced from ref. [3]), (b) SiC, and (c) sapphire with our new approach (6 μm). The scale bars are for 250 μm.

cracks are observed. A similar result can also be observed on the surface of an AlN film grown on a SiC substrate [Fig 4.6 (b)]. On the other hand, there are no cracks on the surface of the 6-μm-thick AlN film on sapphire prepared in this work as shown in Fig. 4.6(c). The result indicates that the interfacial whiskers effectively cushion the influence of the in-plane tensile strain. This can be a strong advantage of our growth method for bulk AlN growth.

4.3 Control of Interface Reaction

In the previous section, we pointed out that the self-separation of AlN from sapphire substrates can assist AlN thick films to grow without cracks. However, excessive self-separation (particularly in the early stage of the growth) degrades the crystalline quality due to rolling of AlN foils, as shown in Fig. 4.7. Therefore, a way to control the degree of self-separation is needed. Here, we propose two methods, (a) nitridation of sapphire substrate and (b) adding alumina (Al_2O_3) powder to the Al source as a material protecting the sapphire surface.

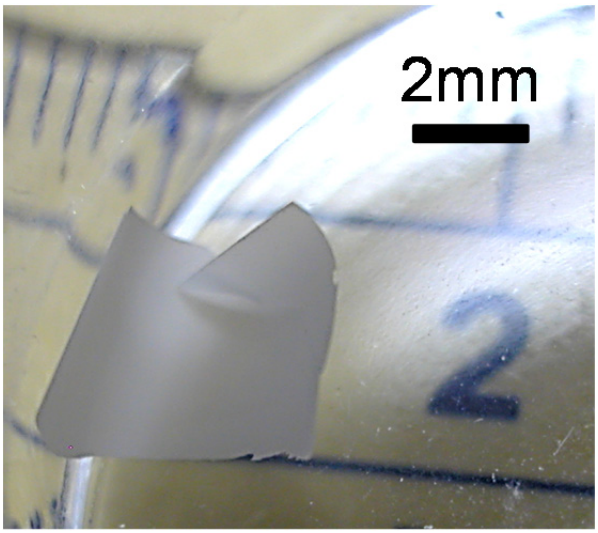

Figure 4.7: AlN peeled-off from a sapphire substrate. The AlN foil rolls.

4.3.1 Nitridation of Sapphire Substrate

Up to here, N_2 and Ar gases are simultaneously introduced into the growth reactor when the temperatures of the source and growth zones reach the target temperatures. In this section, on the other hand, N_2 and Ar gases are loaded into the reactor at the onset of the increase of the growth and source zone temperatures. The whole growth procedure is depicted in Fig. 4.8. Because the Al vapor pressure at 1200°C (see, Fig. 2.8) is as low as 1.2×10^{-5} atm, the initial 55 min (below 1200°C) can be regarded as nitridation treatment of the sapphire substrate with N_2 gas.

Figure 4.9 shows two scanning electron microscopy (SEM) cross-sectional images of interfaces between AlN films and sapphire substrates (a) without and (b) with the nitridation process. Less and smaller voids were observed at the interface with nitridation. (As shown below, those voids are still effective to suppress the crack formation.) The decomposition of sapphire was suppressed effectively with the substrate nitridation pretreatment. The reason may be attributed to an interfacial layer of AlON [4-15] formed with the nitridation pretreatment.

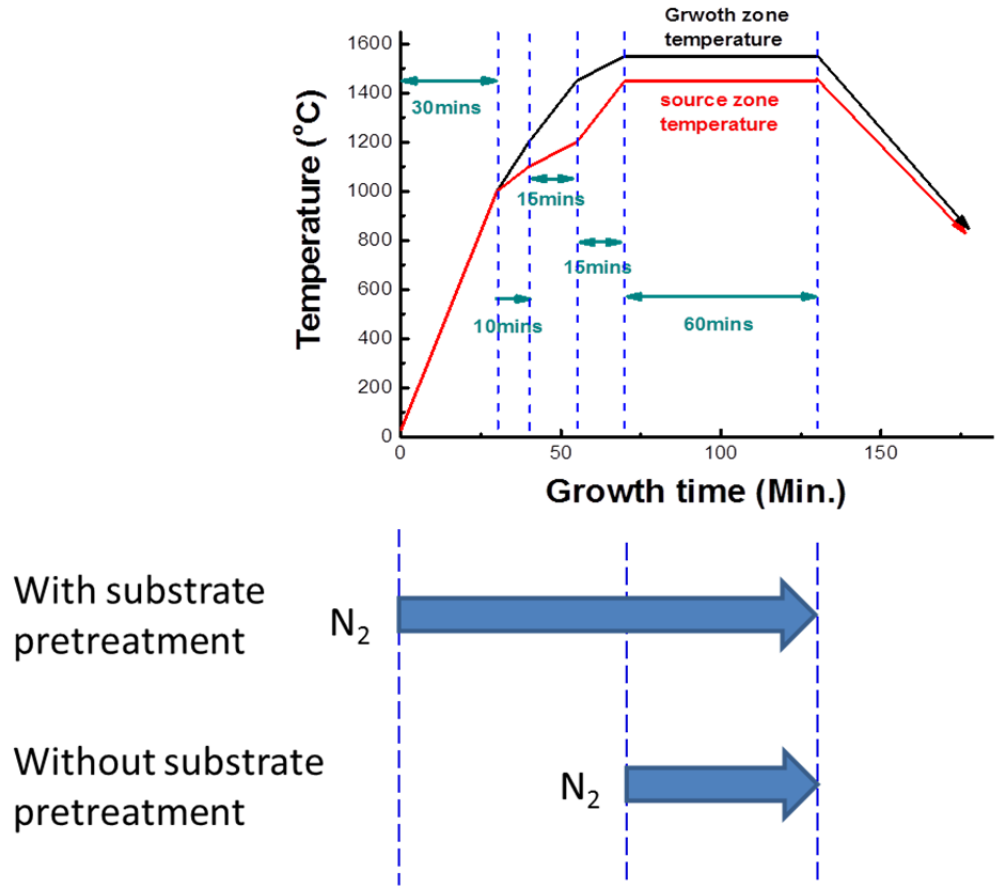

Figure 4.8: Diagram of growth processes with and without nitridation of sapphire substrates.

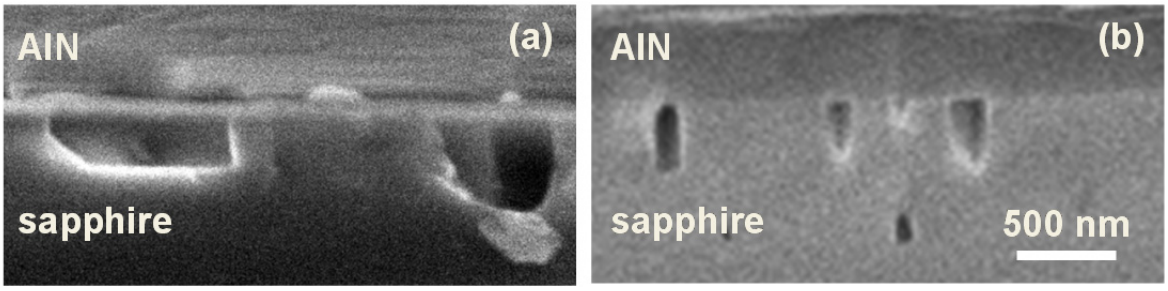

Figure 4.9: Cross-sectional SEM images of the interfaces of AlN and sapphire (a) without and (b) with nitridation.

4.3.2 Alumina as a protective material toward sapphire

In order to suppress the decomposition of sapphire substrates, alumina (Al_2O_3) powder is added into the source materials. That is to say, the gas species supplied from the source zone to growth zone is not limited to Al vapor but expanded to Al and Al-related gases such as Al_2O created through the reaction $2Al_{(g)} + Al_2O_{3(s)} = 2Al_2O_{(g)} + 1/2O_{2(g)}$. It is expected that increasing Al_2O in the growth zone may suppress the decomposition of the sapphire substrate due to Al.

The weight of the added alumina into the source was 0.2 g. The growth temperature and pressure were kept at 1550°C and 10 kPa, respectively. Note that N_2 and Ar gases (V/III = 2200) were introduced at the onset of the temperature increase of the growth zone. Figure 4.10 displays cross-sectional SEM images of AlN grown (a) without and (b) with adding alumina. Plenty of voids form at both AlN/sapphire interfaces. Adding alumina into the source makes voids smaller, but cannot eliminate it, thereby implying a minor effect on the interface control. In addition, using alumina with Al may produce Al_2O additional source gas for the AlN growth, which is considered to cause O related impurities in AlN crystals. Therefore, the

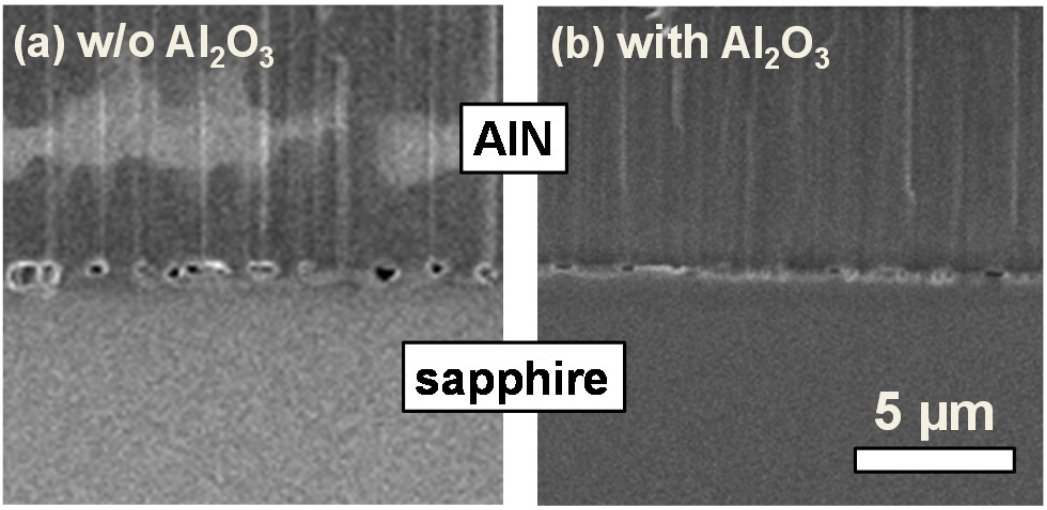

Figure 4.10: SEM cross-sectional images of the AlN/sapphire interfaces grown (a) without (b) with adding alumina.

utilization of alumina as a material protecting the sapphire surface should be determined carefully.

4.4 Growth of Thick AlN Films

4.4.1 Influence of Nitridation

In the previous section, we demonstrated that nitridation of sapphire is an effective process to control the interfacial void formation. In this section, the impact of that process as well as an already revealed important parameter of the V/III ratio on the thick film growth is examined. Note that in this section, alumina was added in the source.

Figures 4.11 and 4.12 show a set of cross-sectional SEM images of AlN films grown under different V/III ratios without and with sapphire nitridation, respectively. The XRD (0002)

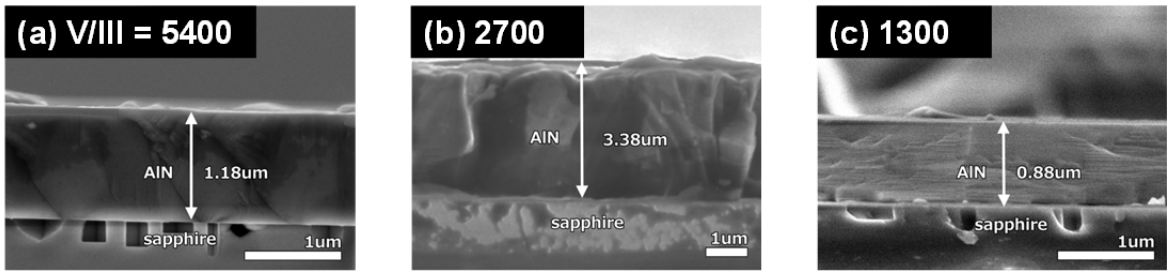

Figure 4.11: SEM cross-sectional images of AlN films grown without sapphire nitridation under various V/III ratios = (a) 5400, (b) 2700 and (c) 1300.

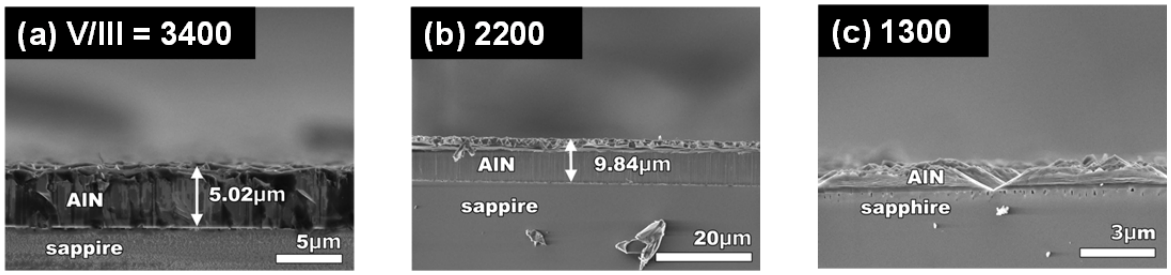

Figure 4.12: SEM cross-sectional images of AlN films grown with sapphire nitridation under various V/III ratios = (a) 3400, (b) 2200, and (c) 1300.

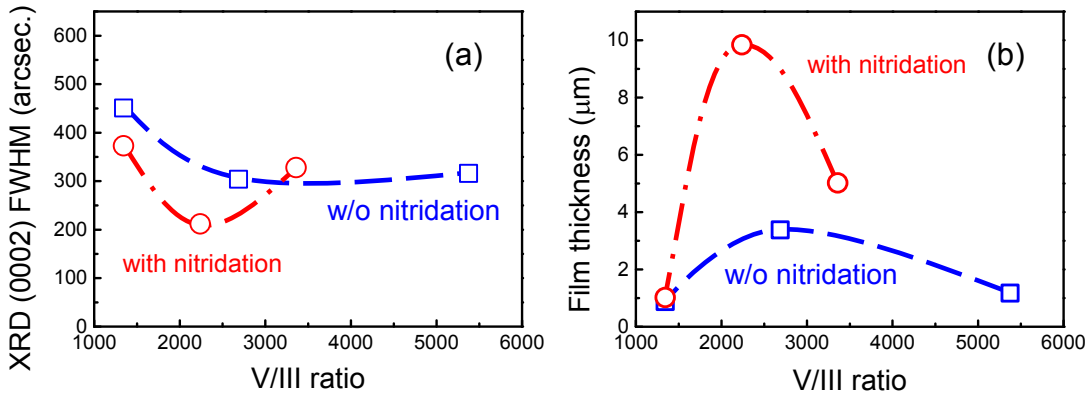

Figure 4.13: (a) XRD (0002) FMWH and (b) thickness of AlN films grown with or w/o nitridation as functions of the V/III ratio.

ω-scan line width and the AlN thickness of the samples shown in Figs. 4.11 and 4.12 are summarized in Fig. 4.13. Nitridation improves the crystalline quality and increases the thickness, indicating the positive impact on the crystal growth. The optimized V/III ratio of AlN film grown on the nitrided sapphire substrate is about 2200.

Then, the structural properties of the fabricated films were assessed by XRD measurements. Figure 4.14 shows the results for the thickest (9.84-μm-thick) AlN [Fig. 4.12(b)]. The XRD 2Θ-ω profile [Fig. 4.14(a)] demonstrates that the AlN film with preferred *c*-orientation is achieved successfully. Figure 4.14 (b) displays the XRD ω-scan profiles of the AlN (0002) symmetric and $(1\bar{1}02)$ asymmetric planes, which have quite narrow full widths at half maximum (FWHM) of 212 and 266 arcsec, respectively. From these values, the edge and screw dislocation densities are estimated to be 5.6×10^8 and 9.8×10^7 /cm^2, respectively. These results indicate that this 9.84-μm-thick AlN film has excellent crystalline quality. Furthermore, the ϕ-scan of the AlN $\{1\bar{1}02\}$ asymmetric planes [Fig. 4.14(c)] shows six-fold symmetry, indicating that the crystal is in the single phase exclusive of other rotation domains. Besides, Fig. 4.14(c) demonstrated that AlN is rotated 30° with respect to sapphire within the (0001) plane. This is to minimize their lattice mismatch, similar to GaN and AlN thin films on sapphire (0001), as shown in Fig. 4.15.

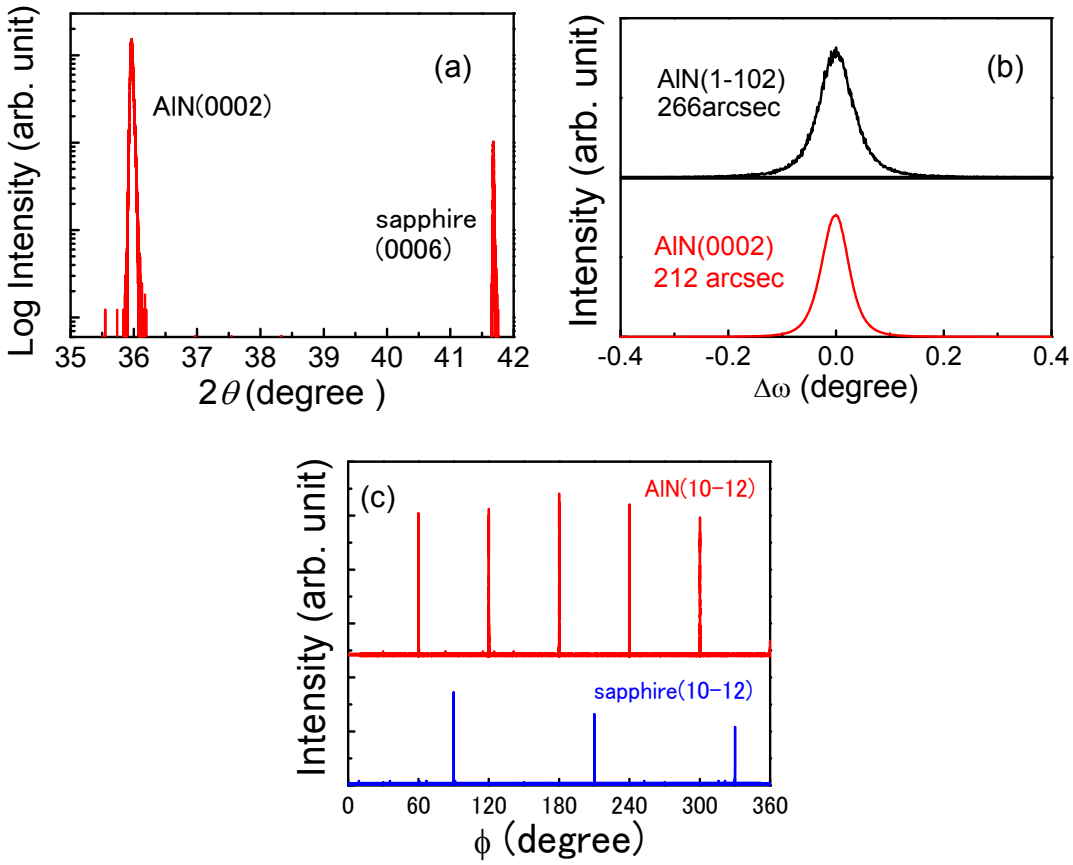

Figure 4.14: XRD (a) 2Θ-ω scan, (b) ω-scan, and (c) ϕ-scan profiles of the AlN film fabricated on the nitrided sapphire substrate with alumina in the source.

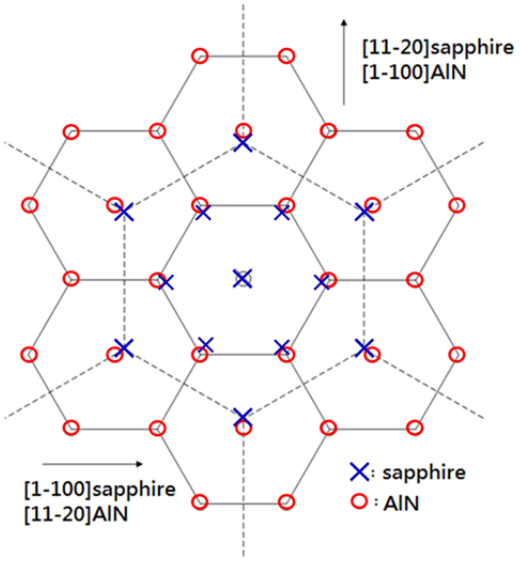

Figure 4.15: Atomic arrangement of AlN on (0001) sapphire.

4.4.2 AlN Grown on Nitrided Sapphire Substrate without Additional Alumina

In this section, AlN is grown with nitridation process but without additional alumina (Al_2O_3) in the source, to see effect of alumina on the growth.

The AlN films were grown with varying V/III ratios at a constant growth temperature of 1550°C. Here, the V/III ratio was varied with the Al flow rate under the constant N_2 flow rate. Since the crystal qualities and film thicknesses of AlN films grown with and without alumina are nearly the same, we plot experimental results of AlN growth with and without alumina together in Fig. 4.16. In Chap. 3, we have shown that lower V/III ratios tend to form AlN whiskers. Referring to that result, we consider that a lower V/III ratio reduces the driving force for film growth but promotes growth along one certain direction forming nanowires. There are similar cases in GaN grown by MOVPE such as ref. [16]. On the one hand, V/III ratios greater than 2300 decrease the growth rate because the Al flow rate that contributes to growth is reduced. Accordingly, the optimal V/III ratio in this study is ~2200. With the optimized growth condition, we achieved the fastest growth rate up to 16 μm/hr in this thesis.

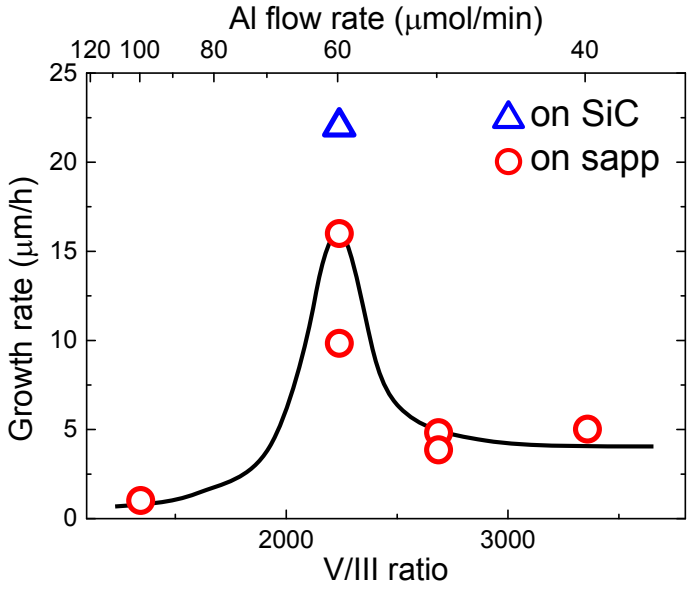

Figure 4.16: AlN growth rate as a function of V/III ratio.

Let us estimate the availability of the Al raw material in our growth method. The 16-μm-thick AlN was grown on a 1 cm × 1.5 cm sapphire substrate. The total supply of the Al source was 3.6 mmol. (See Fig. 4.16. The estimate of 3.6 mmol is given by 60 μmol/min × 60-min growth) If the supplied Al is completely used for the growth, the film thickness should be 300 μm at most. Therefore, the availability of Al source is at least 16/300 ~ 5%. For MOVPE, an Al flow rate of 4 μmol/min results in 1.8 μm/hr [17], which corresponds to 27 μm/hr under the same Al flow rate of 60 μmol/min. Therefore, the availability of the Al source in our growth method is ~60% of that of MOVPE, and the improvement is necessary in the future.

The structural properties of the 16-μm-thick AlN were also assessed. Figure 4.17 shows a cross sectional SEM image. In addition, the controlled interface formation via sapphire

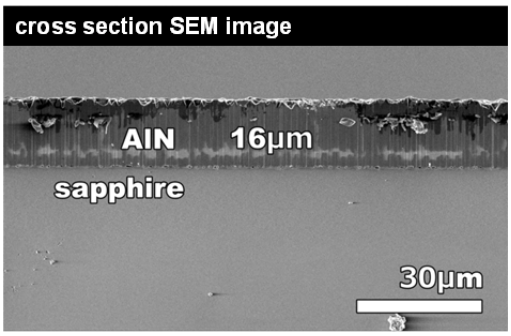

Figure 4.17: SEM cross-sectional image of the 16-μm-thick AlN film.

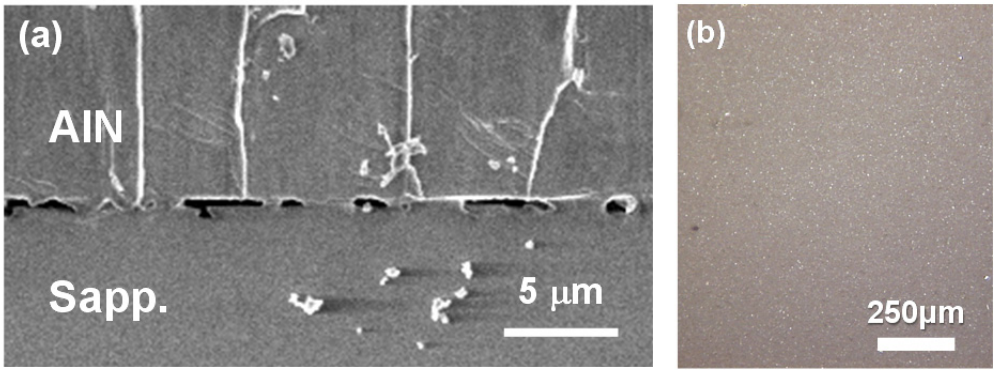

Figure 4.18: (a) SEM image of the interface and (b) surface optical microscope image of the 16-μm-thick AlN film.

nitridation eliminates whiskers but creates voids, as shown in Fig 4.18(a). As discussed in the Sec. 4.2, the tensile strain in AlN is cushioned via the void, and consequently, a thick crack-free AlN film was fabricated successfully [Fig 4.18 (b)].

The structural properties of the 16-µm-thick AlN film were assessed by XRD measurements. The 2Θ-ω profile [Fig 4.19 (a)] indicated the successful growth of AlN. Figure 4.19 (b) displays the ω-scan profiles of the AlN (0002) symmetric and (1$\bar{1}$02) asymmetric planes. The respective FHWMs are 290 and 291 arcsec, and the estimated edge and screw dislocation densities are 4.8×10^8 and 1.8×10^8 /cm^2, respectively. Besides, the ϕ-scan of the AlN {1$\bar{1}$02} asymmetric planes [Fig 4.19(c)] shows a single phase crystal with in-plane 30°

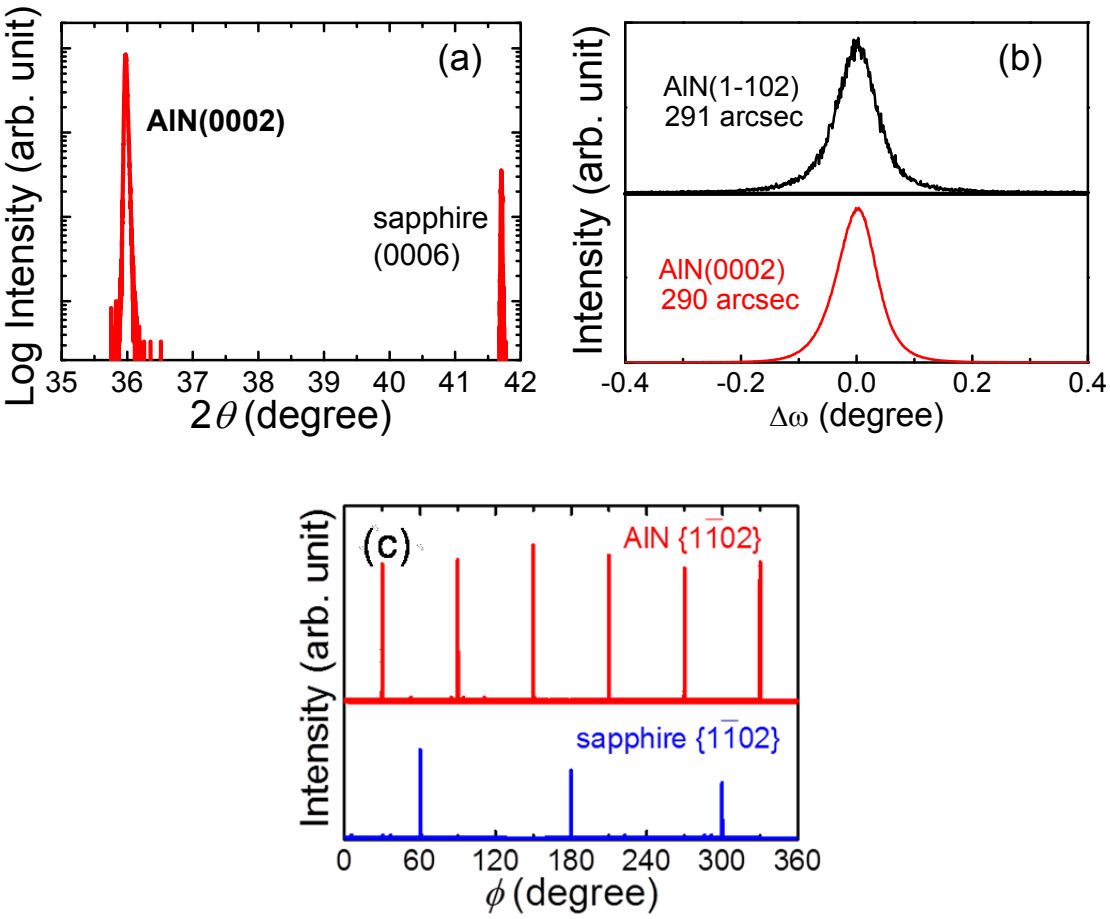

Figure 4.19: XRD (a) 2Θ-ω scan, (b) ω scan, and (c) ϕ scan profiles of the AlN film fabricated on the nitrided sapphire substrate without adding alumina.

rotation. Again, promising characteristics of the proposed growth method are demonstrated.

4.4.3 Influence of Substrate Species

As mentioned in the Sec. 4.2, since the AlN crystal growth may be obstructed if the separation completed in the early stage of the growth, we consider that the decomposition process of sapphire substrate may also affect the growth rate of AlN film. This hypothesis is confirmed in this section.

An AlN film was grown on a Si-face 6H-SiC (0001) substrate at 1550°C with a V/III ratio of 2200 (N_2: 3 SLM and Ar: 0.6 SLM). The growth pressure was kept at 10 kPa. As shown in Fig. 4.20, the thickness of the AlN film is ~20 μm. That is, the growth rate of AlN on SiC is higher than that of AlN on sapphire. Nevertheless, owing to the absence of the voids or whiskers near the interface, the compressive strain at the AlN/SiC interface remains. Consequently, there are a large number of cracks in the AlN film as shown in Fig. 4.6(b). Therefore, SiC is not an ideal alternative to sapphire, and in future work, we expect homoepitaxy for the quality improvement of AlN via direct nitridation method.

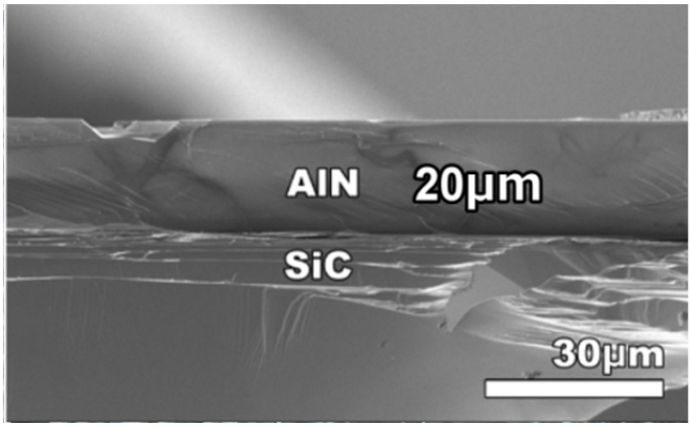

Figure 4.20: Cross-sectional SEM image of the 20 μm AlN film grown on SiC. substrate.

4.5 Determination of Polarity

The wurtzite crystal is not inversion-symmetric along the c-direction. Depending on the bond arrangements, the N-polarity and III metal-polarity are defined as shown in Fig. 4.21. The difference in the surface energies of the two polarities leads to quite different chemical reactivity and surface kinetics. Consequently, the polarity is an important factor that affects the structural, electrical, and optical properties of the AlN films. In this section, we examine the polarity of the AlN thick films grown with / without nitridation of sapphire substrates.

The surface morphologies of the AlN thick film without and with substrate nitridation are quite different as shown in Figs. 4.22(a) and (b), respectively. According to the observations,

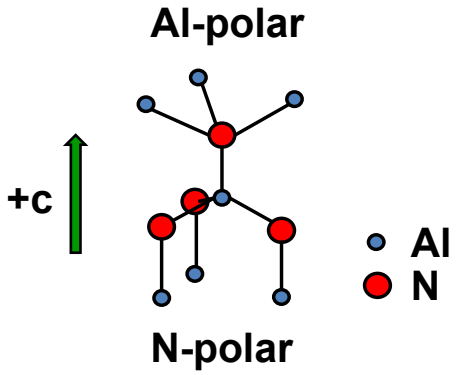

Figure 4.21: Wurtzite III-nitride unit cell.

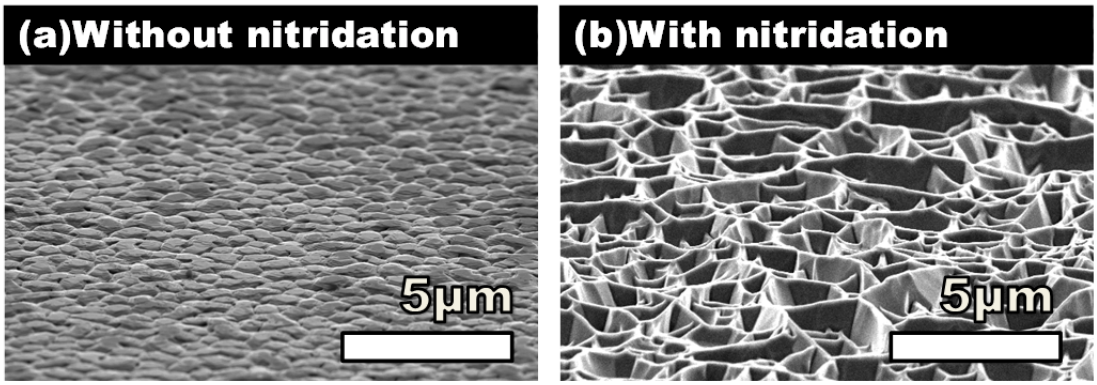

Figure 4.22: SEM images of AlN films grown on sapphire substrates (a) without and (b) with nitridation.

we speculate that their polarities are opposite. Some previous reports claim that polarity inversion tends to take place after substrate nitridation treatment [18,19].

To chemically determine the polarities of the AlN thick films, we etched two samples with and without nitridation with an aqueous potassium hydroxide (KOH) solution (10 wt%) at 70°C for 10 minutes. An aqueous KOH solution will not attack the Al-polar surface, but will generate hexagonal hillocks on the N-polar surface. We used SEM to observe the morphologies of the two samples before and after chemical etching. However, the surface morphologies of both two samples unexpectedly have no obvious change.

To reach the solid conclusion, convergent-beam electron diffraction (CBED) patterns were taken along the AlN [$11\bar{2}0$] direction for the two samples with and without nitridation. For the CBED measurements, specimens were prepared by the conventional Ar^+ milling technique. This specimen thickness was not measured, but was presumably ~100 nm. In Figs. 4.23(a) and (b), the CBED patterns of the two samples look the same, and therefore, we conclude that there is no polarity inversion. Figure 4.23(c) is a simulated CBED pattern for a specimen thickness of 100 nm with an electron acceleration voltage of 200 kV [20]. Similarities are found for the spots designated by $a^{(',")}$, $b^{(',")}$, and $c^{(',")}$ in Figs. 4.23(a), (b), and (c). Therefore, we suppose that the polarities of our AlN thick films are always N-polar. In contrast, AlN films grown by MOVPE are usually Al-polar. These findings suggest that the crystal growth mechanism of AlN prepared in this work is different from that grown by MOVPE. Therefore, the crystal growth mechanism in the proposed method is worthy to be further investigated in the future work.

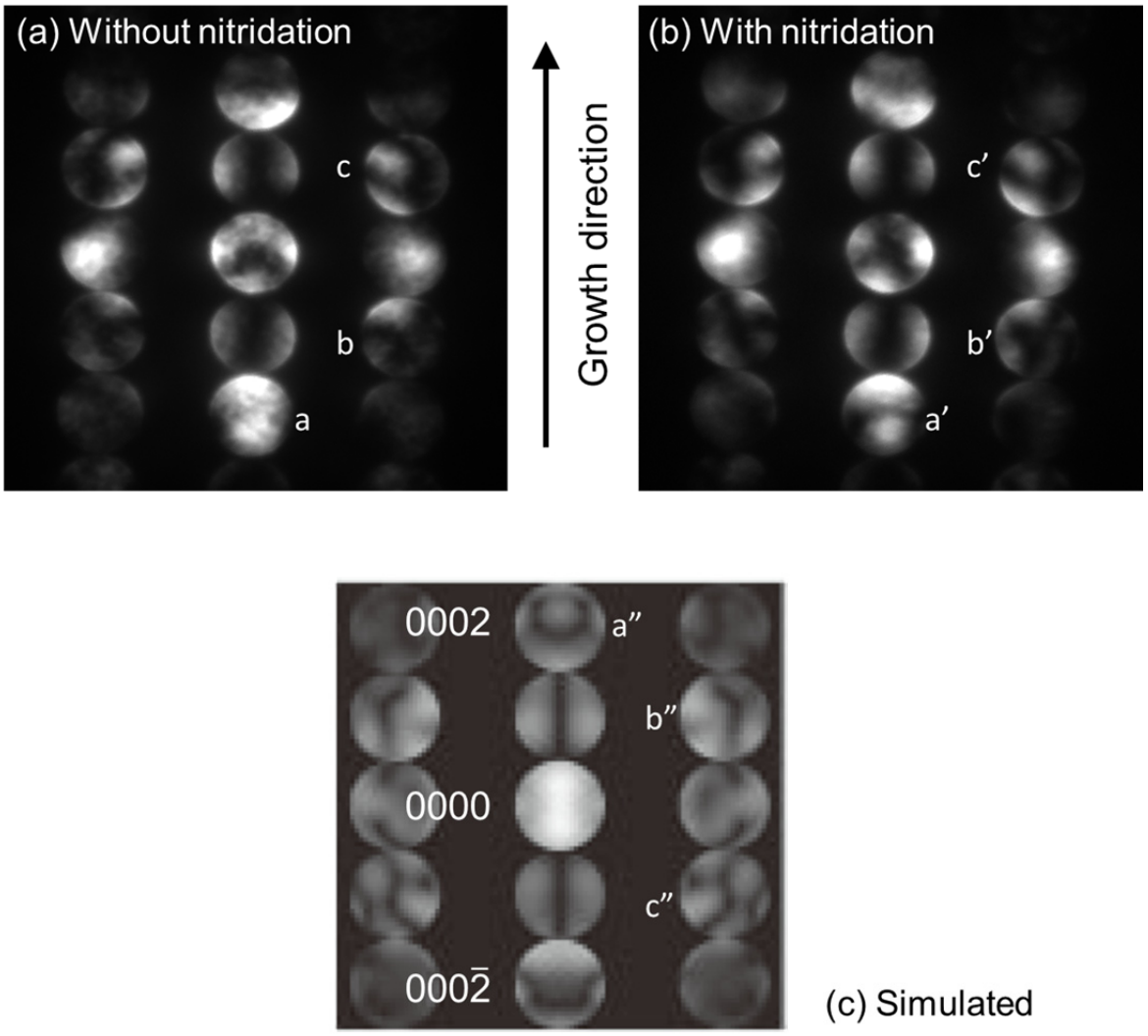

Figure 4.23: CBED patterns of AlN films grown on (a) un-nitrided and (b) nitrided sapphire substrates. (c) Simulated CBED pattern (reproduced from ref. [20]). The patterns were taken along the AlN [11$\bar{2}$0] direction.

4.6 Estimation of Unintentionally Doped Impurity Concentrations

Impurity concentrations in our AlN thick films on sapphire were measured by secondary ion mass spectrometry (SIMS). Two samples were selected: (1) without and (2) with sapphire nitridation. [The source zone and growth zone temperatures were commonly 1400 and

Table 4.1: Impurity concentrations (atoms/cm^3) in our AlN on sapphire measured by SIMS.

	C	Si	O
Sample 1	9×10^{20}	4×10^{20}	2×10^{18}
Sample 2	2×10^{20}	7×10^{19}	4×10^{18}

1550°C, respectively, whereas V/III ratios were 2700 for (1) and 3400 for (2).] The SIMS results are listed in Tab. 4.1. As seen, both two samples contain large quantities of C, Si, and O impurities. Note that the concentrations of oxygen in the two samples are near the background level of the SIMS system around ~1×10^{18} atoms/cm^3.

It has often been reported for GaN that the N-polarity enhances impurity incorporation [21-23]. Because our AlN is N-polar as discussed in Sec. 4.5, one possible reason of the observed high impurity concentrations is the polarity. To examine the effect of the polarity, SIMS was performed for Al-polar AlN, which was prepared by growing AlN on Si-face 6H-SiC (0001) substrate (see Sec. 4.4.3). The result is shown in Tab. 4.2. The impurity concentrations are similarly high in spite of the polarity difference, which strongly suggests that many impurities exist in the growth ambient.

According to these results, we suppose that carbon-related impurities were originating from the chemical reactions between Al and uncoated carbon (graphite) crucibles. In addition, silicon-related impurities were generated from quartz, which is used in the parts of the growth

Table 4.2: Impurity concentrations (atoms/cm^3) in Al-polar AlN grown on 6H-SiC (0001).

	C	**Si**	**O**
Impurity concentrations	2.2×10^{21}	1.8×10^{21}	3.0×10^{18}

apparatus. That is to say, the impurities were almost from the furnace. In order to decrease impurity concentrations, we should modify the apparatus design. For example, ceramic coating around graphite crucibles is a way to diminish carbon-related impurities.

4.7 Threading Dislocations

4.7.1 Characteristics of Dislocation Distribution

Transmission electron microscopy (TEM) is one of the most powerful nano-structural estimation techniques. Through TEM observations, we can characterize the crystal structure and reveal defects with a high resolution. For observations, the TEM specimen needs to be thin enough. In this study, TEM samples were prepared by using an Ar ion milling equipment. The electron beam (200 keV) was incident parallel to the $[11\bar{2}0]_{\mathrm{AlN}}||[1\bar{1}00]_{\mathrm{sapphire}}$ axis. The TEM specimen was manufactured from a 5-μm-thick AlN film which has been introduced in Sec. 4.4.2.

Figure 4.24(a) shows a cross sectional bright field (BF) image of the 5-μm-thick AlN film. Interestingly, threading dislocations (TDs) are concentrated on the voids near the interface. This result implies that the decomposition of sapphire substrates may increase the TD quantity. Consequently, the suppression of substrate decomposition is an effective method to decrease TD density. (Note that too much suppression causes cracks, so that there is a compromise.) Figure 4.24(b) shows a cross section of an AlN thick film grown by MOVPE with a nitridation process of sapphire [24]. Comparison between Figs. 4.24(a) and (b) indicates that the TD density in the AlN film grown in this work is much lower. That is, our AlN thick films with nitridation have better quality than the MOVPE samples with nitridation. In the next section, we discuss the densities of different type dislocations in the 5-μm-thick AlN sample introduced in this section.

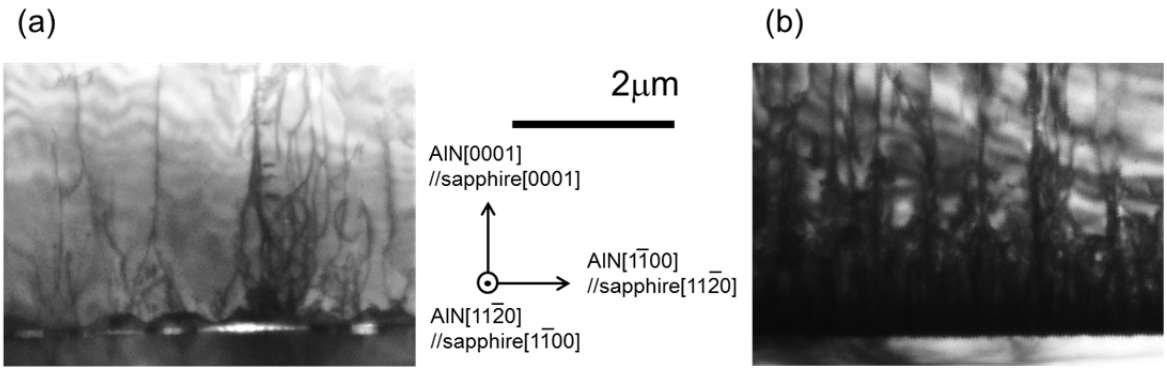

Figure 4.24: TEM-BF images taken along the $[11\bar{2}0]_{\mathrm{AlN}}||[1\bar{1}00]_{\mathrm{sapphire}}$ zone axis of (a) the AlN film grown in this study and (b) grown by MOVPE [24]. Both samples were grown on nitrided sapphire substrates.

4.7.2 Dislocation Density Estimations

In this study, $\boldsymbol{g}\cdot\boldsymbol{b}=0$ invisibility criterion was applied to identify Burgers vectors ($\boldsymbol{b}$) of TDs, where $\boldsymbol{g}$ is the reciprocal vector of the diffraction plane. Briefly, when a perfect dislocation is invisible or only shows a weak residual contrast in a TEM image, its Burgers vector must lie in the diffraction plane. In the wurtzite AlN structure, there are three types of TDs, which are perfect dislocations including type **a** (pure edge), type **c** (pure screw), and type **a+c** (mix) TDs with Burgers vectors of $\frac{1}{3}\langle 11\bar{2}0\rangle$, $\langle 0001\rangle$, and $\frac{1}{3}\langle 11\bar{2}3\rangle$, respectively [25]. Therefore, in order to identify the types of the TDs, a series of observations under two-beam conditions with $\boldsymbol{g}=[0002]$ and $[1\bar{1}00]$ were performed. Through different two-beam conditions, the quantity of pure edge dislocation and pure screw dislocation can be estimated approximately. According to the $\boldsymbol{g}\cdot\boldsymbol{b}=0$ invisibility criterion, the images of type **a** TDs in the AlN film are out of contrast under $\boldsymbol{g}=[0002]$ diffraction condition, whereas type **c** and **a+c** TDs are visible. On the other hand, under $\boldsymbol{g}=[1\bar{1}00]$ diffraction condition, those visible TDs are considered type **a** and **a+c** TDs. (Note that type **a** TDs with Burgers vector $\frac{1}{3}[11\bar{2}0]$ are also out of contrast under $\boldsymbol{g}=[1\bar{1}00]$ diffraction condition. Therefore,

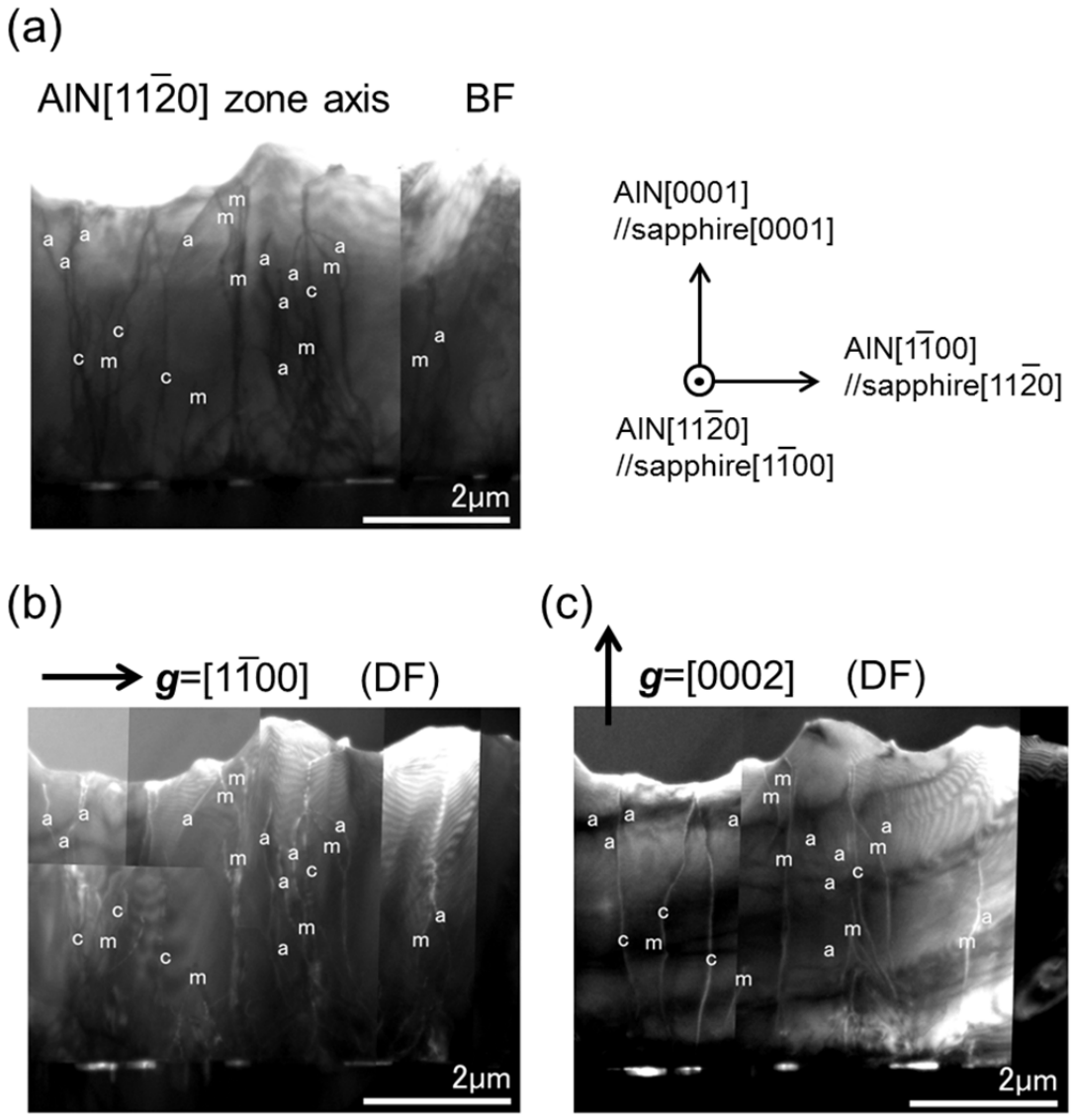

Figure 4.25: TEM images of the AlN thick film taken along the $[11\bar{2}0]_{AlN}$ axis. (a) BF image, (b) dark field (DF) image with $\boldsymbol{g} = [1\bar{1}00]$ two beam condition and (c) DF image with $\boldsymbol{g} = [0002]$.

the visible type **a** TDs are 2/3 of the total type **a** TDs.)

Based upon the TEM analyses using the invisibility criterion, the estimated density of type **a** TDs (except type **a** TDs with Burgers vector $\frac{1}{3}[11\bar{2}0]$) is 1.7 $\times$ 10^9 cm^{-2} (marked as **a** in Fig. 4.25). Hence, the total density of pure edge TDs should be 2.6×10^9 cm^{-2}. The estimated

density of pure screw TDs is 7 × 10^8 cm^{-2} (marked as **c**). Likewise, the estimated density of type **a+c** TDs is 2.0×10^9 cm^{-2} (marked as **m**). Here, the TEM specimen thickness was assumed to be 100 nm. Also, there may be an error in counting the dislocation numbers. Therefore, the estimates may include an error of a few tens %. Having said this, the values from TEM are close to the values calculated from the XRD profiles (Pure screw: 2.3 × 10^8 cm^{-2} and pure edge: 1.7 × 10^9 cm^{-2}).

4.8 Optical Properties

4.8.1 Photoluminescence

The emission properties are investigated by photoluminescence (PL). The excitation source was an ArF excimer laser (193 nm) with a pulse width of 4 ns. Figure 4.26(a) shows the PL spectra of the 16-μm-thick AlN film grown in this study acquired at 11.6 K and room temperature (RT). For comparison, Fig. 4.26(b) shows PL spectra of 600-nm-thick AlN grown by MOVPE [17]. Comparing them reveals that the near bandgap emission is not observed, but intense deep level emissions are observed in AlN grown in this study. Furthermore, the impurity concentrations in the AlN film in this study are much higher than that grown by

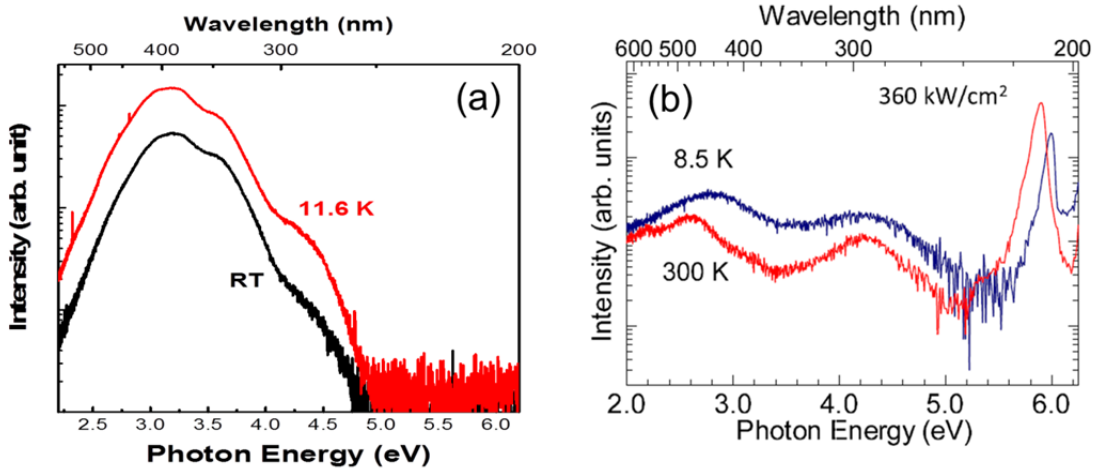

Figure 4.26: (a) PL spectra of the 16-μm-thick AlN film grown in this study. (b) PL spectra of 600-nm-thick AlN grown by MOVE, for comparison. (b) is reprinted from ref. [17]

MOVPE (data not shown). Therefore, reducing impurities and vacancies is an important task in future to improve the optical properties of AlN grown by the proposed method. Again, we would like to stress that this can be achieved by modifying the furnace design.

If we assume that non-radiative processes are negligible at low temperatures, the internal quantum efficiency of the AlN layer prepared in this work is as high as 34% at RT.

4.8.2 Transmittance and Absorption

The optical transmission spectrum of the 16-μm-thick AlN film was assessed at RT using a D_2 lamp (200 – 400 nm) and Laser-Driven Light Source (LDLS) lamp (400 – 800 nm). Because the surface of the 16-μm-thick AlN film was rough as shown in Fig. 4.22(b), the surface was polished and the resultant thickness was reduced to 10 μm. However, the surface is still rough and causes light scattering. Furthermore, the sapphire substrate was not removed. Both of them make an analysis difficult, and we make some assumptions.

In order to acquire an approximate optical transmission spectrum, we assumed (a) no multipath reflection inside the film, (b) no absorption at longer wavelengths around 800 nm, and (c) no dispersion of reflectivity. With assumption (a), the external transmission (T_{ext}) through an AlN/sapphire structure is generally described as $T_{\mathrm{ext}} = \frac{I}{I_0} = t_1 t_2 t_3 \exp(-\alpha d)$, where I_0 is the intensity of the incident light, I is the intensity of the transmitted light, and t_i (i = 1,2,3) are the transmittances at air/AlN (i = 1), AlN/sapphire (i = 2), and sapphire/air interfaces (i = 3). α is the absorption coefficient and d is the thickness of the AlN film. In practice, because the surface of our sample is rough even after polishing, it is difficult to accurately deal with t_i. Therefore, we made assumptions (b) and (c) to extract the internal transmission of $T_{\mathrm{int}} = \exp(-\alpha d)$ with the following procedure.

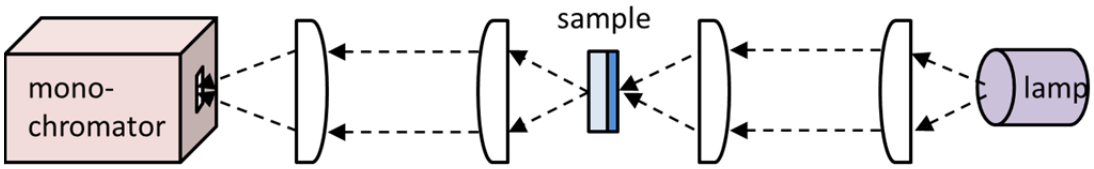

Figure 4.27: System of optical transmittance measurement.

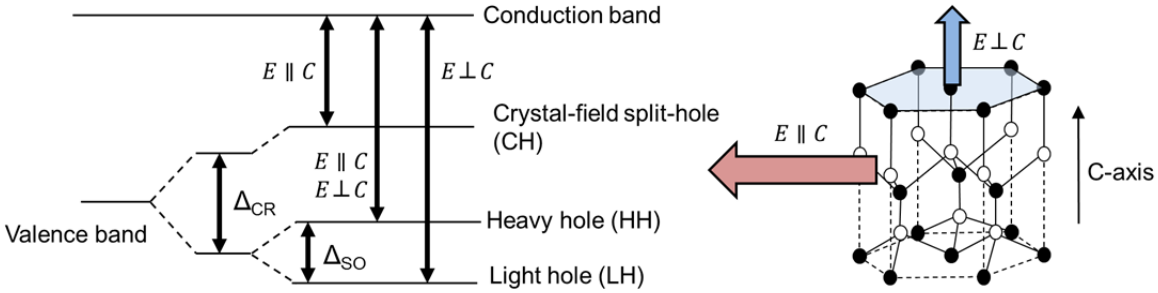

Figure 4.28: Band structure and optical transitions of AlN.

Figure 4.27 shows the system setting for optical transmittance measurements. The angle of incidence was normal to the sample surface, that is, along the [0001] axis of AlN. We used a blank sapphire substrate as a reference. Here, the band structure of AlN should be noted. As illustrated in Fig. 4.28, the topmost valence band in AlN is the crystal-field splitting hole band. The optical transition related to this valence band is polarized along the [0001] c axis due to the nature of the *p* state composed of the band. Therefore, under the present experimental configuration, where the electric vector of the incident light is perpendicular to the [0001] axis, the absorption may be underestimated.

Initially, we measured the external optical transmission spectra of the blank sapphire substrate and the 16-μm-thick AlN film on sapphire. Subsequently, to compensate for the sapphire and system dispersions, we divided the transmission spectrum of the 16-μm-thick AlN film by that of the reference blank sapphire. Lastly, the transmittance at ~800 nm was considered to be 100%, based on the assumption (b). Thus obtained transmission spectrum

approximated an internal transmission spectrum, which is shown in Fig. 4.29. The absorption occurs below 300 nm, similar to AlN by sublimation, reflecting high impurity concentrations revealed in Sec. 4.6.

Besides, from the estimated internal transmission spectrum, we estimated the absorption

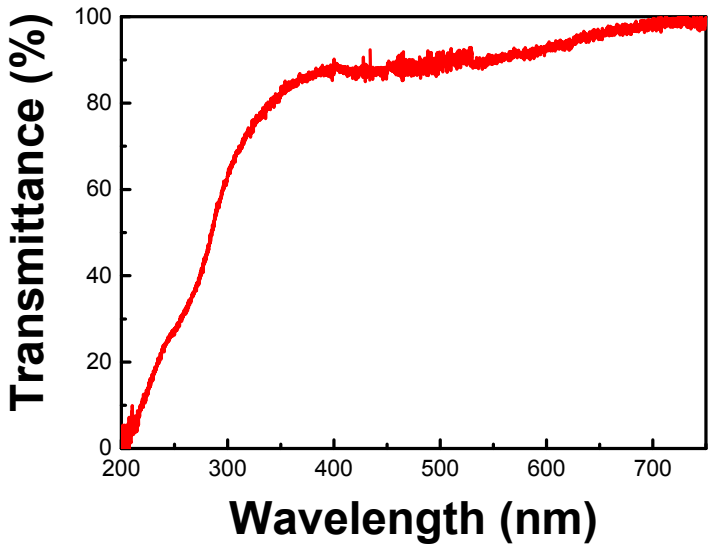

Figure 4.29: Estimated internal optical transmission spectrum of the 16-μm-thick AlN film at RT.

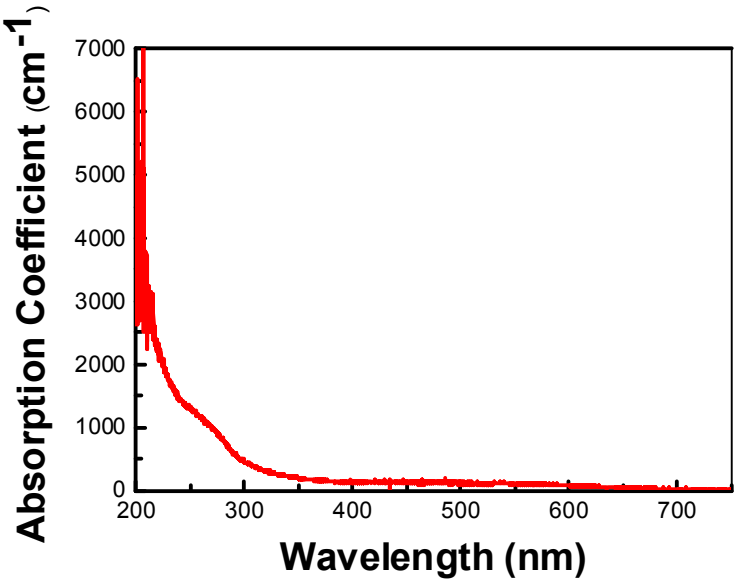

Figure 4.30: Dispersion of the absorption coefficient of the 16-μm-thick AlN film at RT.

coefficient using $T_{\mathrm{int}} = \exp(-\alpha d)$. Note that after polishing, the thickness of the 16-μm-thick AlN film was decreased to 10 μm. The result is shown in Fig. 4.30. Below-gap absorption appeared at wavelengths longer than 207 nm is confirmed.

4.9 Summary

In this chapter, the mechanism of self-separation of AlN films from sapphire substrates was discussed. We attributed it to the sapphire decomposition caused by the Al vapor: The Al vapor transferred from the source zone may reduce sapphire (Al_2O_3) substrate to yield Al-related gases. Such a reaction increases local Al-related molecules and decreases the local V/III ratio at the sapphire surface. As mentioned in Chap. 3, a low V/III ratio promotes whisker growth, which is why the AlN whiskers are formed only near the sapphire surface. Because the whiskers are physically weak, the AlN film grown on top of them is likely free from the influence of the sapphire substrate. This suggests that even in thick AlN, crack generation due to the thermal expansion mismatch may be avoided without any special treatment. In fact, crack free 16-μm-thick AlN was demonstrated.

However, the degree of self-separation affects the AlN film growth significantly. Therefore, we proposed two methods to control the degree of the interface reaction between AlN and sapphire. One is nitridation of sapphire substrates, and the other is adding alumina to the source. The results showed that the effect from adding alumina was merely, whereas the nitridation well controlled interface formation. We utilized the results to fabricate AlN thick film and obtained a high quality 16-μm-thick AlN film successfully.

References

[1] W. M. Yim, E. J. Stofko, P. J. Zanzucchi, J. I. Pankove, M. Ettenberg, S. L. Gilbert, J. Appl. Phys. 44, 292 (1973).

[2] W. M. Yim, R. J. Paff, Appl. Phys. 45, 1456 (1974).

[3] R.G. Banal, Y. Akashi, K. Matsuda, Y. Hayashi, M. Funato, Y. Kawakami, Jpn. J. Appl. Phys. 52, 08JB21 (2013).

[4] T. D. Moustakas, R. J. Molnar, T. Lei, G. Menon, J. C. R. Eddy, Mater. Res. Soc. Symp. Proc. 242, 427 (1992).

[5] S. Hirai, M. Ozawa, H. Katayama, Y. Uemura, Mater. Trans. Jpn. Inst. Metals, 56, 541 (1992).

[6] K. Uchida, A. Watanabe, F. Yano, M. Kouguchi, T. Tanaka, S. Minagawa, J. Appl. Phys. 79, 3487 (1996).

[7] Z. Yang, L. K. Li, W. I. Wang, J. Vac. Sci. Technol. B 14, 2354 (1996).

[8] T. Tokuda, A. Wakahara, S. Noda, A. Sasaki, J. Cryst. Growth 183, 62 (1998).

[9] C. Heinlein, J. Grepstad, S. Einfeldt, D. Hommel, T. Berge, A. P. Grande, J. Appl. Phys. 83, 6023 (1998).

[10] F. Widmann, G. Feuillet, B. Daudin, J. L. Rouviere, J. Appl. Phys. 85, 1550 (1999).

[11] H. Fukuyama, W. Nakao, M. Susa, K. Nagata, J. Am. Ceram. Soc. 82, 1381 (1999).

[12] M. Losurdo, P. Capezzuto, G. Bruno, J. Appl. Phys.88, 2138 (2000).

[13] M. Losurdo, P. Capezzuto, G. Bruno, G. Namkoong, W.A. Doolittle, A. S. Brown, J. Appl. Phys. 91, 2108 (2002).

[14] W. Nakao, H. Fukuyama, J. Crystal Growth 259, 302 (2003).

[15] W. Nakao, H. Fukuyama, K. Nagata, J. Am. Ceram. Soc. 85, 889 (2002).

[16] K. Choia, M. Arita, Y, Arakawa, J. Crystal Growth 357, 58 (2012).

[17] R.G. Banal, PhD thesis, Kyoto University (2009).

[18] Q.S. Paduano, D.W. Weyburne, J. Jasinski, Z. Liliental-Weber, J. Crystal Growth 261, 259 (2004).

[19] Y. Wu, A. Hanlon, J. F. Kaeding, R. Sharma, P. T. Fini, S. Nakamura, J. S. Speck, Appl. Phys. Lett. 84, 912 (2004).

[20] M. Imura, U. Gautam, K. Nakajima, Y. Koide1, H. Amano K. Tsuda, Jpn. J. Appl. Phys. 52, 08JE15 (2013).

[21] M. Sumiya, K. Yoshimura, K. Ohtsuka, S. Fuke, Appl. Phys. Lett. 76, 2098 (2000).

[22] N. A. Fichtenbaum, T. E. Mates, S. Keller, S. P. DenBaars, S. P. Speck, J. Cryst. Growth 310, 1124 (2008).

[23] S. C. Cruz, S. Keller, T. E. Mates, U. K. Mishra, S. P. DenBaars, J. Cryst. Growth 311, 3817 (2009).

[24] S. Shibaoka, Master thesis, Kyoto University (2014).

[25] T. Metzger, R. Hopler, E. Born, O. Ambacher, M. Stuzmann, R. Stommer, M. Schuster, H. Gobel, S. Christiansen, M. Albrecht, H. P. Strunk, Philos. Mag. A 77, 1013 (1998).

Chapter 5 – Conclusions

5.1 Conclusions

In this thesis, a novel growth method for AlN bulk crystals has been demonstrated. The growth method requires only Al element and N_2 gas as source raw materials. Furthermore, the growth temperature is relatively low. Therefore, compared with the previous growth methods such as HVPE and sublimation, the proposed method provides an environmentally friendly route to fabricate a wide bandgap semiconductor of AlN. The achievements are as follows.

In Chap. 2, the possibility of the AlN growth from Al and N_2 is discussed in terms of thermodynamics, which strongly suggests a spontaneous reaction between them to create AlN. Conventionally, direct nitridation of Al with N_2 is used to sinter AlN powder, but simply copying that method is not suitable for AlN layer growth because unexpected AlN forms on the Al source surface and prevents continuous supply of Al vapor. Therefore, initially, we designed and constructed a suitable apparatus for the layer growth. The growth apparatus has two zones for source and growth. The zone temperatures can independently be controlled. Furthermore, the source zone is divided into two channels. The upper channel is for N_2 gas, while the lower channel is for Al vapor, thereby enabling separate supply of those precursors to the growth zone.

In Chap. 3, the reactivity between Al and N_2 was experimentally confirmed through direct nitridation. AlN powders were successfully obtained. Then, the two sources were separately supplied onto sapphire substrates. It was found that the growth zone temperatures and V/III ratios determine AlN crystal morphology. A growth zone temperature of 1550°C requires the

least V/III ratio to achieve the film growth, which, we consider, is determined by the competition between N_2 and sapphire decomposition. As for the V/III ratio, higher (lower) V/III ratios bring films (whiskers). In addition, the optical properties of the obtained AlN crystals are investigated. Although the main emissions of our samples are deep level emissions most likely due to Al vacancies, those are intense especially for AlN powders. This result suggested that AlN powders sintered by our growth method may be used as UV phosphors. To compensate for the Al vacancies, we grew AlN whiskers under an Al-rich atmosphere. Excitonic emission was obtained, which supports the assertion of an Al-vacancy-related origin of the deep level emission.

In Chap. 4, self-separation phenomena of AlN from sapphire substrates were revealed, and the mechanism was discussed. Sapphire decomposition caused by the Al vapor is the most plausible cause, because it increases Al-related molecules and decreases the V/III ratio in the vicinity of the sapphire surface. According to Chap. 3, low V/III ratios tend to cause whisker growth, and therefore AlN whiskers were formed only at the AlN/sapphire interface. Physically weak whiskers mitigate the influence of sapphire in the AlN film. The tensile strain in AlN is thus reduced, and consequently, crack-free AlN films were achieved. It was revealed that the appropriately controlled self-separation may help us to obtain high-quality AlN thick layers with a high growth rate. For this, sapphire nitridation was found to be effective. In this thesis, a 16-μm-thick AlN film was successfully obtained with a growth rate ~16 μm/hr. The XRD measurements indicated the growth of single phase wurtzite crystals with edge and screw dislocation densities of 4.8×10^8 and 1.8×10^8 /cm^2, respectively. These are one of the lowest values ever reported for AlN-on-sapphire heterostructures.

Table 5.1 compares the achievements in this study with the common AlN bulk crystal growth methods such as sublimation and HVPE. (The transmittance was estimated using the absorption coefficient discussed in Sec. 4.8.2.) The advantages of our proposed growth

Table 5.1: Comparison among sublimation, HVPE, and the proposed method.

	Sublimation	HVPE	this work
Raw materials	AlN powder, N_2(g)	Al powder, HCl(g), H_2(g), NH_3(g)	Al element, N_2(g)
Growth Temp. (°C)	~2000	<1500	~1550
Growth rate (μm/hr) (single crystal)	＞500	~25	~16
Impurities	More than HVPE (From AlN powder and crucible materials)	O, H, Si, Cl…	C, Si, O
Dislocation Density (cm^{-2})	10^2~10^3 (AlN seed growth)	>10^7 (sapphire/SiC)	~10^8 (sapphire)
Transmittance at 220–300nm (%) (with ~100 μm thickness)	~18%	~63%	~1% (estimated)

method include high environmentally friendliness and high crystalline quality, and may offer another route for the growth of promising optoelectronics material, AlN.

5.2 Future Works

Through this study, a new growth method for AlN crystal was demonstrated. However, it remains in its infancy. Several issues should be solved to improve the growth rate and crystalline quality. Here, some future works are mentioned.

■ Improving the furnace design

The availability of Al raw material in this thesis was ~5%, as estimated in Sec. 4.4.2. Therefore, one of the topics for the future works is to increase the availability of the Al raw material. For instance, tilting the substrate holder (susceptor) into a slope may be a way to

increase the growth rate.

Additionally, the SIMS measurements suggested that the impurities such as C and Si were derived from the furnace. We consider that ceramics coating around graphite parts and modifying the furnace design to separate quartz parts from the heated region may decrease the impurity concentrations.

If further reduction of the growth temperature is necessary, the utilization of activated nitrogen is an option, such as plasma-enhanced nitrogen and radical nitrogen.

■ Improving the crystal quality of AlN on sapphire substrates

As mentioned in Chap.1, compared with SiC or AlN substrates, the remarkable advantages of sapphire substrates are cost effectiveness and abundance. Although a drawback may be difficulty in separating AlN from sapphire, this can be overcome through the further control of sapphire decomposition, similar to void-assisted separation (VAS) method for GaN on sapphire [1]. Therefore, sapphire substrates are still very alluring.

Another issue is high dislocation densities in heteroepitaxial layers. Recall that the edge and screw dislocation densities of the 16-μm-thick AlN film grown on sapphire substrate are estimated as 4.8×10^8 and 1.8×10^8 /cm^2, respectively. To improve the crystalline quality, there are several possible ways. One of them is a polarity inversion technique. In Chap 4, we have revealed that the AlN films grown in this work are N-polar. If the polarity can be inverted to Al-polar, threading dislocations may bend or even diminish near the Al-/N-polarity inversion boundary. To realize the polarity inversion, the growth mechanism of N-polar AlN grown by our method must be clarified.

Another technique could be annealing under CO atmosphere, which has recently been proposed to improve the AlN quality [2], and is also applicable to our AlN layers.

■ Toward AlN bulk growth

For AlN bulk growth, increase of the growth rate of AlN film crystal is an important issue. In this thesis, the maximum value was about 16 μm/hr (on the sapphire substrate). Compared with the growth rates in sublimation and HVPE, that of this study remains insufficient. In order to improve the growth rate, further optimization of growth conditions such as V/III ratio and growth temperature is necessary. In addition, the aforementioned improvement of the growth apparatus may also be effective.

Although sapphire is mainly used in this thesis, other seed crystals such as AlN bulk crystals and AlN templates are worth being tried to improve the crystalline quality. In the future, AlN grown by our method can be a seed crystal.

■ Suppressing the deep-level emission

The optical properties of AlN powders, whiskers, and films were discussed in Chaps. 3 and 4. The main emissions were related to deep levels derived from Al vacancies (V_{Al}). To suppress V_{Al} and consequent deep level emissions, a simple guess suggests growth under Al-rich conditions. In fact, AlN whisker grown under an Al-rich condition indicated excitonic emission. However, as revealed in Chap. 3, Al-rich conditions (that is, low V/III ratios) promote whisker growth and are not suitable for layer growth. Therefore, other methods such as *ex-situ* post-growth annealing under Al-rich condition, much be developed.

■ Further applications

The core principles of the method proposed in this thesis are (a) vaporization of an element in the source zone and (b) chemical reaction between the vaporized element and a reactant gas

in the growth zone. As long as these principles are satisfied, the growth method may be used for other material systems. Here, let us consider several material systems.

(a) Vaporization:

Figure 5.1 shows the vapor pressures of Al, Ga, In, and Zn. The former three were calculated using ref. [3], while the latter was calculated from the equilibrium constant. Ga, In, and Zn have vapor pressures higher than that of Al, so that in terms of vaporization, those elements can be used with our growth system.

(b) Reactivity:

Figure 5.2 shows the calculated Gibbs free energy changes for representative material systems using Al, Ga, In, and Zn. Particularly, oxide materials such as ZnO and III_2O_3 have comparable or even better reactivity, compared with AlN, which indicates that the growth of those materials with our newly developed method is quite promising.

Hence, we expect that our environmentally friendly growth method can widely be utilized for the fabrications of other materials without using toxic and hazard sources.

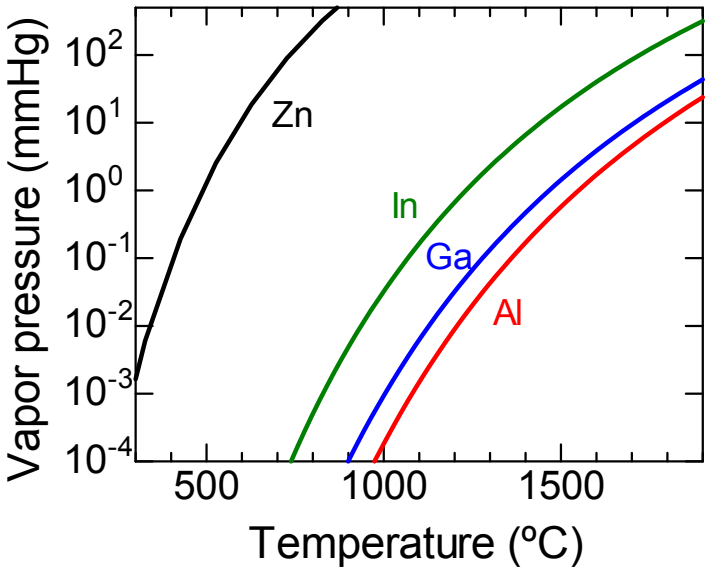

Figure 5.1: Estimations of the vapor pressures of Al, Ga, In and Zn.

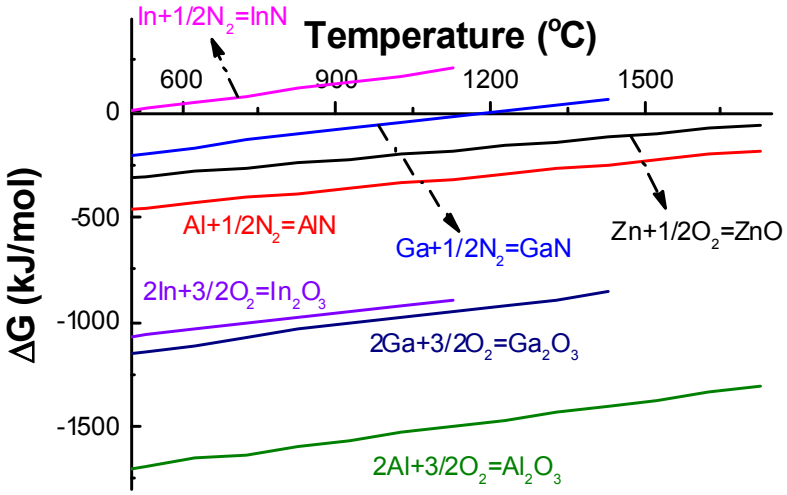

Figure 5.2: Estimations of the Gibbs free energy changes of various reactions.

References

[1] Y. Oshima, T. Eri, M. Shibata, H. Sunakawa, K. Kobayashi, T. Ichihashi, A. Usui, Jpn. J. Appl. Phys. 42, L1 (2003).

[2] G. Nishio, S. Suzuki, H. Miyake, K. Hiramatsu, H. Fukuyama, IEICE Technical Report, ED2013-80, CPM2013-139, LQE2013-115, 75 (2013).

[3] J.C. Bailar, H.J. Emeléus, S.R. Nyholm, A.F. Trotman-Dickenson, Comprehensive Inorganic Chemistry, Pergamon, Oxford (1973).

List of Publications

A. Journal papers

1. PeiTsenWu, Mitsuru Funato, and Yoichi Kawakami, “Environmentally friendly method to grow wide-bandgap semiconductor aluminum nitride crystals” (submitted)
2. PeiTsenWu, Mitsuru Funato, and Yoichi Kawakami, “Syntheses of AlN powders, whiskers, and films from Al metal and N_2 gas” (in preparation)
3. PeiTsenWu, Mitsuru Funato, and Yoichi Kawakami, “Control of interfacial void formation during vapor phase epitaxy of AlN on sapphire using Al and N_2” (in preparation)

B. International conference

1. PeiTsenWu, Mitsuru Funato, and Yoichi Kawakami, “Synthesis of aluminum nitride powders emitting in near ultraviolet spectral range”, The Sixth Asia-Pacific Workshop on Widegap Semiconductors, May 12-15, 2013, Tamsui, New Taipei, Taiwan. PT19 (Poster)

C. Domestic conferences

1. PeiTsenWu, Mitsuru Funato, and Yoichi Kawakami, “A novel method for crystallizations of aluminum nitride”, IEICE Technical Committee on Lasers and

Quantum Electronics, Nov. 28, 2013, Osaka University, Japan. (Oral)

2. PeiTsenWu, Mitsuru Funato, and Yoichi Kawakami, “Growth of crack-free AlN thick films on c–sapphire using Al powders and nitrogen gas”, The 55th Annual Symposium of the Vacuum Society of Japan, Nov. 18-20, 2014, Osaka Prefecture University, Japan. (Poster)
3. PeiTsenWu, Mitsuru Funato, and Yoichi Kawakami, “Vapor phase epitaxy of AlN thick films from environmentally-friendly sources of Al powders and nitrogen gas”, The 62nd Spring Meeting, The Japan Society of Applied Physics, March 11-14, 2015, Tokai University, Japan. (Oral)

D. Related conference

1. PeiTsenWu, Mitsuru Funato, and Yoichi Kawakami, “Role of interfacial nanowhiskers for crack-free AlN thick films grown on c-plane sapphire”, The 2nd Nano-mix Young Researcher Alliance Meeting, Nov. 13, 2014, Kyoto University, Japan. (Oral and Poster)